Photoinduced micro-fabrications of polymer films driven by the actions of topmost surface

Issei Kitamura

Department of Molecular and Macromolecular Chemistry
Nagoya University

2021

Contents

Chapter III
Photo-triggered large mass transport driven only by a photoresponsive surface skin layer

Chapter I
General Introduction

1-1. Introduction

Polymer materials are extensively essential in our lives, with a wide range of applications in the fields of structural materials as well as medical, electronic technology, adhesives, coatings and printing. Surfaces and interfaces of polymer materials exhibit a variety of performance and characteristics, such as wettability, adhesion, friction, and biocompatibility, but surface properties are difficult to fully understand because surfaces and interfaces have different energy states from the interior of the material. The contribution of surfaces and interfaces is becoming increasingly important, especially as modern materials are trend in the direction of miniaturization and thinner films. In this background, the development of methods for analysis and interpretation of the surface and interface of polymer materials have been explored. With the recent establishment of surface analysis process and the precision polymerization methods, understanding of the surface and interface of polymer materials have been rapidly progressing in these days.

This thesis focuses on the inkjet printing technic as a new approach to polymer surface and interface study, which is different from previous research directions. This study launched up by proposing a new research concept that allows direct observation of the objective polymer surface and interface by using three-dimensional heteropolymer structures fabricated by the sub-femto-litter inkjet printing. This surface and interface strategy with inkjet printing is expected to open the door to create new functionalities starting from the topmost surface of the polymer film.

In this introduction chapter, the study background on the photochromic azobenzene (Az) molecule and the Marangoni effect are firstly overviewed. Then, the important concept for the strategy of functionalization of polymer films is explained from the view point of topmost polymer film surface. Finally, the objective and the outline for this thesis are described.

1-2. Photochromic Material: Azobenzene

1-2-1. Photoisomerization of azobenzene

Azobenzene (Az) is one of the most typical photochromic molecules. The first synthesis of Az dates back to the 1858's report by P. Griess. The unique feature of azobenzene is to show photochromism from the trans form to cis form under UV light irradiation and return from the cis to trans form under visible light irradiation (Fig. 1-1a). From thermodynamics viewpoint of Az, the cis form is more thermally unstable than the trans one, which provides a thermal back reaction to trans form at room temperature for several hours to several days in the dark. Photoisomerization of Az is caused by the weakening of the N=N double bond in the S_1 state under photoirradiation[1]. The thermal cis-to-trans back reaction proceeds along the potential energy curve in the S_0 state[2,3].

1-2-2. Applications of phtoresponsive azobenzene materials

Az shows a molecular shape change by the trans-cis photoisomerization, resulting in changes of volume and dipole moments[4]. This is why Az-containing materials have been the target to create the wide range of photoresponsive functional materials utilizing the above photoinduced physical properties changes[5–17].

Photoalignment of Az have been demonstrated using the feature of transition dipole moment of azobenzene derived from its rod-like structure. When Az is irradiated with linearly polarized light, the trans-cis-trans isomerization cycle and rearranges of the transition dipole moment occur to be perpendicular to the linearly polarized light (Weigert effect)[18] (Fig. 1-1b). Based on the Weigert effect, Wendorff et al. have demonstrated the refractive index changes and developed an optical hologram system by photo-orienting Az-introduced acrylic polymers[19,20].

Az is very compatible with liquid crystalline (LC) properties due to its rod-like shape (Fig. 1-1c). Ichimura, Seki et al. have been investigated the orientation control of nematic LC. They reported a homeotropic-planar alignment control technique for LC using the Weigert effect in Az monolayers on a solid substrate (Command Surface)[21,22] (Fig. 1-2a). Recently, a new system for alignment control of LC by the free surface strategy: surface segregation and inkjet printing has been demonstrated[23–26]. (details are described in Section 1-5). This is recognized as a new command surface by the free surface, which is different from the conventional command layer placed on solid interfaces.

So far, the functions of Az have been described primarily with respect to nm-scale functions, such as molecular orientation. On the other hand, countless studies extended to macro-scale functions from nm-scale changes associated with photoisomerization have been developed. Seki et al. demonstrated reversible change of surface area of monolayers of side chain liquid crystalline (SCLC) Az-introduced polyvinyl alcohol on the water surface by photoirradiation[27]. In this system, the key to the control of surface area change of monolayer on water surface is photoinduced polarity change of Az and its affinity for water. For the photoinduced deformation of self-

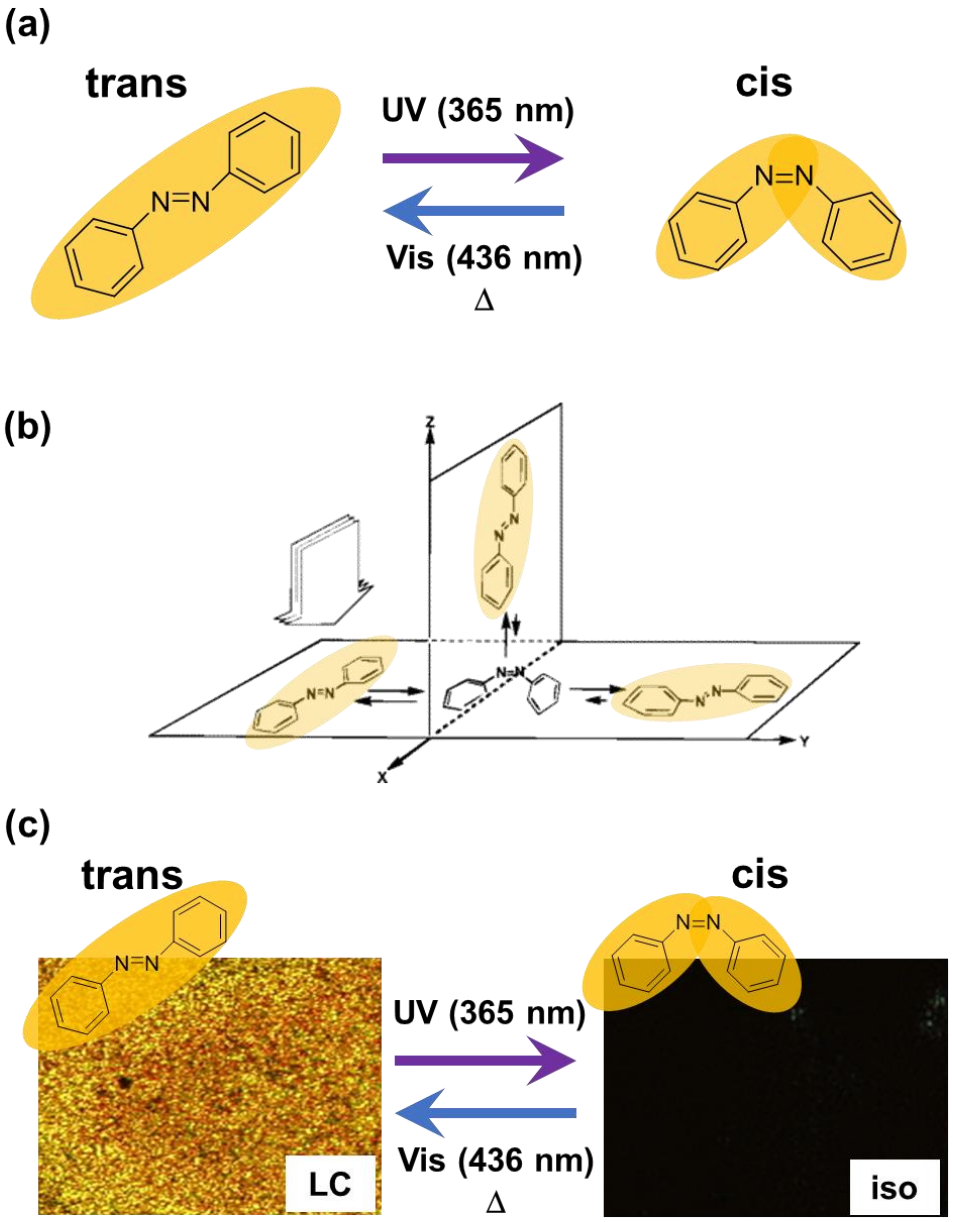

Figure 1-1. Photoisomerization of Az (a). In-plane and out-of-plane photoorientation of azobenzene by linearly polarized light irradiation (Weigert effect) (b). Photoinduced phase transition of LC Az (c) Reproduced with permission from Ref 18.

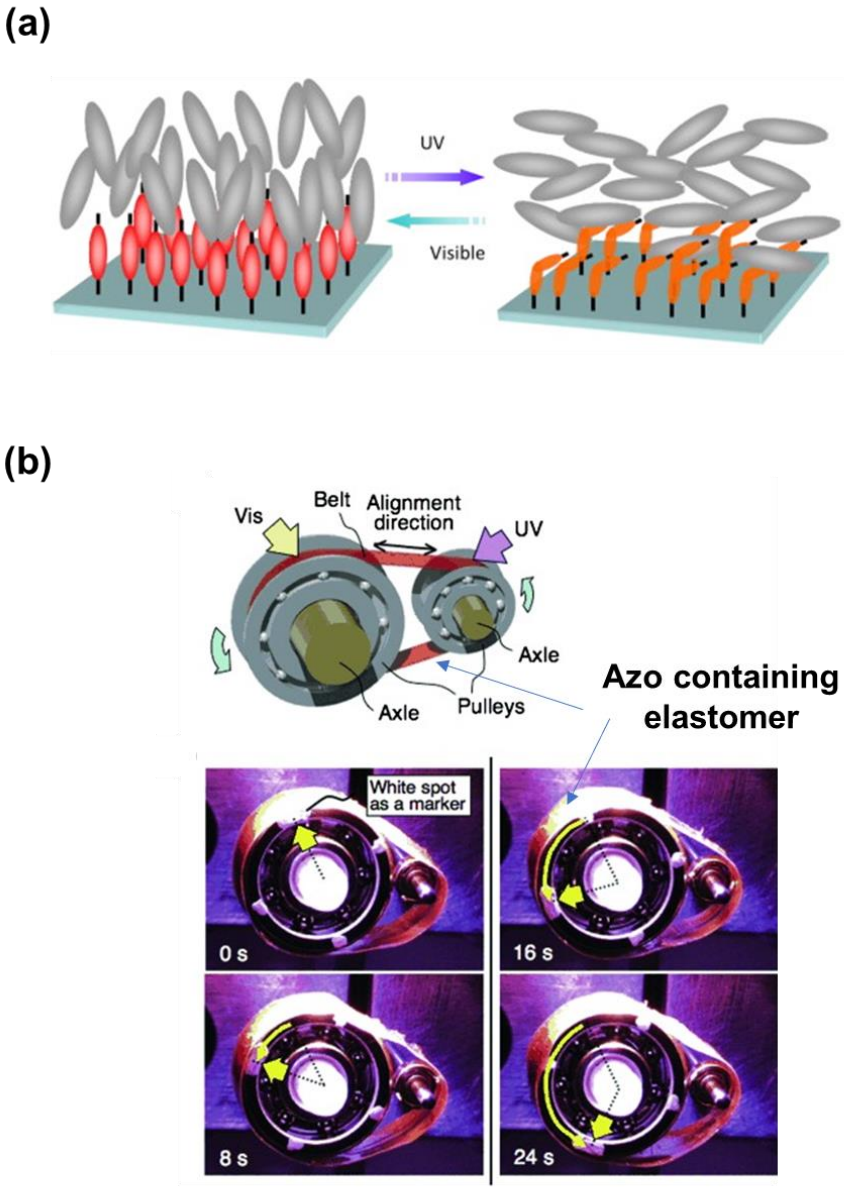

Figure 1-2. Reversible LC alignment change by command surface (a). Photomechanical materials composed of Az containing LC elastomer (b). Reproduced with permission from Ref 21 and 34.

supported azobenzene polymer films. Barrett et al. reported a reversible film thickness changes driven by free volume changes using polyacrylate with Az in the side chain[28].

Surface Relief Gratings (SRGs) formation has been a subject of extensive studies using Az polymer (PAz) films. In 1995, Natanshon et al. and Tripathy et al. reported the formation of SRGs due to mass migration of the amorphous azobenzene film by performing interferometric Ar ion laser irradiation[29,30]. Subsequently many attempts to induce the SRGs formation have been made, which triggered a great enhancement of the number of papers on the Az functionalization[5]. The details of the research on SRGs formation is shown in Section 1-3.

About 10 years after the first SRGs report, Ikeda and Yu et al. reported in 2003 that the films were bent by photoirradiation in uniaxially aligned cross-linked LC Az polymer films[31] (Fig. 1-2b). In this system, the light energy is converted to mechanical energy and can act as a motor which is called photomechanical materials. The phase transition is induced by photoisomerization of the surface layer of the cross-linked LC Az polymer film, resulting in shrinkage and bending of polymer film[32–35]. As noted in this section, wide variety of functions have been reported using photoresponsive Az materials, ranging from molecular scales of nm to visually perceptible mm scales.

1-3. Surface Relief Grating (SRGs) formation in azobenzene materials

1-3-1. SRGs formation in azobenzene polymer films

In 1995, a Canada group (Natanshon et al.) and a USA group (Tripathy et al) at the same time reported the SRGs formation resulted from the mass migration of the amorphous PAz film after interferometric irradiation with Ar ion laser at room temperature[29,30]. The key to this mass migration is that photoinduced isomerization of Az

molecules of nm scale convert to mass transport of micro-scale. From the interest of basic scientific perspective and expect for the photonics applications leading to rewritable holograms, optical data storage and microfabrication[36], SRGs studies are starting from the elucidation of mechanisms and extending to induction of mass migration in amorphous polymers[5,29,30,37–53], side-chain liquid crystalline polymers (SCLCPs)[7,54–60] and supramolecular systems[58,60–62], amorphous small-molecule materials[63], and inorganic materials[64–66]. Further SRGs formations in other photochromic molecules were also developed[67–69].

Ubukata, Seki et al. reported a highly efficient SRGs formation process by adding 5CB to azobenzene-infused polyvinyl alcohol. This system exhibits the light sensitivity with three orders of magnitude lower than that required for the earlier amorphous materials systems[54,55] (Fig. 1-3a). This highly efficient SRGs formation is explained by two factors: significant softening by LC-isotropic phase transition and acceleration of mass flow by viscosity reduction by soft doped 5CB. In addition, the function of SRGs structures have also been extended to optical applications such as recording media[36], patterns guides for block copolymer (Direct Self-assembly)[70,71], distributed feedback laser[72,73] and alignment of colloidal nanoparticle arrays[55].

1-3-2. Mechanism of SRGs formation in azobenzene polymer films

SRGs formations have been studied using a wide variety of materials, in parallel, many researches have been conducted to elucidate the mechanism of SRGs formation. So far, Various mechanistic models for mass transfer have been proposed: isomerization pressure due to volume change[40,41], gradient force[42–44], mean-field model[45], directed softening or fluidization[46–48], molecular diffusion[49–51], molecular orientation force[52,53] etc.

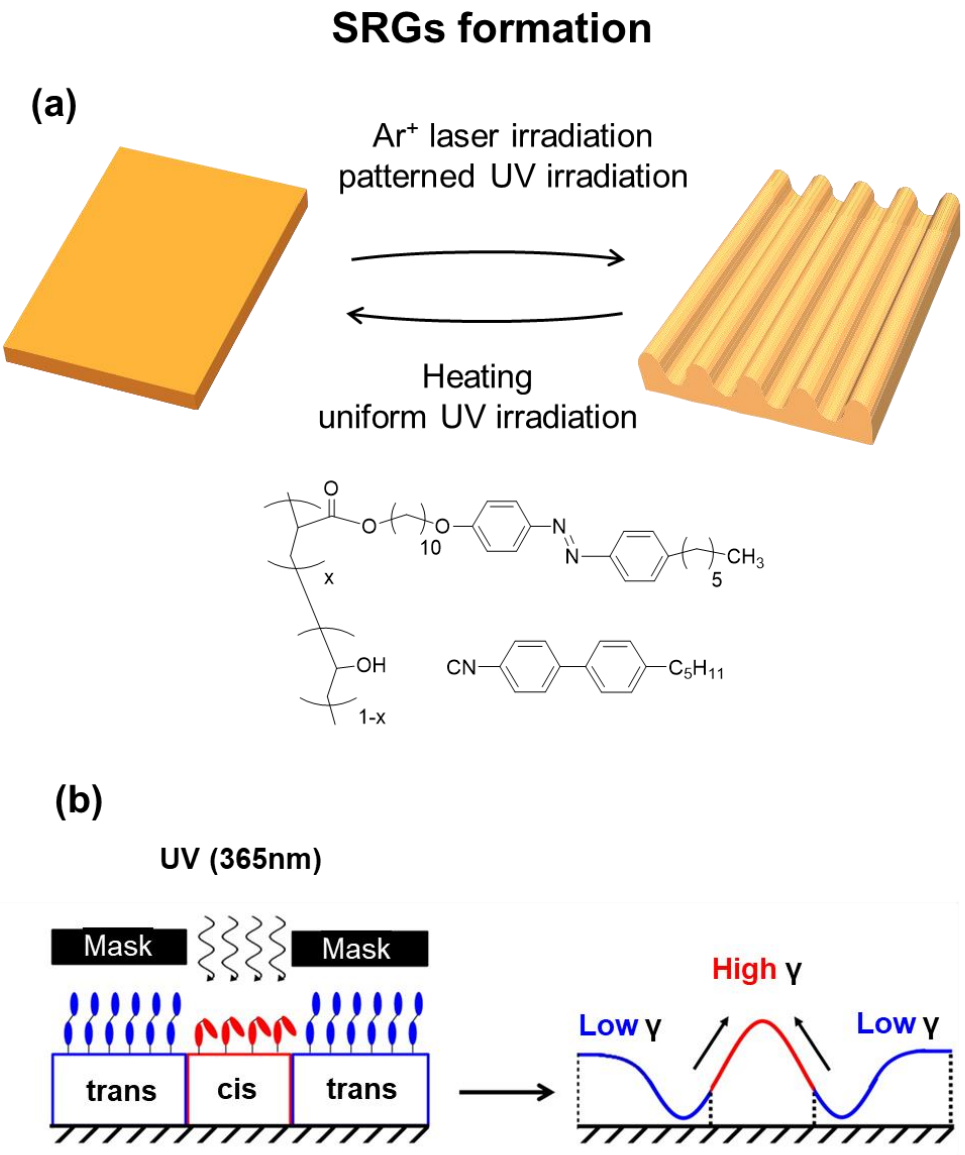

Figure 1-3. Efficient SRGs formation in LC Az polymer films (a). Explanation of SRGs mechanism by the Marangoni effect (b). Reproduced with permission from Ref 54 and 74.

However, a universal explanation on the mechanism has yet to be provided because each researcher have studied the SRGs formation with different Az polymers (amorphous type, LC type, low molecular wight type etc.) with different structures.

Recent studied have emphasized the importance of surface tension. Ellison et al. have proposed that SRGs are formed as a result of Marangoni flow by the surface tension difference of PAz film caused by photoirradiation[74] (Fig. 1-3b).Similar microfabrication were demonstrated by photochemical reactions in other photoresponsive polymer films[75–77]. The Marangoni effect is explained as a phenomenon of material flowing from a lower surface tension area toward a higher surface tension one driven by the surface tension gradient due to the temperature and concentration distributions. The details of the Marangoni effect are noted in the next section (1-4). After Ellison's paper in 2016, the number of reports referring the contribution of Marangoni effect to the SRGs formation is increasing and new interpretations are provided[78,79]. As mentioned above, even now after 25 years after first reports of SRGs, research field in the surface microfabrications resulted from mass migration in PAz materials is still under active discussion.

1-4. The Marangoni effect

When surface tension instability is occurred on the fluid surface, the flow is induced from areas of lower surface tension towards ones of higher surface tension (Fig. 1-4). This phenomenon of fluid flow driven by the surface tension difference is known as the Marangoni effect. A well-known example of the Marangoni effect is the "tear of wine" which describes wine droplet crawls along the inside of a wine glass. "Tear of wine" was firstly reported in 1855 by Thomson, but in 1871, Marangoni et al explained in detailed, then this mass motion driven by surface tension difference was named the Marangoni

effect[80]. The Marangoni effect has been studied in connection with many fields, including silicon crystal fabrication process[81], coating[82,83] inkjet printing[84] and colloidal particles[85] and liquid crystal molecular orientation[86] manipulation. In the coating process, slight contaminations existing in a material lead to substantial defects in applied paint. When a surface tension difference exists at the free surface of coating, flow motions are induced by the well-known Marangoni effect. For polymer film materials with a moderately high viscosity, this effect may deform the film surface, and then the deformed shape is fixed after solvent evaporation or vitrification by cooling. In general, such surface distortions and defects in polymer films are serious nuisances, preventing smooth film coatings. Examples can be found in crater formation during the painting process, striation defect generation in spincast films[87], and difficulties in droplet shape control in inkjet printing. On the other hand, useful manipulation of the Marangoni effect on polymer films have been reported by Singer's[88,89] and Elashnikov's[90] group. They demonstrated the heating induced Marangoni flow on the polymer film by focused laser beam irradiation. This mass motion is robust technique for the simple surface microfabrication of polymer films.

1-5. Surface effect on molecular orientation of block copolymer and SCLC polymer

The microphase separation (MPS) structure of block copolymer in the thin film is significantly different from that of the bulk properties due to the influence of the solvent annealing, surface free energy, period length of MPS and thickness of the film. Krausch et al. reported that the MPS structure of ABC block copolymers films on solid substrates were observed by AFM and showed a unique phase separation structure that depending on the film thickness which differs from the bulk one[91].

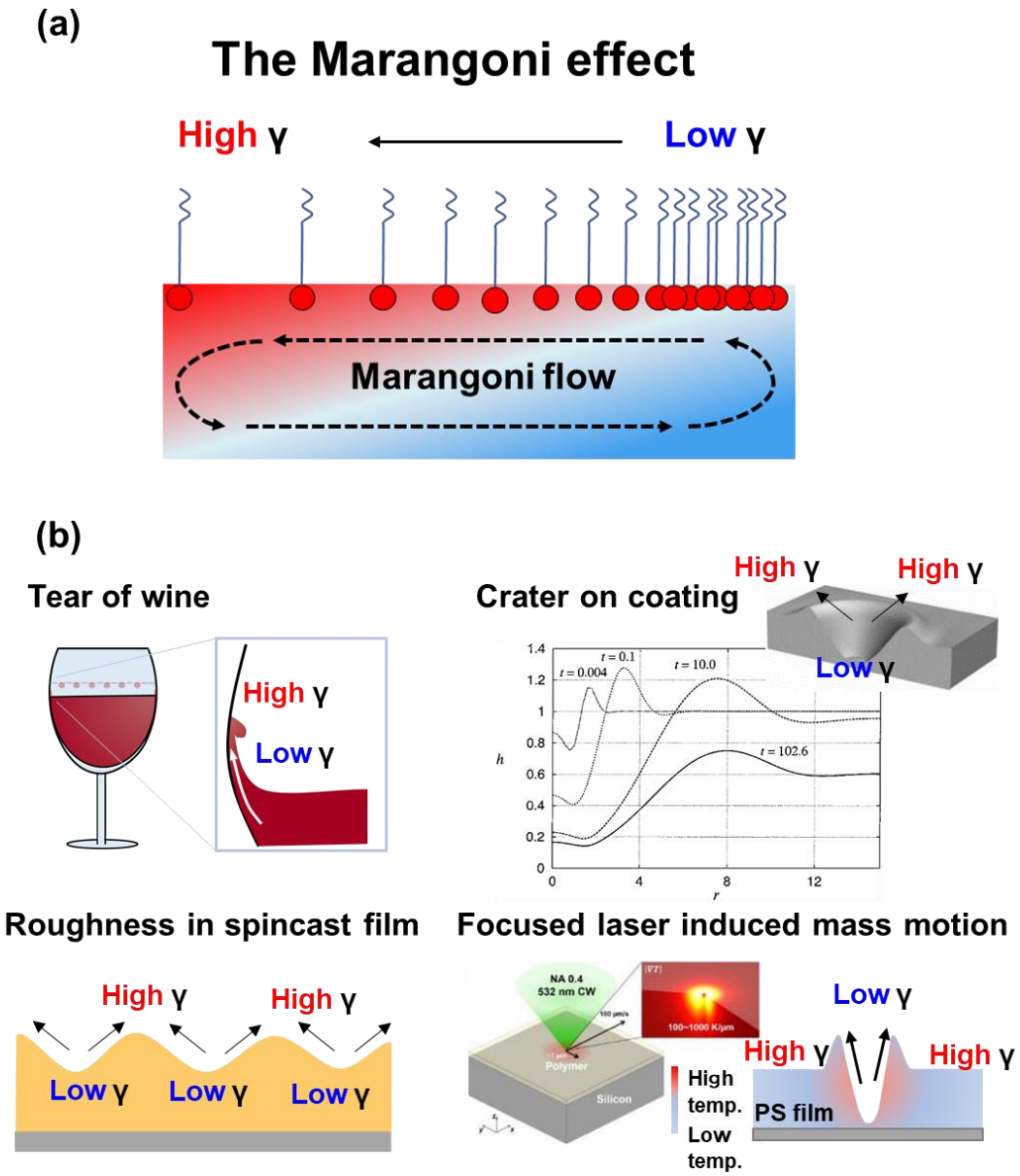

Figure 1-4. The Marangoni effect by concentration instability of surfactant on water (a). Various mass motion driven by the Marangoni effect (b). Reproduced with permission from Ref 82 and 89.

One of the features of MPS orientation is that it affected by the free surface and interfaces. Bate et al. demonstrated induction of vertically aligned lamellar MPS of diblock polymer by surface topcoating (Fig. 1-5a). This mechanism is explained that the top-coating polymer acts as a neutral layer for both block chains, resulting in a vertically aligned lamellar MPS structure[92]. This is the first example of how the orientation of the block copolymer is dominated by the free surface.

For simple and universal preparation of neutral layer for both block chains, Oh et al. reported cross linking system of the surface skin layer by plasma treatment(Fig. 1-5b). Cross-linked skin layer acts as a neutral layer for both block chains[93]. The simple strategy with 2 nm- thick surface cross-linked layer can extend to various kind of block copolymer for vertical alignment of MPS. After induction of vertically aligned MPS, surface cross-linked layer can be eliminated by quick etching process.

The strategy to control of orientation for π-conjugated polymer (polyalkyl thiophene, P3HT) by the free surface strategy has also been investigated by Tajima et.al. P3HT shows edge-on and face-on orientations in spincast film. On the other hand, the end-on alignment of P3HT is accomplished by induction of a small amount of fluorocarbon chains at the end of P3HT[94,95]. Fluorocarbon chains with low surface tension segregate to the film surface, leading vertical alignment of P3HT. This specific induced end-on alignment of P3HT gives a great contribution in design for effective carriers migration direction control for solar cell devices.

The effect of the free surface tailors to the molecular orientation of SCLCPs. In general, rod-shaped mesogens are oriented homeotropically at the air interface by the influence of exclusion volume effects between the mesogen and the flexible and low surface free energy alkyl tails. Therefore MPS with cylinder structure of block

copolymers containing side-chain liquid crystalline polymers is aligned in vertical orientation to the substrate[96,97].

Nagano and Sano et al. suggested the use of low surface energy amorphous block to induce LC planer orientation[98]. They adopted surface segregation of low surface energy amorphous block leading to formation of parallel intermaterial dividing surface of block copolymer, resulted LC planer orientation. Furthermore, Fukuhara et al. reported that the LC orientation inside the film is dominated by the orientation of the LC at the free surface prepared by surface segregation[24] of surface active SCLCP in blended film or inkjet printing[25,99] (Fig. 1-6). Further, photoresponsive SCLCP are provided in the free surface, allowing for the photoalignment and photo-switching in the entire film[24,25]. In the similar line, Kawatsuki et al. demonstrated LC photoalignment by the supramolecular LC system fabricated by inkjet printing and chemical vaper method[100–102].

Iyoda et al. developed horizontally aligned MPS of cylinder structure consisting of poly(ethyrene oxide) (PEO) and Az-containing block copolymer covered with poly(dimethyl siloxane) (PDMS)[97]. In this case, Az mesogen indicate planer alignment. Similar effect was observed in PEO-*b*-PAz block copolymer covered with poly(vinyl pyrrolidone) (PVP)[103]. The surface amorphous layer on the polymer film can be easily removed by solvent immersion, which is expected to facilitate its application to lithographic materials.

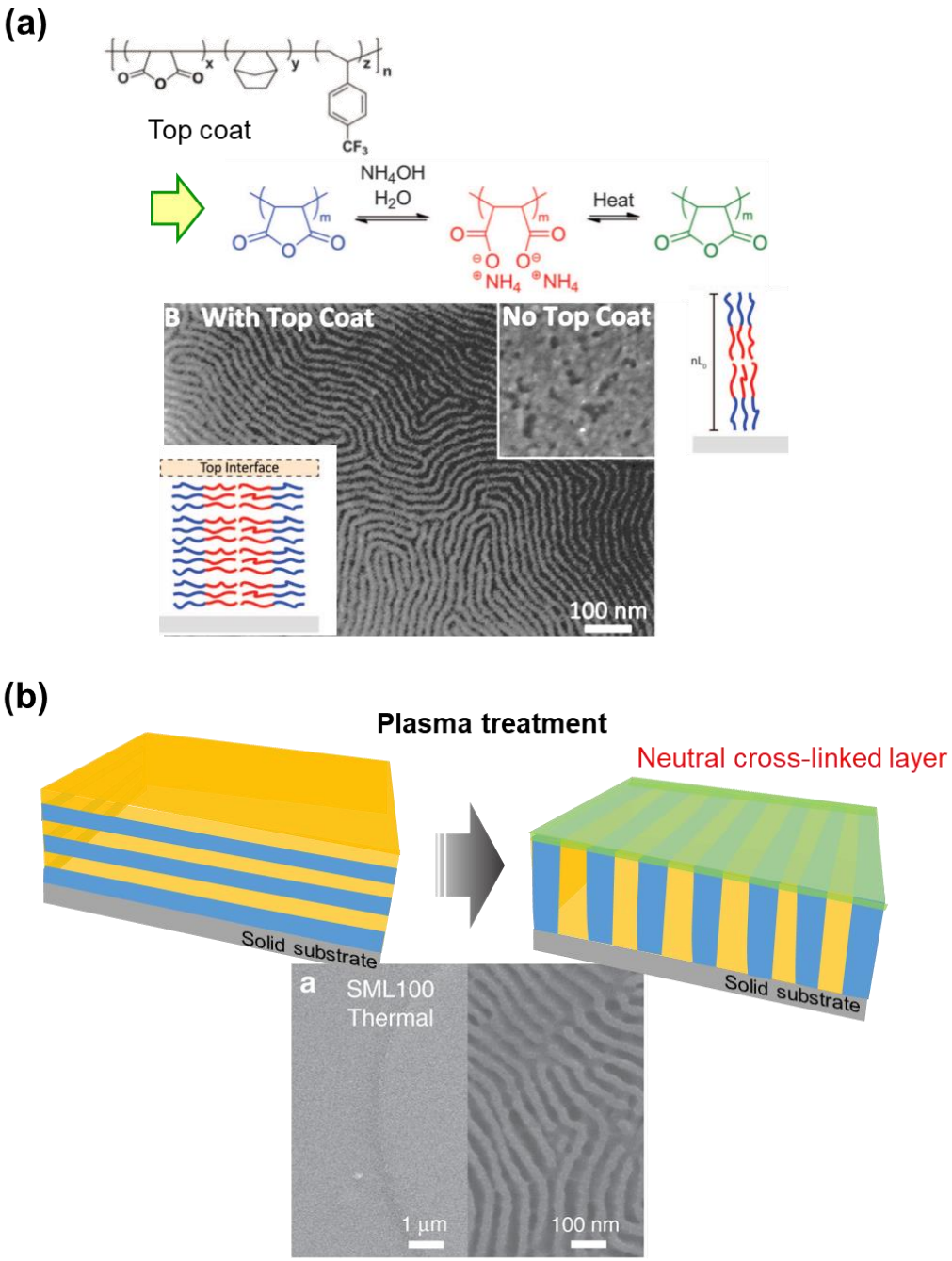

Figure 1-5. The orientation control of MPS structure of BCP by surface coating (a) and surface crosslinking by plasma treatment. Reproduced with permission from Ref 92 and 93.

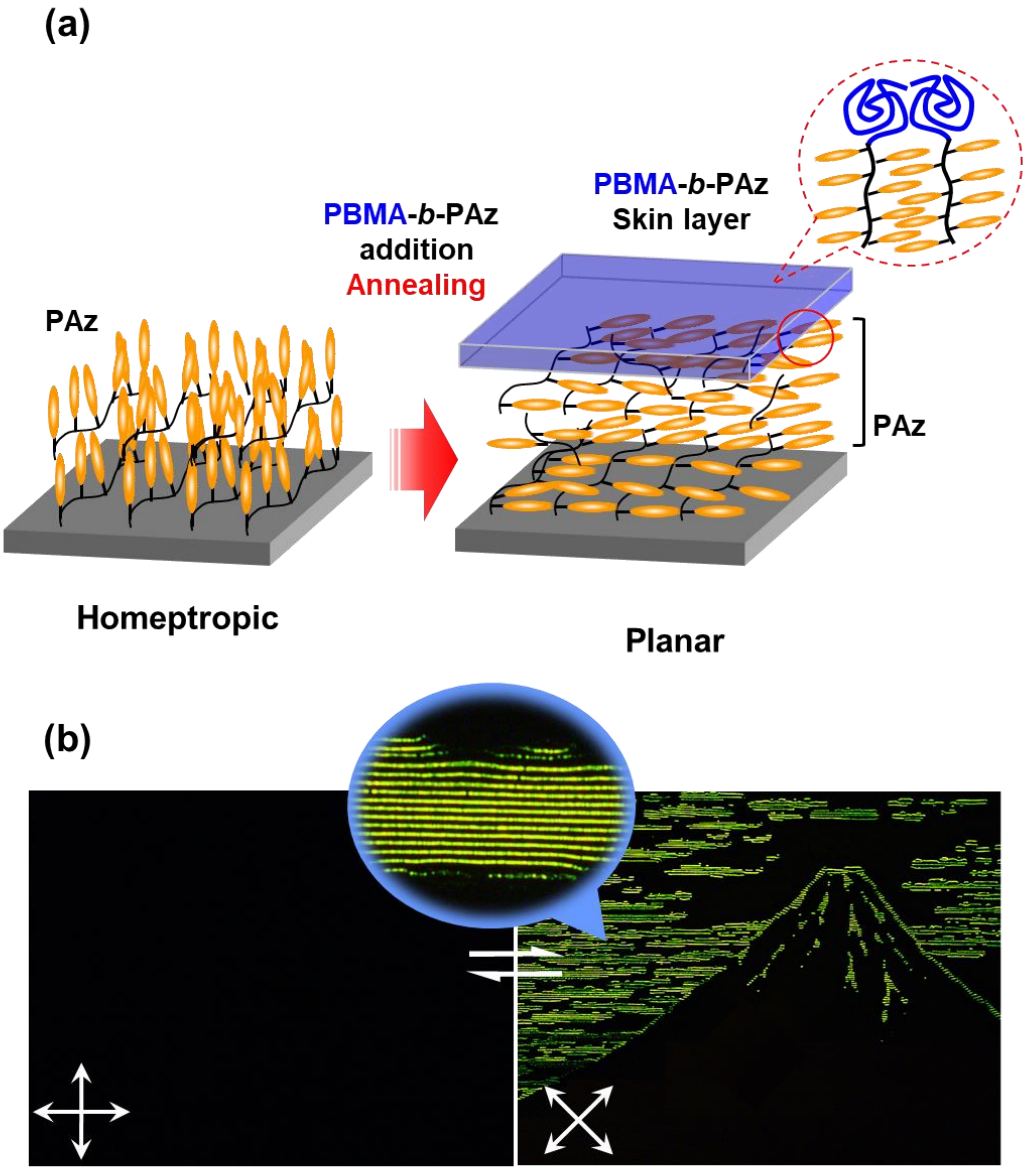

Figure 1-6. The LC alignment control by surface segregation of surface active amorphous block chains (a) and inkjet printing (b). Reproduced with permission from Ref 24 and 25.

1-6. Scope in This Thesis

1-6-1. Objectives

Studies on polymer surfaces and interfaces are essential to further enhance the wettability tuning, adhesion, friction, biocompatibility, and other functions of polymer surfaces. Conventional studies of polymer surfaces and interfaces are generally performed at two-dimensional interfaces, such as spin-coated films[104] on solid substrates and their laminations[105]. Previous studies have revealed that polymer surfaces exhibit different physical properties (e.g., glass transition temperature, crystallization, and orientation) than the inside of the films. It has been shown that the orientation of MPS of block copolymers and SCLCPs are influenced by free surface[24,92,93102,103]. Recently, it has been pointed out that the essential contribution of surface tension to the surface relief formation in PAz films[74]. The above knowledge inspired us to examine the role of topmost surface of polymer film for further development of polymer film functions.

This thesis focus on the super-inkjet printing allowing nano-scale three-dimensional polymer printing on thin polymer thin films, as a new approach to polymer surface and interface study. Then, based on the knowledge obtained from the explorations by inkjet printing, this thesis proposes a new guideline for the creation of novel functionalities originating from the polymer film surface.

1-6-2. Outline of This Thesis

This thesis is consisted of five chapters, from Chapter I to V.

In Chapter II, as a new direction for polymer surface and interface research, super-inkjet printing method on a photoresponsive SCLCP thin films is shown. Quick mass migration initiated from the inkjet patterns on the photoresponsive SCLCP thin films

is induced by photoirradiarion. This process can be named as the photoinduced Marangoni flow taking place from a low to a high surface tension region.

In Chapter III, patterned UV irradiation is conducted on a bilayered film composed of a photoresponsive Az SCLCP skin layer on non-photoreactive base SCLCP film. Mass transport of both of Az SCLCPs and non-photoreactive SCLCPs is induced by patterned UV irradiation. The surface tension difference caused by photoisomerization of Az induces the Marangoni flow, resulting in the SRGs formation. The importance of surface photo-responsiveness for photoinduced mass transfer in azobenzene polymer films is demonstrated. This shows an important and novel issue that SRGs are formed also for photo-inert polymer films.

In Chapter IV, the SRGs formation propagated from the photoresponsive top skin layer is applied to a widely used amorphous styrene polymer (PS). The tailored SRGs formation in PS film suggests the generalization of mass transfer driven from the topmost photoresponsive skin layer. Because the commercially available polymer films can be used, great potential for applications is suggested toward recording media and optical materials such as diffraction gratings and liquid crystal alignment films.

Finally, this thesis is summarized, and the future outlook is provided in Chapter V.

References

[1] H. M. D. Bandara, S. C. Burdette, *Chem. Soc. Rev*. **2012**, 41, 1809–1825.

[2] G. S. Hartley, *Nature* **1937**, 14, 281.

[3] G. S. Hartley, *J. Chem. Soc.* **1938**, 633-642.

[4] M. Irie, Y. Hirano, S. Hashimoto, K. Hayashi, *Macromolecules* **1981**, 14,262-

267.

[5] A. Natansohn, P. Rochon, *Chem. Rev*. **2002**, 102, 4139–4175.

[6] T. Seki, J. Mater. Chem. C. 2016, 4, 7895–7910.

[7] T. Seki, *Macromol. Rapid Commun*. **2014**, 35, 271–290.

[8] T. Seki, *Bull. Chem. Soc. Jpn*. **2018**, 91, 1026–1057.

[9] T. Seki, S. Nagano, M. Hara, *Polymer* **2013**, 22, 6053–6072.

[10] K. Ichimura, *Chem. Rev*. **2000**, 100, 1847–1873.

[11] H. K. Bisoyi, Q. Li, *Chem. Rev*. **2016**, 116, 15089–15166.

[12] D. Dattler, G. Fuks, J. Heiser, E. Moulin, A. Perrot, X. Yao, N. Giuseppone, *Chem. Rev*. **2020,** 120, 310–433.

[13] S. L. Oscurato, M. Salvatore, P. Maddalena, A. Ambrosio, A. *Nanophotonics* **2018**, 7, 1387–1422.

[14] T. Ikeda, *J. Mater. Chem.* **2003**, 13, 2037–2057.

[15] H. Yu, *J. Mater. Chem. C*. **2014,** 2, 3047–3054.

[16] T. J. White, D. J. Broer, *Nat. Mater*. **2015**, 14, 1087–1098.

[17] X. Pang, J. Lv, C. Zhu, L. Qin, Y. Yu, *Adv. Mater*. **2019**. 31, 1904224.

[18] M. Han, S. Morino, K. Ichimura, *Macromolecules*, **2000**, 33, 6360-6371.

[19] M. Eich, J. Wendorff, . *J. Makromol. Chem*. **1987**, 8, 467–471.

[20] M. Eich, J. Wendorff, B. Reck, H. Ringsdorf, *J. Makromol. Chem*. **1987**, 8, 59–63.

[21] K. Ichimura, Y. Suzuki, T. Seki, A. Hosoki, K. Aoki,. *Langmuir* **1988**, 4, 1214–1216.

[22] T. Seki, M. Sakuragi, Y. Kawanishi, Y. Suzuki, T. Tamaki, R. Fukuda, K. Ichimura, *Langmuir* **1993**, 9, 211–218.

[23] S. Nagano, *Langmuir* **2019**, 35, 5673–5683.

[24] K. Fukuhara, Y. Fujii, Y. Nagashima, M. Hara, S. Nagano, T. Seki, *Angew. Chem. Int. Ed*. **2013**, 52, 5988–5991.

[25] K. Fukuhara, S. Nagano, M. Hara, T. Seki, *Nat. Commun.* **2014**, 5, 3320.

[26] T. Nakai, D. Tanaka, M. Hara, S. Nagano, T. Seki, *Langmuir* **2016**, 32, 909–914.

[27] T. Seki, T. Tamaki, *Chem. Lett.* **1993**, 22, 1739–1742.

[28] O. M. Tanchak, C. J. Barrett, *Macromolecules* **2005**, 38, 10566–10570.

[29] P. Rochon, E. Batalla, A. Natansohn, *Appl. Phys. Lett.* **1995**, 66, 136-138.

[30] D. Y. Kim, S. K. Tripathy, L. Li, J. Kumar, *Appl. Phys. Lett.* **1995**, 66, 1166-1168.

[31] Y. Yu, M. Nakano, T. Ikeda, *Nature* **2003**, 425, 145.

[32] T. Ikeda, M. Nakano, Y. Yu, O. Tsutsumi, A. Kanazawa, *Adv. Mater.* **2003**, 15, 201–205.

[33] M. Kondo, Y. Yu, T. Ikeda, T. *Angew. Chem. Int. Ed*. **2006**, 45, 1378–1382.

[34] M. Yamada, M. Kondo, J. Mamiya, J. Y. Yu, M. Kinoshita, C. J. Barrett, T. Ikeda, *Angew. Chem. Int. Ed.* **2008**, 120, 5064–5066.

[35] M. Yamada, M. Kondo, R. Miyasato, Y. Naka, J. Mamiya, M. Kinoshita, A. Shishido, Y. Yu, C. J. Barrett, T. Ikeda, *J. Mater. Chem.* **2009**, 19, 60–62.

[36] E. Ishow, A. Brosseau, G. Clavier, K. Nakatani, R. B. Pansu, J. J. Vachon, P. Tauc, D. Chauvat, C. R. Mendonça, E. Piovesan, *J. Am. Chem. Soc.* **2007**, 129, 8970–8971.

[37] N. K. Viswanathan, D. Y. Kim, S. Bian, J. Williams, W. Liu, L. Li, L. Samuelson, J. Kumar, S. K. Tripathy, *J. Mater. Chem.* **1999**, 9, 1941–1955.

[38] K. G. Yager, C. J. Barrett, *Curr. Opin. Solid State Mater. Sci*. **2001**, 5, 487–494.

[39] Y K. G. Yager, C. J. Barrett, *J. Photochem. Photobiol. A* **2006**, 182, 250–261.

[40] C. J. Barrett, A. Natansohn, P. L. Rochon, *J. Phys. Chem.* **1996**, 100, 8836–8842.

[41] C. J. Barrett, P. L. Rochon, A. Natansohn, *J. Chem. Phys.* **1998**, 109, 1505–1516.

[42] J. Kumar, L. Li, X. L. Jiang, D. Y. Kim, T. S. Lee, S. Tripathy, *Appl. Phys. Lett*. **1998**, 72, 2096–2098.

[43] O. Baldus, S. J. Zilker, *Appl. Phys. B: Laser Opt*. **2001**, 72, 425–427.

[44] K. Sumaru, T. Fukuda, T. Kimura, H. Matsuda, T. Yamanaka, *J. Appl. Phys*. **2002**, 91, 3421–3430.

[45] T. G. Pedersen, P. M. Johansen, N. C. R. Holme, P. S. Ramanujam, S. Hvilsted, *Phys. Rev. Lett*. **1998**, 80, 89–92.

[46] P. Karageorgiev, D. Neher, B. Schulz, B. Stiller, U. Pietsch, M. Giersig, L. Brehmer, *Nat. Mater.* **2005**, 4, 699–703.

[47] S. Lee, H. S. Kang, J. K. Park, *Adv. Mater.* **2012**, 24, 2069–2103.

[48] N. Hurduc, B. C. Donose, A. Macovei, C. Paius, C. Ibanescu, D. Scutaru, M. Hamel, N. Branza-Nichita, L. Rocha, *Soft Matter* **2014**, 10, 4640–4647.

[49] N. Mechau, D. Neher, V. Börger, H. Menzel, K. Urayama, *Appl. Phys. Lett*. **2003**, 81, 4715–4717.

[50] A. Ambrosio, L. Marrucci, F. Borbone, A. Roviello, P. Maddalena, *Nat. Commun*. **2012**, 3, 989.

[51] A. Ambrosio, P. Maddalena, L. Marrucci, *Phys. Rev. Lett.* **2013**, 110, 146102.

[52] M. Saphiannikova, V. Toshchevikov, *J. Soc. Inf. Disp*. **2015**, 23, 146–153.

[53] V. Toshchevikov, J. Ilnytskyi, M. Saphiannikova, *J. Phys. Chem. Lett.* **2017**, 8, 1094–1098.

[54] T. Ubukata, T. Seki, K. Ichimura, *Adv. Mater.* **2000**, 12, 1675–1678.

[55] T. Ubukata, M. Hara, K. Ichimura, T. Seki, *Adv. Mater.* **2004**, 16, 220–223.

[56] N. Zettsu, T. Fukuda, H. Matsuda, T. Seki, *Appl. Phys. Lett*. **2003**, 83, 4960–

4962.

[57] N. Zettsu, T. Ogasawara, R. Arakawa, S. Nagano, T. Ubukata, T. Seki,. *Macromolecules* **2007**, 40, 4607–4613.

[58] N. Zettsu, T. Ogasawara, N. Mizoshita, S. Nagano, T. Seki, *Adv. Mater.* **2008**, 20, 516–521.

[59] J. Isayama, S. Nagano, T. Seki, *Macromolecules* **2010**, 43, 4105–4112.

[60] J. Gao, Y. He, F. Liu, X. Zhang, Z. Wang, X. Wang, *Chem. Mater*. **2007**, 19, 3877–3881.

[61] S. Mitsui, S. Nagano, M. Hara, T. Seki, *Crystals* **2017**, 7, 52.

[62] J. E. Koskela, J. Vapaavuori, R. H. A. Ras, A. Priimagi, *ACS Macro Lett*. **2014**, 3, 1196–1200.

[63] H. Nakano, T. Takahashi, T. Kadota, Y. Shirota, *Adv. Mater.* **2002**, 14, 1157–1160.

[64] O. Kulikovska, L. M. Goldenberg, L. Kulikovsky, J. Stumpe, *Chem. Mater*. **2008**, 20, 3528–3534.

[65] K. Nishizawa, S. Nagano, T. Seki, *J. Mater. Chem*. **2009,** 19, 7191–7194.

[66] K. Nishizawa, S. Nagano, T. Seki, *Chem. Mater*. **2009**, 21, 2624–2631.

[67] T. Ubukata, Y. Moriya, Y. Yokoyama, *Polym. J*. **2012**, 44, 966–972.

[68] T. Ubukata, M. Nakayama, T. Sonoda, Y. Yokoyama, H. Kihara, *ACS Appl. Mater. interfaces* **2016**, 8, 21974–21978.

[69] A. Kikuchi, Y. Harada, M. Yagi, T. Ubukata, Y. Yokoyama, J. Abe, *Chem. Commun*. **2010**, 46, 2262–2264.

[70] Y. Morikawa, T. Kondo, S. Nagano, T. Seki, *Chem. Mater.* **2007**, 19, 1540–1542.

[71] K. Aissou, J. Shaver, G. Fleury, G. Pécastaings, C. Brochon, C. Navarro, S. Grauby, J-M. Rampnoux, S. Dilhaire, G. Hadziioannou, *Adv. Mater*. **2013**, 25, 213–217.

[72] T. Ubukata, T. Isoshima, M. Hara, *Adv. Mater*. **2005**, 17, 1630–1633.

[73] L. M. Goldenberg, V. Lisinetskii, Y. Gritsai, J. Stumpe, S. Schrader, *Adv. Mater.* **2012,** 24, 3339–3343.

[74] C. B. Kim, J. C. Wistrom, H. Ha, S. X. Zhou, R. Katsumata, A. R. Jones, D. W. Janes, K. M. Miller, C. J. Ellison, *Macromolecules* **2016**, 49, 7069–7076.

[75] J. M. Katzenstein, D. W. Janes, J. D. Cushen, N. B. Hira, D. L. McGuffin, N. A. Prisco, C. J. Ellison, *ACS Macro Lett.* **2012**, 1, 1150–1154.

[76] T. A. Arshad, C. B. Kim, N. A. Prisco, J. M. Katzenstein, D. W. Janes, R. T. Bonnecaze, C. J. Ellison, *Soft Matter* **2014**, 10, 8043–8050.

[77] A. R. Jones, C. B. Kim, S. X. Zhou, H. Ha, R. Katsumata, G. Blachut, R. T. Bonnecaze, C. J. Ellison, *Macromolecules* **2017**, 50, 4588–4596.

[78] A. Bobrovsky, K. Mochalov, D. Solovyeva, V. Shibaev, M. Cigl, V. Hamplová, A. Bubnov, *Soft Matter* **2020**, 16, 5398–5405.

[79] A. Miniewicz, A. Sobolewska, W. Piotrowski, P. Karpinski, S. Bartkiewicz, E. Schab-Balcerzak, *Materials* **2020**, 13, 2464.

[80] L. E. Scriven, C. V. Sternling, *Nature* **1960**, 187, 186–188.

[81] B. J. Keene, *Surf. Interface Anal.* **1987**, 10 , 367-383.

[82] P. L. Evans, L. W. Schwartz, R. V. Roy, *J. Coll. Interf. Sci.* **2000**, 227, 191–205.

[83] L. O. Kornum, H. K. R. Nielsen, *Prog. Org. Coat.* **1980**, 8, 275-324.

[84] T. Kajiya, W. Kobayashi, T. Okuzono, M. Doi, *J. Phys. Chem. B* **2009**, 113, 15460-15466.

[85] M. Anyfantakis, S. N. Varanakkottu, S. Rudiuk, M. Morel, D. Baigl, *ACS Appl. Mater. interfaces* **2017**, 9, 37435–37445.

[86] M. Tsuei, M. Shivrayan, Y.-K. Kim, S. Thayumanavan, N. L. Abbott, *J. Am.*

Chem. Soc. **2020**, 142, 6139-6148.

[87] D.P. Birnie, *Langmuir* **2013**, 29, 9072-9078 (2013).

[88] J. P. Singer, P.-T. Lin, S. E. Kooi, L. C. Kimerling, J. Michel, E. L. Thomas, *Adv. Mater.* **2013**, 25, 6100–6105.

[89] J. P. Singer, S. E. Kooi, E. L. Thomas, *J. Polym. Sci., Part B: Polym. Phys*. **2016, 54,** 225–236.

[90] R. Elashnikov, P. Fitl, V. Svorcik, O. Lyutakov, *Appl. Surf. Sci.* **2017**, 394, 562–568.

[91] A. Knoll, A. Horvat, K. S. Lyakhova, G. Krausch, G. J. A. Sevink, A. V. Zvelindovsky, R. Magerle, *Phys. Rev. Lett*. **2002**, 89, 355011–355014.

[92] C. M. Bates, T. Seshimo, M. J. Maher, W. J. Durand, J. D. Cushen, L. M. Dean, G. Blachut, C. J. Ellison, C. G. Willson, *Science* **2012**, 338, 775–779.

[93] J. Oh, H. S. Suh, Y. Ko, Y. Nah, J. C. Lee, B. Yeom, K. Char, C. A. Ross, J. G. Son, *Nat. Commun*. **2019**, 10, 2912.

[94] Q. Wei, K. Tajima, Y. Tong, S. Ye, K. Hashimoto, *J. Am. Chem. Soc.* **2009**, 131, 17597–17604.

[95] J. Ma, K. Hashimoto, T. Koganezawa, K. Tajima, *J. Am. Chem. Soc.* **2013**, 135, 9644–9647.

[96] Y. Morikawa, S. Nagano, K. Watanabe, K. Kamata, T. Iyoda, T. Seki, *Adv. Mater.* **2006**, 18, 883–886.

[97] M. Komura, A. Yoshitake, H. Komiyama, T. Iyoda, *Macromolecules* **2015**, 48, 672–678.

[98] S. Nagano, Y. Koizuka, T. Murase, M. Sano, Y. Shinohara, Y. Amemiya, T. Seki, *Angew. Chem. Int. Ed.* **2012**, 51, 5884–5888.

[99] D. Tanaka, Y. Nagashima, M. Hara, S. Nagano, T. Seki, *Langmuir* **2015**, 31, 11379–11383.

[100] N. Kawatsuki, K. Miyake, M. Kondo, *ACS Macro Lett.* **2015**, 4, 764–768.

[101] K. Miyake, H. Ikoma, M. Okada, S. Matsui, M. Kondo, N. Kawatsuki, *ACS Macro Lett*. **2016**, 5, 761–765.

[102] N. Kawatsuki, R. Fujii, Y. Fujioka, S. Minami, M. Kondo, *Langmuir* **2017**, 33, 2427–2432.

[103] H-L. Xie, X. Li, H. S. Suh, J-X. Ren, L. S. Wan, G. S. W. Craig, C. G. Arges, P. F. Nealey, *J. Polym. Sci., Part B: Polym. Phys*. **2017**, 55, 1569–1574.

[104] B. Frank, A. P. Gast, T. P. Russell, H. R. Brown, C. Hawker, *Macromolecules*. **1996**, 29, 6531-6534.

[105] D. Kawaguchi, Y. Ohta, A. Takano, Y. Matsushita, *Macromolecules*. **2012**, 45, 6748-6752.

Chapter II

Photoinitiated Marangoni flow morphing in a liquid crystalline polymer film directed by super-inkjet printing patterns

2-1. Introduction

The free surface plays an important role in the motions of fluid materials. When a surface tension difference exists at the free surface, flow motions are induced, widely known as Marangoni effect[1]. Such flow progression are ubiquitous in nature, and can be seen in everyday life[1,2]. For polymer film materials with a moderately high viscosity[3], this effect may deform the film surface, and then the deformed shape is fixed after solvent evaporation or vitrification by cooling. In general, such surface distortions and defects in polymer films are serious nuisances, preventing smooth film coatings. Examples can be found in crater formation during the painting process[4–6], striation defect generation in spincast films[7], and difficulties in droplet shape control in inkjet printing[8–11].

If the flow-induced deformation of polymer surfaces can be controlled as designed, this will provide a powerful tool for surface microfabrication. In this regard, Ellison et al.[12–16] have proposed the pioneering concept of arbitrary inscription of polymer surfaces based on the Marangoni flow via photopatterning on the free surface. A melt-flow is induced according to photopatterns upon annealing above the glass transition temperature (T_g) of the base polymer. Singer et al.[17,18] have studied a focused laser-induced Marangoni de-wetting for amorphous polymer films, and Elashnikov et al.[19] have demonstrated a laser-heating-directed Marangoni flow on a dye-doped poly(ethyl methacrylate) film. Along the same line, Ubukata et al.[20] have also observed a relevant mass transfer phenomenon of an amorphous film, which is discussed from a different

viewpoint of material diffusion affected by photochemical crosslinking.

This chapter demonstrates a new free surface-mediated optical effect exhibiting large and instantaneous surface morphing directed by super fine-inkjet printing patterns in a photoresponsive side chain liquid crystalline polymer (SCLCP) film. The mass migration motion due to the Marangoni flow was initiated by a photoinduced phase transition[21] in an azobenzene-containing SCLCP film printed using low surface tension polymer ink. The resulting surface morphology was obtained as a dip in the center and embossments in the periphery regions, a characteristic feature of crater formation by contaminations in paint. The superfine inkjet-printing drawing provides spatially designed micrometer-scaled heterointerfaces without damages to the surface of the base polymer film. The volume of transferred polymer reaches a level of a hundred times that of printed polymer ink. In this sense, the printed ink pattern on the surface works as a latent image, and UV irradiation corresponds to a dry development process, leading to the surface microfabrication.

2-2. Experimental

2-2-1. Materials and polymer synthesis

Azobenzene-containing SCLCP poly[4′-10-(methacryloyloxy)decyloxy-4-(heptylpheynylazo)phenyl] (PAz, Fig. 2-1)[22], Poly(butyl methacrylate) (PBMA Fig. 2-1)[22], Poly(butyl methacrylate)-*block*-PAz (PBMA-*b*-PAz, Fig. 2-1)[23], cyanobiphenyl containing SCLCP poly{4′-[6-(methacryloyloxy)hexyloxy]-4-cyanobiphenyl)} (PCBMA, Fig. 2-1)[24,25] and poly(dimethylsiloxane)-*block*-PAz (PDMS-*b*-PAz, Fig. 2-1)[26] were synthesized by the atom transfer radical polymerization (ATRP) method according to the previous papers. Chemical structures of all polymers used in this study are

displayed in Fig. 2-1 and the characterization data are listed in Table 2-1.

2-2-2. Film preparation

PAz films were prepared by spin coating (2000 rpm, 60 s) (Mikasa, Japan) from toluene solutions (typically 7.0 wt% in toluene) onto clean quartz substrate (typical film thickness: approximately 350 nm).

2-2-3. Inkjet printing

The inkjet printing of PBMA, PBMA-*b*-PAz, PCBMA and PDMS-*b*-PAz ink onto PAz film was performed using a subfemto-liter inkjet printing apparatus (SIJ Technology Inc.,Japan) as shown in Fig. 2-2. The arbitrary drawing was achieved as programmed in a computer. Typically, inkjet printing was achieved by applying a 30-50 Hz square wave form of 250-350 V amplitude. The nozzle speed was 0.01-0.03 mm s^{-1}. The polymer ink solutions were prepared with 0.5 wt% of polymer in mixed solvent of o-dichlorobenzene and N-methyl-2-pyrrolidone (30:1 by volume). In the conditions employed, the solvent was nearly evaporated during the flight from the inkjet nozzle to the PAz film surface, suggesting that the solvent hardly disrupted the PAz film surface.

2-2-4. Light irradiation

UV light irradiation (365 nm) was performed with an Hg-Xe lamp (UV supercure 203s, Sanei Electronic Co., Japan) at 0.25-10 mW cm^{-2}, exposing the inkjet-printed PAz surface at a controlled temperature. The 365 nm and 436 nm lines were selected by passing through combinations of glass filters of UV-35/UV35D (Toshiba) and 3–73 and 6–67 (Corning), respectively. The schematic illustration of inkjet printing and UV-

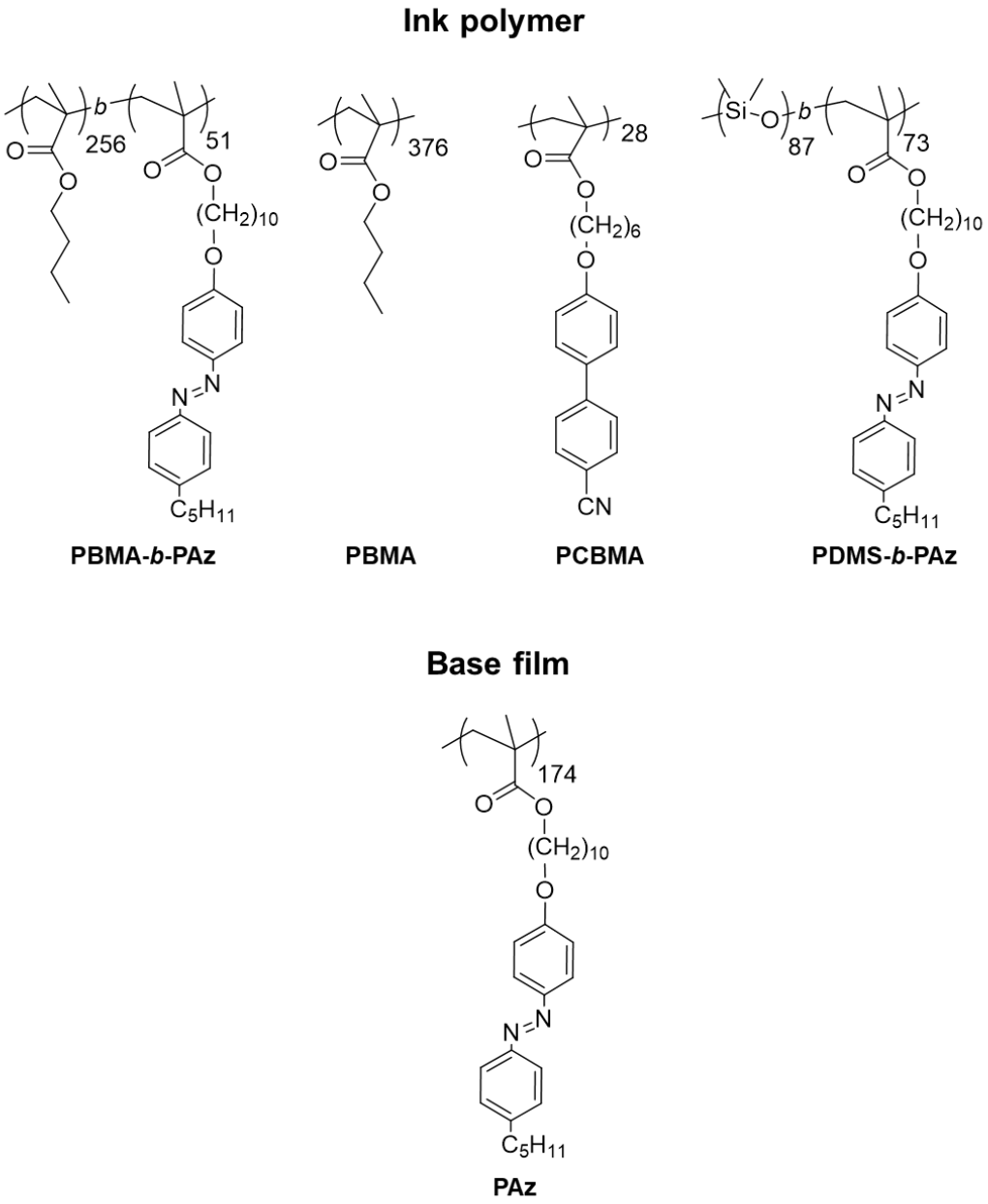

Figure 2-1. Chemical structures of polymers used in this study.

Table 2-1. Characterizations of the polymers used in this study.

Polymer	M_n (M_w/M_n)	Degree of polymerization	Thermophysical Properties / ° C	Contact angle of glycerol (θ_{gly}) / deg		
				25 ° C	90 ° C	130 ° C
PAz	8.6×10^4 (1.54)	174	g (55) sm C (87) sm A (116) iso	102.5 ± 0.9	103.2 ± 0.7	93.3 ± 1.8
PAz (UV)				89.1 ± 1.8	85.1 ± 1.6	83.7 ± 1.5
PBMA-*b*-PAz	5.4×10^4 (1.10)	256 (PBMA), 51 (PAz)	g (54) sm C (83) sm A (115) iso	93.3 ± 1.0	102.0 ± 1.1	101.0 ± 2.5
PBMA	5.3×10^4 (1.16)	376	g (ca.20)	93.0 ± 0.8	101.0 ± 1.1	100.7 ± 1.5
PCBMA	1.0×10^4 (1.13)	28	g (53) sm A (115) iso	84.9 ± 1.2	84.2 ± 1.0	80.3 ± 1.4
PDMS-*b*-PAz	5.6×10^4 (1.20)	87 (PDMS), 73 (PAz)	g (53) sm C (81) sm A (112) iso	110.0 ± 0.7	116.7 ± 1.1	102.6 ± 1.8

PAz (UV): under UV light irradiation, g: glass, Sm: smectic, iso: isotropic

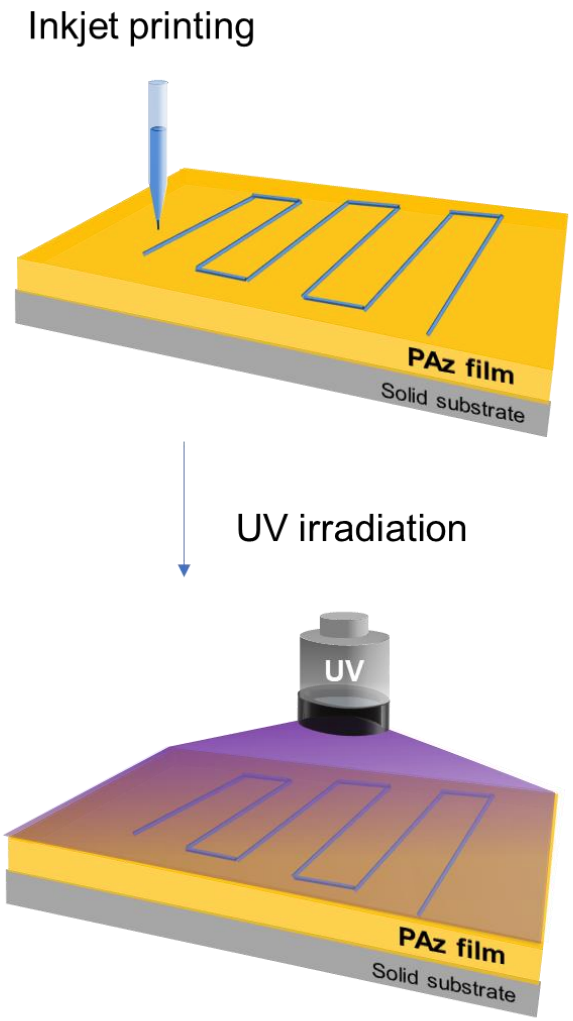

Figure 2-2. Schematic of procedure adopted in this work.

irradiation process is demonstrated in Fig. 2-2.

2-2-5. Measurement

The Molecular weight and the molecular weight distribution were measured by gel permeation chromatography or high-performance liquid chromatography (Showa Denko K. K., Japan).

The liquid crystal transition temperatures and glass transition temperatures were evaluated by DSC (TA Instrument Q200, USA) and a polarized optical microscope (BX-51, Olympus Corp., Japan).

The film thicknesses were measured with a white-light interferometric microscope (WLIM, BE-S501, Nikon Corp., Japan).

The static contact angles of glycerol and water on the polymer films were obtained using a CA-XP (Kyowa Interface Science Co. Ltd., Japan) at various temperatures.

The UV-Vis absorption spectral measurement was performed via UV/Vis absorption spectroscopy (Agilent 8453 spectrometer, Agilent Technologies, USA). The real time UV-Vis absorption spectral measurement was performed using UV/Vis absorption spectroscopy (QE6500/DH-200-BAL, Ocean Optics, Japan) and light source (REX-250, Asahi Spectra, Japan). The content of cis-azobenzene (M(t)) in the photostational state after irradiation with 365 nm and 436 nm light was determined spectroscopically by comparing absorbances at 370 nm (A_{370}) and at 308 nm (A_{308}) (isosbetic point) followed by the below equation[27], where a is a numerical constant.

$$M(t) = 1 - a(A(t)_{370}/A(t)_{308})$$

Steady flow viscosity measurements of the PAz polymer were performed at

controlled temperatures using a MCR-301 rotatinal rheometer (Anton Paar GmbH, Austria) with corn-plate of 3.0 cm diameter. The viscosity measurements (share rate: 0.01-100 s^{-1}) under UV irradiation were achieved by introducing the light with an optical fiber to the rear side of the plate.

The morphological changes were observed by WLIM (BE-S501, Nikon, Japan) or AFM (MFP-3D, Asylum Research, UK). AFM imaging was performed in repulsive region by using an Al-coated cantilever (OMCL-AC240TS, Olympis, Japan).

The real time morphological change observations were performed by an optical microscope (BX-51, Olympus Corp., Japan) equipped with a light irradiation apparatus.

Surface analysis of time of flight secondary ion of mass spectroscopy (ToF-SIMS) were performed with a PHI TRIFT V nano TOF (ULVAC-PHI Inc., Japan) at Aichi Center for Industry and Science Technology in Toyota city. In this measurement, the 30 kV Bi^{3+} primary ion beam (100 nm diameter) under vacuum irradiated an area of 150 × 150 μm and 500 ×500 μm with pixel resolution of 256 × 256.

2-3. Results and discussions

2-3-1. Contact angle measurement

The contact angles of a glycerol droplet (θ_{gly}) (γ_{gly} = 63 mN m^{-1} at 25 °C) are summarized in Table 2-1 for the measure of surface tension of the polymer film surface. Glycerol was used based on the requirement of high temperature measurements at approximately 100 °C. The contact angles of a water droplet (γ_w = 72 mN m^{-1} at 25 °C) on these polymer films at 25 °C are indicated in Fig. 2-3a for reference. The static contact angles of a glycerol droplet (θ_{gly}) on the film surfaces of PAz and PBMA-*b*-PAz under UV-light irradiation at 90 °C were 85 ± 1.5° and 102 ± 1.1°, respectively (Table 2-1),

(a)

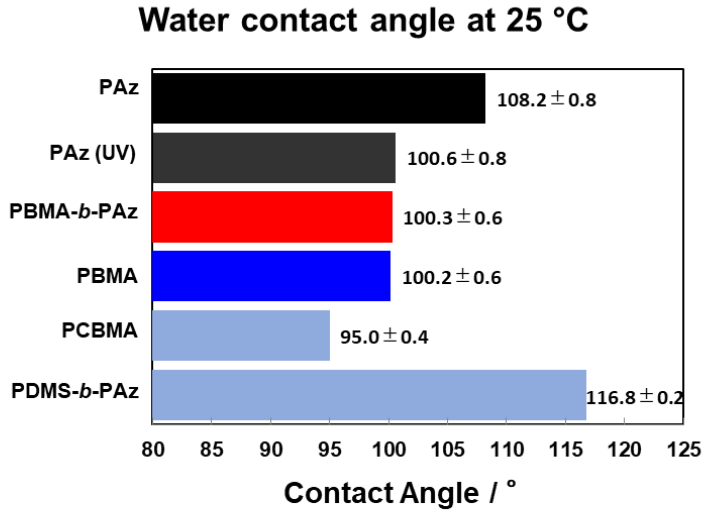

(b)

Droplet	γ / mN · m^{-1}	b.p. / °C
Glycerol	63.4	290

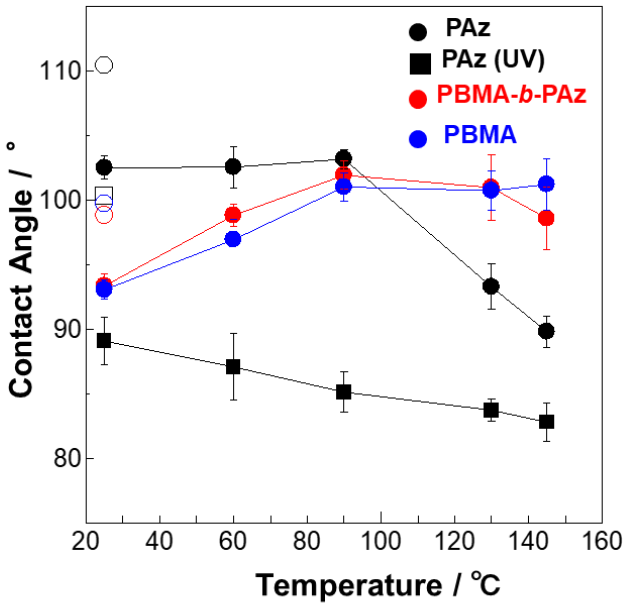

Figure 2-3. Contact angle measurements. (a) The contact angle of a water droplet on various polymer film surface. (b) The contact angle of glycerol (θ_{gly}) on polymers at various temperatures.

indicating that the surface tension of the PAz surface was larger than that of PBMA-*b*-PAz. Thus, the migration direction occurred from lower to higher surface tension regions. In Fig. 2-3b, the θ_{gly} values at various temperatures under UV irradiation are indicated. At all temperatures, θ_{gly} on cis-isomerized PAz was smaller than that of PBMA-*b*-PAz.

2-3-2. Photoinitiated mass migration

The dot of PBMA-*b*-PAz ink was deposited onto PAz film of 350 nm thickness using an inkjet apparatus. The dimensions of the dot were 5 μm in diameter and 100 nm in height. When the dot (Fig. 2-4, left) was irradiated with UV light at 365 nm at 60 °C, a mass transfer occurred form a crater toward periphery (Fig. 2-4, right). Such a dip formation surrounded by a rim is a characteristic of crater defects in paint coatings originating from a contamination existing on the surface [4–6].

Having this result, line patterns were hereafter routinely drawn under the same conditions by continual ejection for experimental and analytical conveniences (a scheme of the procedures is shown in Fig. 2-2). The mass migration occurred essentially only in a one-dimensional manner, namely perpendicular to the printed line, leading to the reliable and reproducible evaluation of mass transfer process from the linewidth. After a line of PBMA-*b*-PAz was drawn by inkjet printing, the whole surface was uniformly irradiated with UV light at a constant temperature. The widths of the printed line were typically 5 μm with a 70 nm height at the center.

Figure 2-5 shows topographical AFM data of the surface morphology and profile with time under irradiation with UV light (10 mW cm^{-2}) at 25 °C. Under these conditions, the azobenzene unit was isomerized to the cis-form and reached the photostationary state (cis content: 76%, see Measurement 2-2-4) in 20 s. As shown, the mass migration

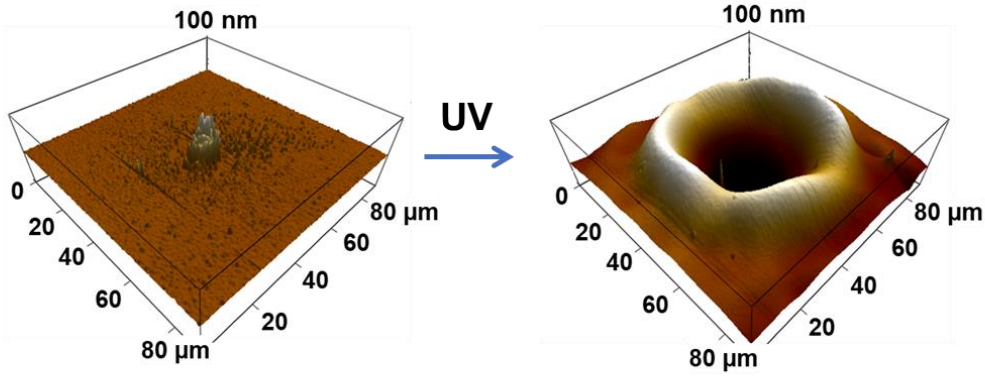

Figure 2-4. Photoinitiated mass transfer process. Dot inkjet drawings (before UV light irradiation; left, after UV light irradiation; right) leading to crater observed by AFM

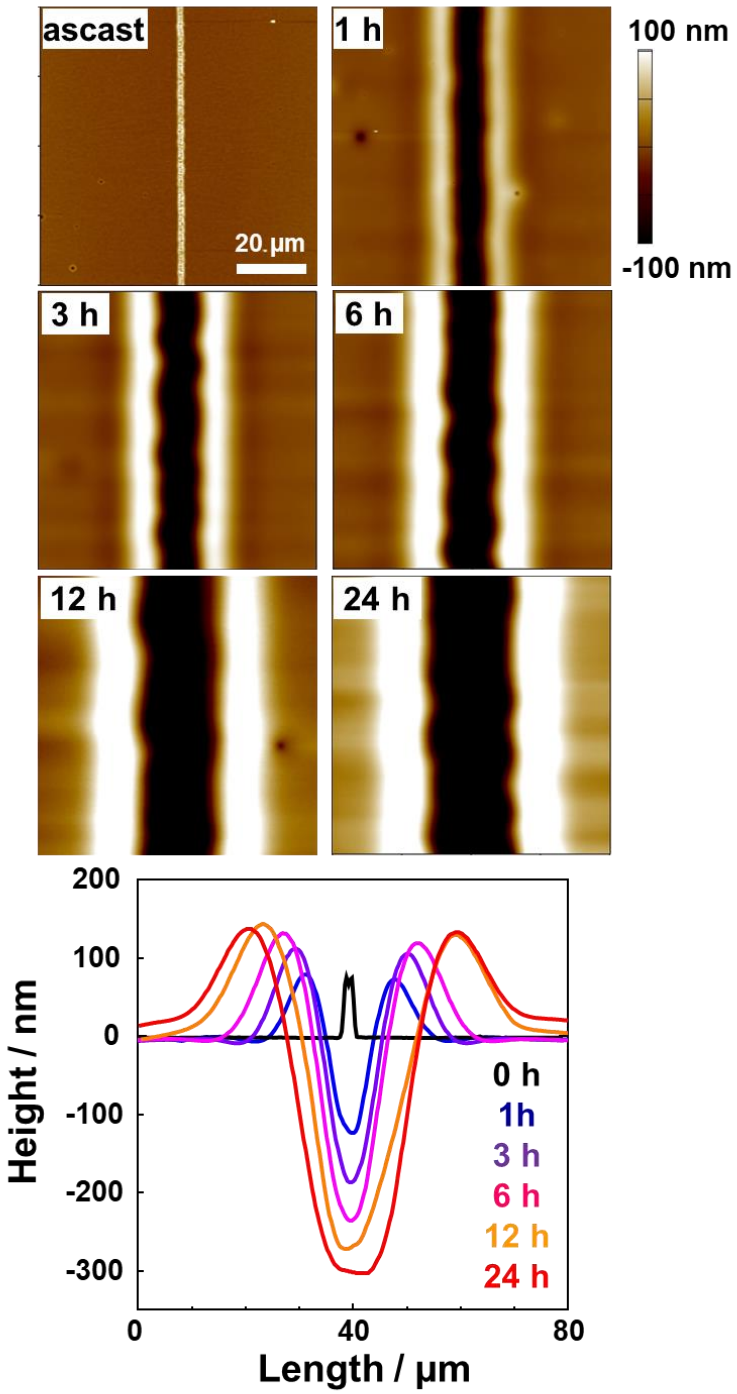

Figure 2-5. Topographical AFM images demonstrating the mass transfer of a PAz film with a thickness of 350 nm under UV light irradiation (10 mW cm^{-2}) at 25 °C.

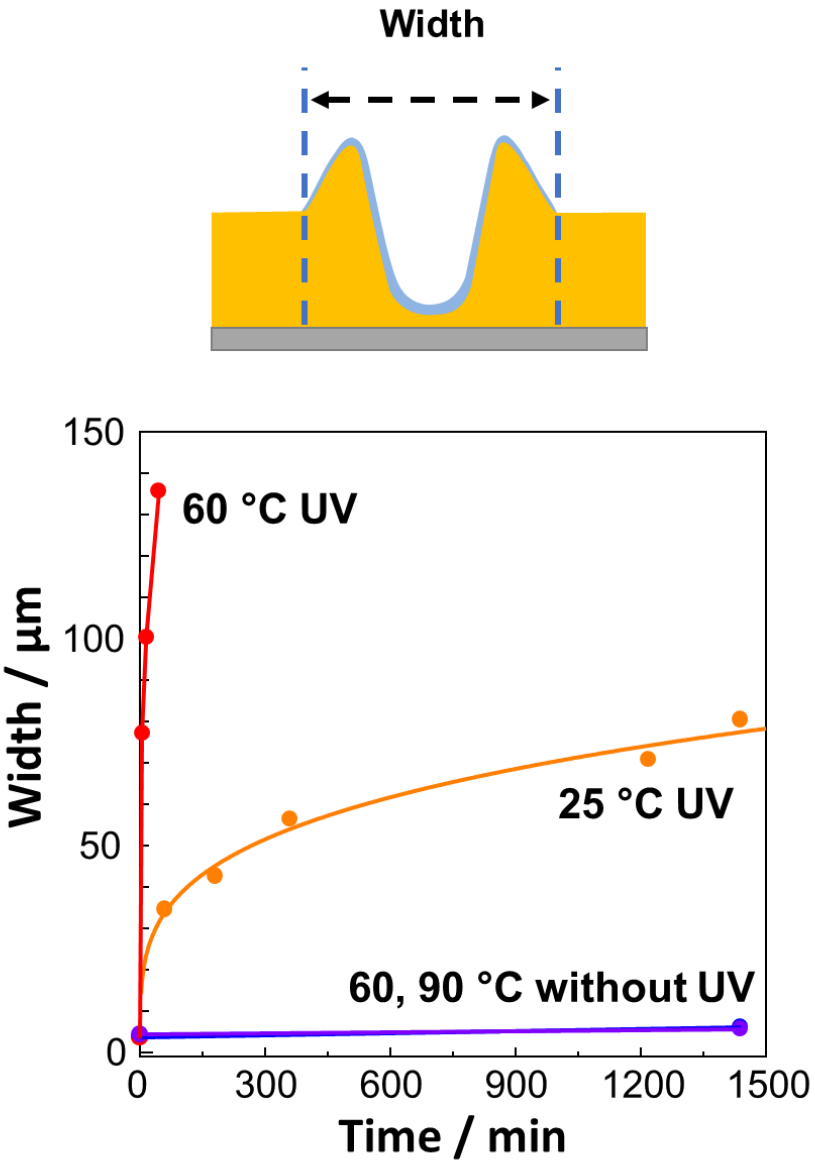

Figure 2-6. Changes in the line-width with time without UV irradiation at 60, 90 °C and with UV irradiation (10 mW cm^{-2}) at 25 °C and 60 °C.

occurred slowly over a range of hours to form a trench and ridges on both progression sides. The linewidth defined as the distance between the two ridge edges was monitored as a function of time (Fig. 2-6). Compared to the data at 25 °C, the migrating motion was prominently accelerated at 60 °C. Contrastingly, the linewidth was hardly changed when the UV light was not shone. It is well known that an isothermal liquid crystalline to isotropic phase transition is induced by UV-light irradiation as a result of the accumulation of cis-azobenzene[28]. This phase transition leads to a liquefaction of such polymers[28–30].

Steady flow viscosity measurements were made for PAz using a cone-plate rotational rheometer. The irradiation was achieved from the bottom of the shear cell in the apparatus. Large differences in shear viscosity were observed between the irradiated and non-irradiated samples depending on the shear rate in the dark and under UV irradiation (10 mW cm^{-2}) (Fig. 2-7a). However, the data observed under UV-light irradiation here does not reflect the actual viscosity of the UV photostationary state because the sample thickness (50 μm (cone center) to 480 μm (periphery)) was far beyond the light penetration depth (below 1 μm). The photoisomerization to cis-form of azobenzene occurred partly only on the surface of the illuminated side. Nevertheless, the apparent viscosity change was evident, namely, the viscosity was substantially lowered under the UV irradiation conditions at low shear ratios (Fig. 2-7b, c). This significant reduction in viscosity of the PAz base film should be ascribed to the induction of the linewidth evolution.

Under optimal temperature conditions, the migrating motion became instantaneous following the photoisomerization progression (Fig. 2-8). At 90 °C (approximately 20 °C lower than the isotropization temperature (T_{iso})), the motion ceased

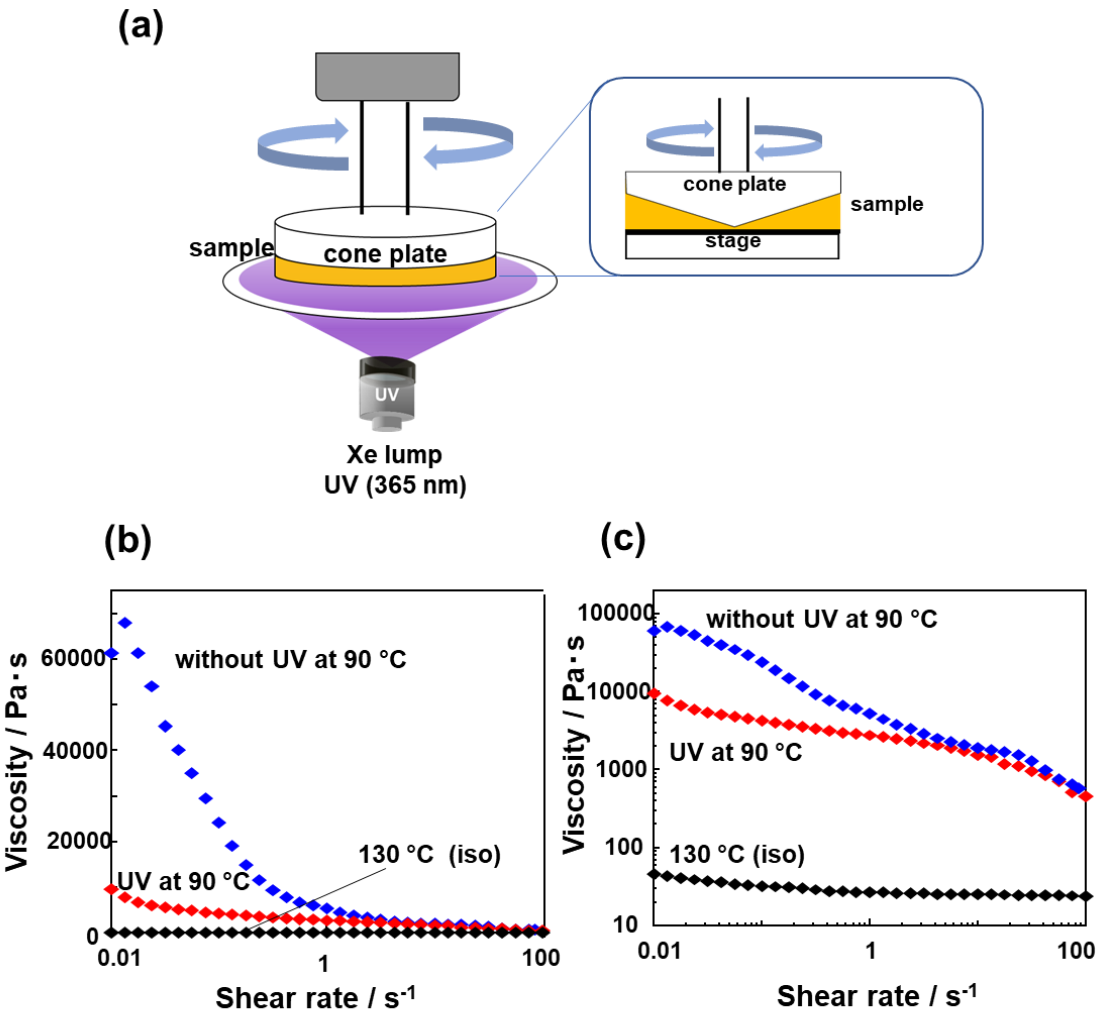

Figure 2-7. Steady flow viscosity measurement without and without UV irradiation. (a) Schematic of viscosity measurement apparatus under UV-light irradiation. The light was introduced from the bottom of the stage of viscometer. (b) Viscosity of PAz as a function of share rate. Blue and red diamonds corresponds to measurements made without and with UV irradiation at 90 °C. Black diamonds are data taken at 130 °C, isotropic state of PAz. (c) The same data displayed in the logarithm scale in the viscosity axis.

over nearly the same time course as the photoreaction (20 s). Figure. 2-8 show surface morphology changes evaluated by WLIM observations. Before UV-light irradiation, the surface profile indicated small protrusions of the printed line (Fig. 2-8a, lower). In contrast, after UV irradiation for 30 s, enormous surface deformations were observed (Fig. 2-8b). As shown in the images of Fig. 2-8, the initial printed line was nearly invisible, and in contrast, the mass migration by the irradiation, gave a large trench formation approximately 300 nm in depth and 200 nm ridges approximately 200 nm in height on both edges. Using an ordinary optical microscope, the migrating motion could be monitored. In this study, real-time surface morphology changes under irradiation were performed. In the real-time observation, the mass migration was initiated immediately after the UV-light irradiation.

UV light irradiation was performed on PBMA-*b*-PAZ line on PAz film at 90 °C at various UV light intensity (0.25-10 mW cm^{-2}). Fig. 2-9a shows the time evolution of the line width for each UV light intensity. At UV light intensities above 0.5 mW cm^{-2}, mass migration efficiently occurred and trench structure was formed, contrary below 0.25 mW cm^{-2}, no mass transfer occurred and the inkjet line was retained. Therefore, the threshold of UV light intensity required to induce mass migration exists between 0.25-0.5 mW cm^{-2} . As mention above, this mass migration is initiated by a significant viscosity reduction by photoisomerization. Under the condition of low UV light intensity, the cis ratio should not be higher enough for induction of mass migration. Then, real-time UV-Vis absorption spectroscopy was performed under UV irradiation of various intensity (0.25-10 mW cm^{-2}) at 90 °C and cis ratio was calculated followed by previous paper[27]. Fig. 2-9b shows time evolution of cis ratio for each UV light intensity. The cis ratio increased with the UV light intensity. The cis ratio was 31% at 0.25 mW cm^{-2} where mass

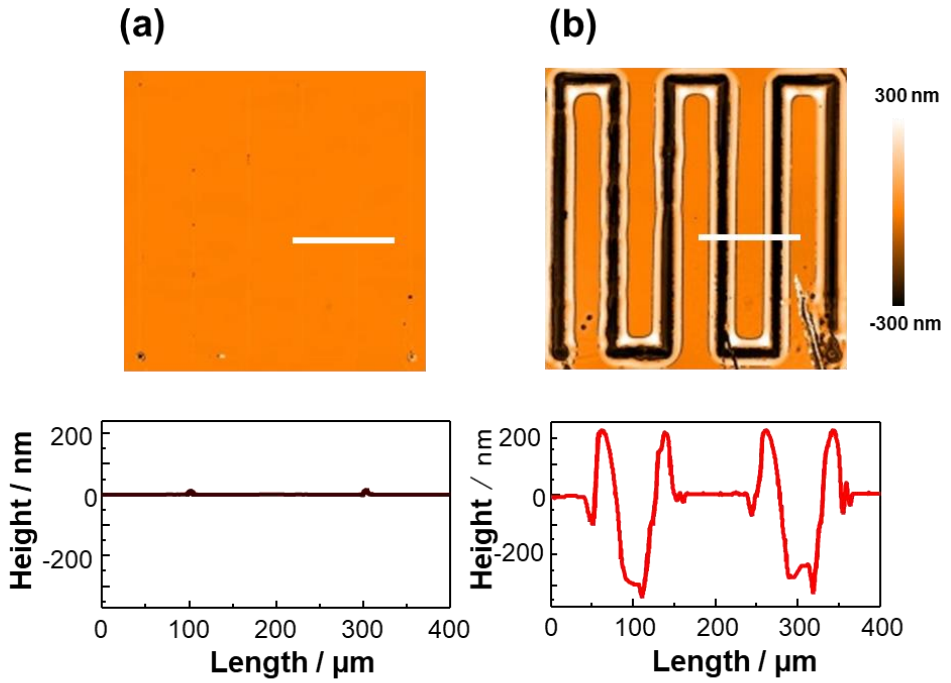

Figure 2-8. Instantaneous photoinitiated surface morphology change under optimized conditions. (a) A surface morphological image for an initial as-printed film taken by WLIM; 2D image (upper) and cross sectional height profile traced along the wight line (lower). (b) The same measurement as (a) after UV light irradiation (10 mW cm^{-2}) at 90 °C for 30 min.

transfer does not occur and 40% at 0.5 mW cm^{-2} where mass transfer occurs. Consequently, the threshold for the cis-ratio required for induction of mass transfer was between 31-40%. Mass transfer was not induced at a low cis ratio because the reduction in viscosityby photo-pahse transition of the PAz film should not be satisfied.

The data obtained by static contact angles of a glycerol droplet (θ_{gly}) shows that θ_{gly} on cis-isomerized PAz was smaller than that of PBMA-*b*-PAz at all temperature (Fig. 2-3), indicating that the surface tension of the PAz surface was larger than that of PBMA-*b*-PAz. These facts strongly suggests that the driving mechanism of the above photoinitiated migrations is the surface tension driven flow by the Marangoni effect, as has been suggested in former studies using photopatterned amorphous polymer films upon heating above T_g [12–16]. The rate of mass migration in this work was notably fast compared with those of these previous examples. This can be a particular feature for a system utilizing the photoinduced phase transition in liquid crystalline polymers.

Furthermore, the print-assisted deformation can be concave or convex, depending on the relative surface tensions of the ink material and the base polymer. This work is focused on concave (trench) formation, but the same strategy can be applied for convex (embossment) formation using a different polymer ink with a higher surface tension of PCBMA (Fig. 2-10). This mass migration is also driven by the Marangoni flow from periphery of printed area with lower surface tension toward center of ink with higher surface tension.

After UV irradiation, once the trench was formed in PBMA-*b*-PAz line on PAz film, the surface morphology was extremely stable. The valley structure was essentially unchanged, even at 130 °C for 7 days (Fig. 2-11). This means that the resultant morphology is persistently maintained as far as a different polymer component exists on

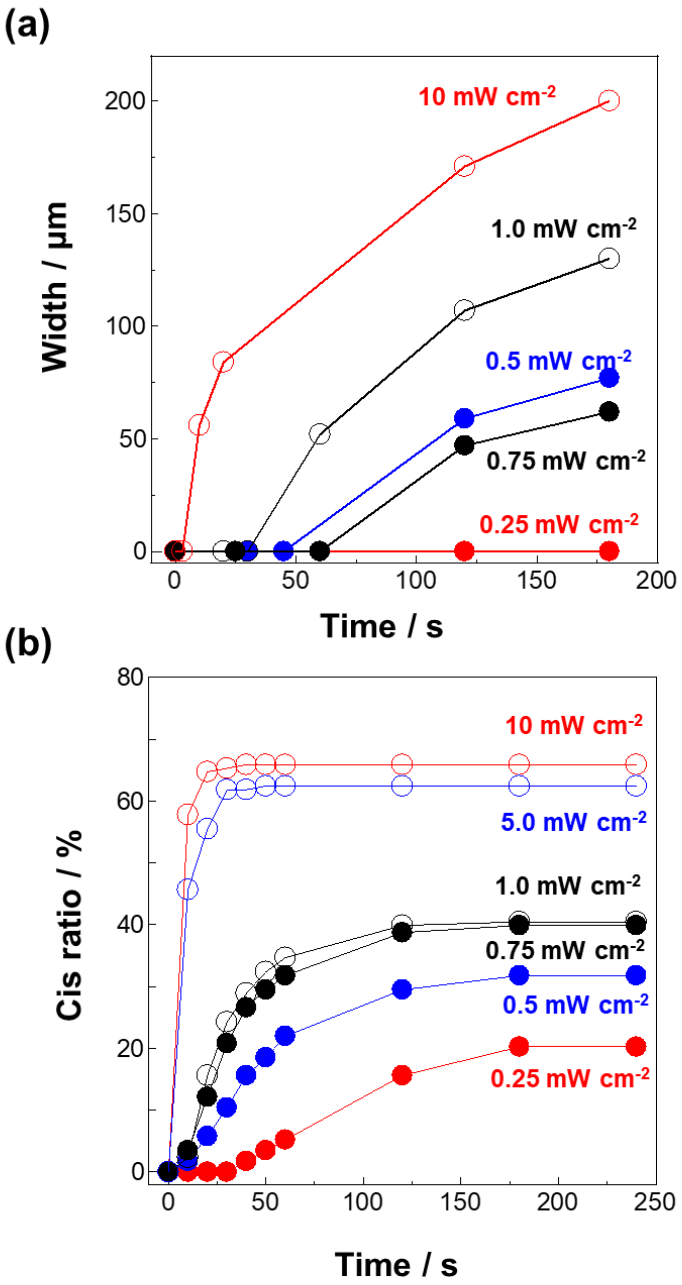

Figure 2-9. In-situ measurement of line width evolution and cis ratio. (a)Changes in the line-width with time under UV irradiation (various intensity) at 90 °C. (b) Changes in cis ratio with time under UV irradiation (various intensity) at 90 °C.

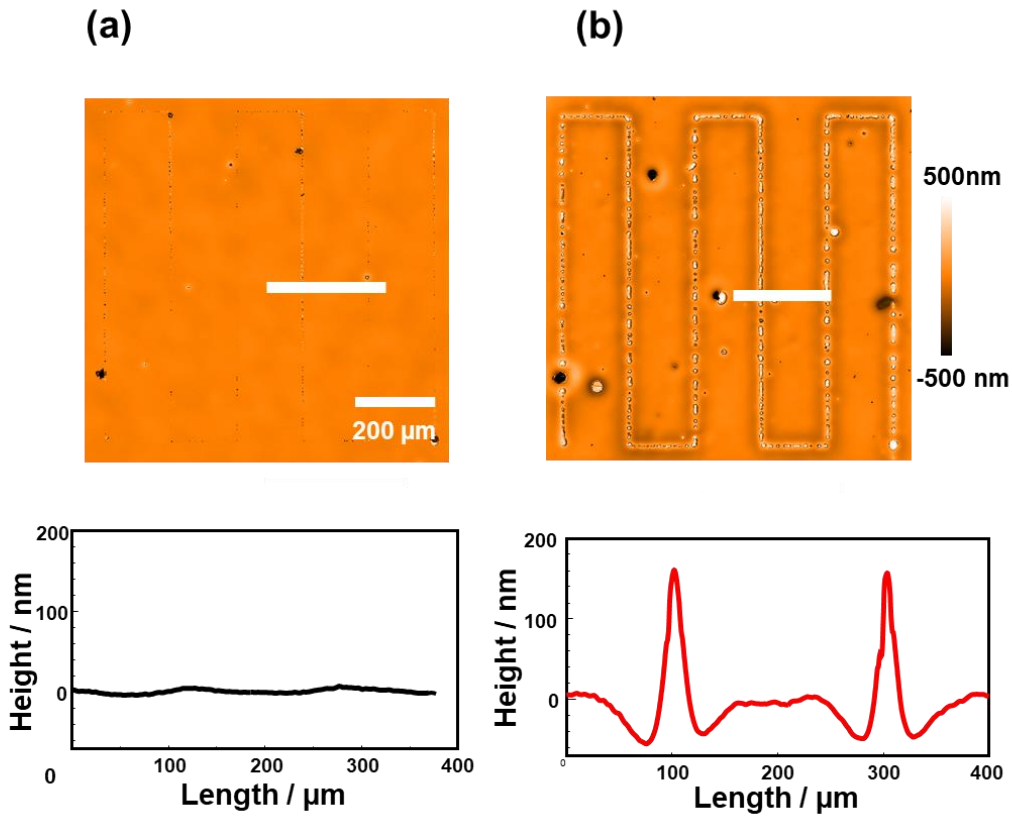

Figure 2-10. Ridge formation at the center triggered from a PCBMA line on a PAz film. (a) as-cast, (b) after heating at 130 °C for 10 min

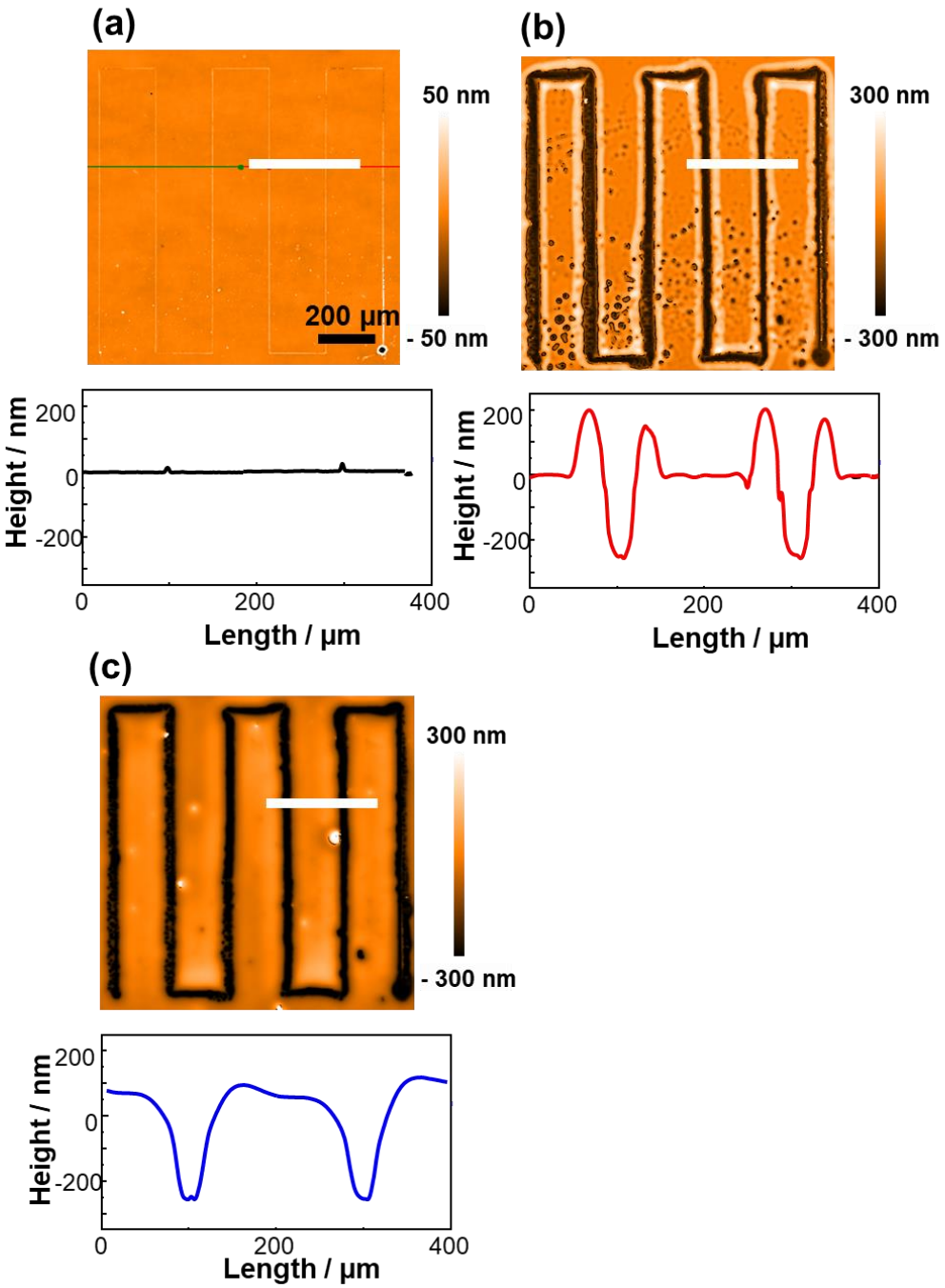

Figure 2-11. Stability of the photogenerated morphology. Surface morphologies evaluated by WLIM. (a) as-cast, (b) after UV irradiation at 60 °C for 5 min, and (c) annealed at 130 °C for 7 days from the state of (b).

the free surface. If the polymer ink is removed from the surface, the capillary force due to the surface tension should flatten the surface. To confirm this, the printed ink was selectively rinsed from the surface-inscribed surface. In this experiment, PBMA instead of PBMA-*b*-PAz was printed on the PAz film surface. The PBMA homopolymer was also found to induce the mass migration, and with this polymer selective removal of the printed ink was possible because of the large solubility difference between PBMA and PAz in cyclohexane (Fig. 2-12a, b). From the surface-deformed film of PAz, PBMA was selectively rinsed with cyclohexane at room temperature for 2 min. The rinsing did not affect the morphology at this stage. UV irradiation of this film at 90 °C resulted in a flat surface formation (Fig. 2-12c). As indicated in Fig. 2-11c, the ridges were flattened after 7 day heating. In this way, the effect of capillary force was admitted as a very slow process when the ink exists on the top.

By evaluating the cross-sectional area of the height profile after UV-light irradiation, the volume of the ridge portions was roughly in agreement with that of the trench. This fact unequivocally indicates that the morphology change is due to mass migration. The volume of PAz film driven by the surface ink of PBMA-*b*-PAz ($V_{PAz}/V_{PBMA\text{-}b\text{-}PAz}$ (=*f*)) was roughly estimated by the areas of cross section profile. This can be regarded as the amplification factor. Under the same conditions (60 °C, UV: 10 mW cm^{-2} for 5 min), the value of f increased with film thickness in the same conditions. When the film thicknesses of PAz film were 350, 600, and 1000 nm, the *f* values were 58, 210, and 440, respectively. The thicker film provided the larger amplification factor.

2-3-3. Features of the printing-assisted photo-driven process

The inkjet printing briefly enables arbitrary drawings. Figure 2-13a displays

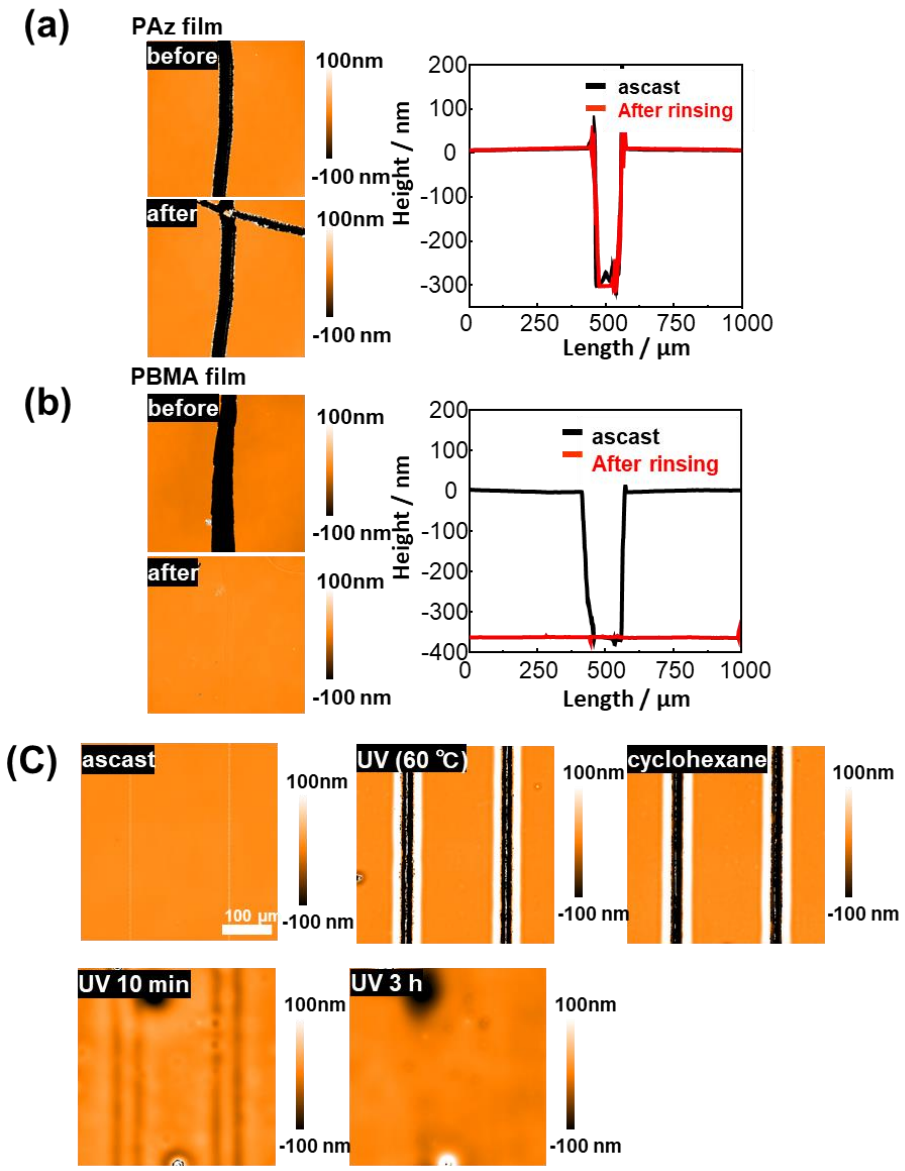

Figure 2-12. Selected removal of the printed polymer ink and the morphology change. (a) Solubility tests showing that PAz is not dissolved in cyclohexane (b) while PBMA fill was fully dissolved in this solvent as revealed with scratched film of PAz and PBMA films. (C) Morphologies of an as-printed film with PBMA, the inscribed film by UV-light irradiation (UV (60 °C)), after rinsing with cyclohexane selectively removing PBMA ink on the top, and UV irradiation with 10 min and 3 h at 60 °C. All images were taken by WLIM.

examples of curved drawings (Nazka humming bird (upper) and spiral circle (lower)). The real-time motions were performed by optical microscope. The particular features of the photoinitiated mass migration process, instead of the heat-assisted one, can be identified by two aspects. First, irradiation is remotely achievable, which enables a selective inscription. In Fig. 2-13b, two letters, N and U, were inkjet printed. The figures of N and U were inscribed independently with UV irradiation on the left- and right-hand sides of this field, respectively. This type of spatial selection is difficult in heating processes. Second, on-off switching of the mass migration is readily performed. Figure 2-14 shows the time course of the linewidth upon alternative irradiation with UV (365 nm, cis-azobenzene content: 76%) and visible (436 nm, cis-azobenzene content: 11%) light at 75 °C. The linewidth evolution progressed under UV-light irradiation, and slowed under visible-light irradiation that switches back to the smectic A phase. This control could be achieved repeatedly. This fact indicates that the linewidth can be controlled arbitrarily by the UV irradiation time. The slowing by visible light was not sharply achieved because several seconds were needed to alter the irradiation wavelength. In the heat-melt process, such prompt switching should also be difficult. The above two features are expected to expand the possibilities of the Marangoni flow process for the formation of engineered surfaces.

2-3-4. Evaluation of polymer ink spreading

To gain further insight into this dynamic process, we attempted to observe the lateral distribution of the printed polymer ink after the mass transfer. The evaluation by a surface profile measurement such as AFM was difficult because the surface deformation was too large to detect the subtle embossment of the polymer ink. A rough estimation

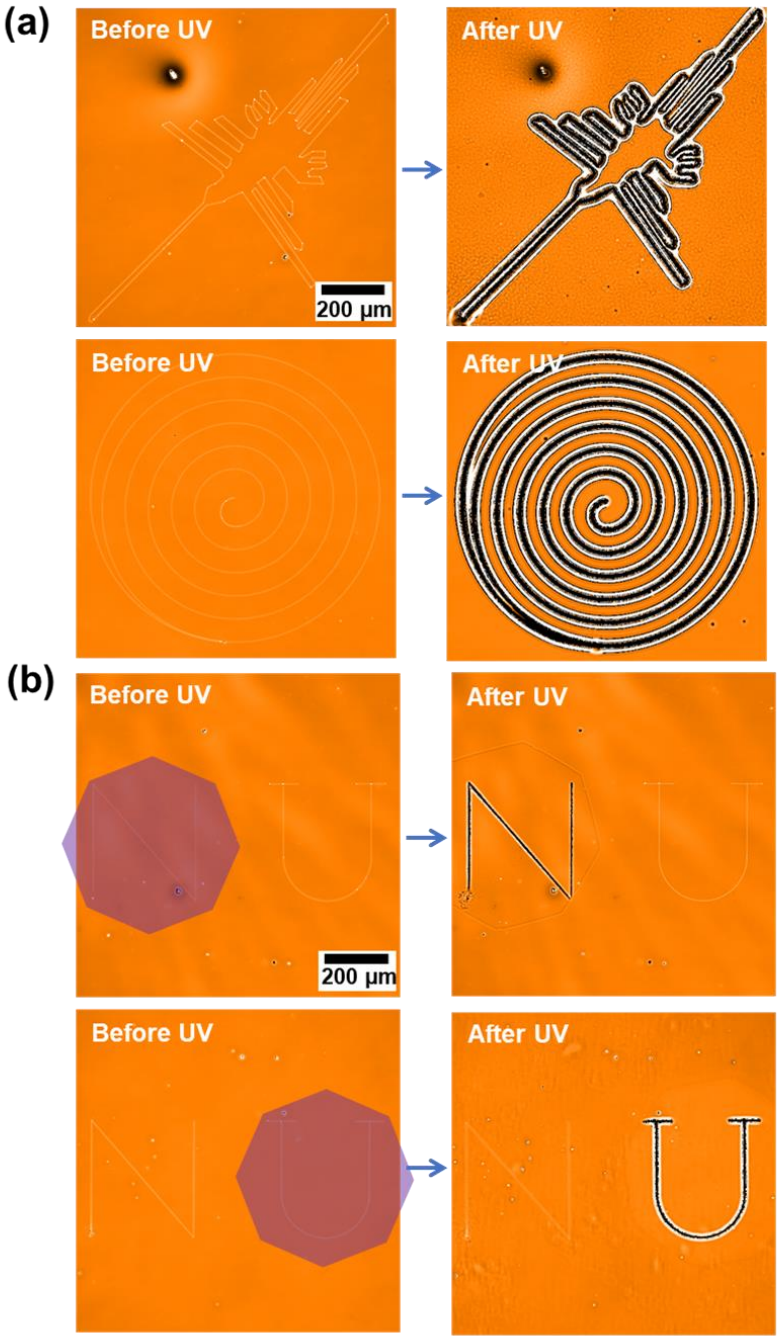

Figure 2-13. Various in the photoinitiated mass transfer process. (a) Various inkjet drawings (Nazka humming bird; upper, spiral; below) leading to curved trenches observed by WLIM. (b) Two letters that are individually irradiated. Only the selectively irradiated letter within the octagonal area appeared.

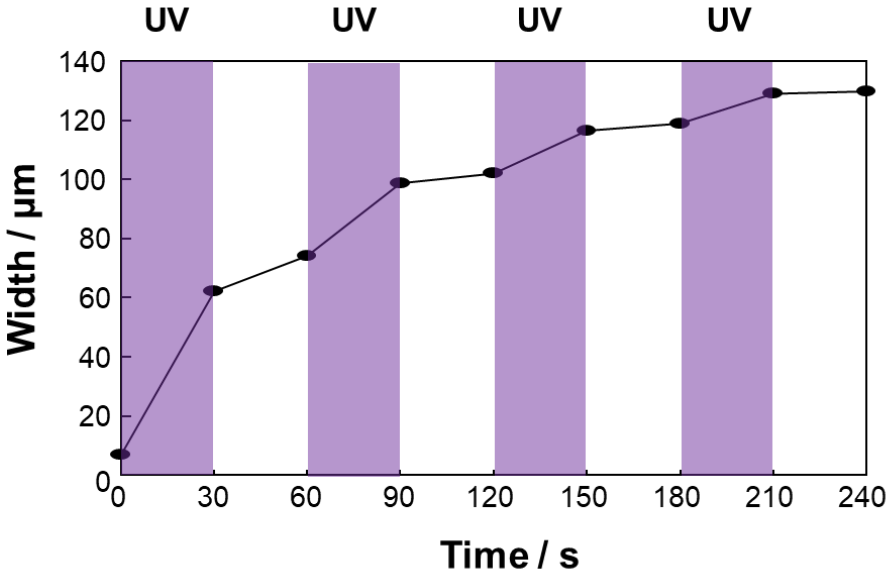

Figure 2-14. On-off switching control of the transfer motion by alternating irradiation with UV and visible light.

after mass migration by AFM provided approximately 5 nm as thickness of the spread ink. To obtain the accurate spreading behavior, a time-of-flight ion secondary ion mass spectroscopy (ToF-SIMS) measurement was made[6] using PDMS-*b*-PAz instead of PBMA-*b*-PAz. With this polymer, elemental Si can be the probe for 2D mapping of the ink distribution. Fig. 2-15a, b show a surface profile obtained from WLIM measurement and a ToF-SIMS image after sufficient UV irradiation, respectively. In Fig. 2-15c, a profile indicating the abundance of elemental Si (red line) is superimposed with the height profile in the regions of the white bar in a and b. As revealed, the Si was distributed almost between the edge regions of the two ridges. Therefore, it was confirmed that the printed polymer line laterally expanded over the two ridges as a consequence of the mass migration. This fact should indicate that the amount of mass migration depends on the amount of printed ink. When the ink is fully spread, the migration motion should cease. In fact, a larger ink amount resulted in a larger mass migration until this spreading level was attained (Fig. 2-16).

2-3-5. Thermally induced mass migration

The thermally induced transition in the dark was explored in addition to the photoinduced transition because more precise understandings were expected to be obtained. Figure 2-17 shows the evolution of linewidth in the dark at various temperatures. Essentially no morphology change was induced below 90 °C. At 110 °C ($T \simeq T_{iso}$), the line showed some expansion, but no dip formation was observed; only the printed ink showed spreading on the surface. A drastic change was observed at temperatures above Tiso. At 130 °C, a clear mass migration quickly proceeded to form a trench with a ridge on each both side. Thus, in both the photochemical and thermal cases,

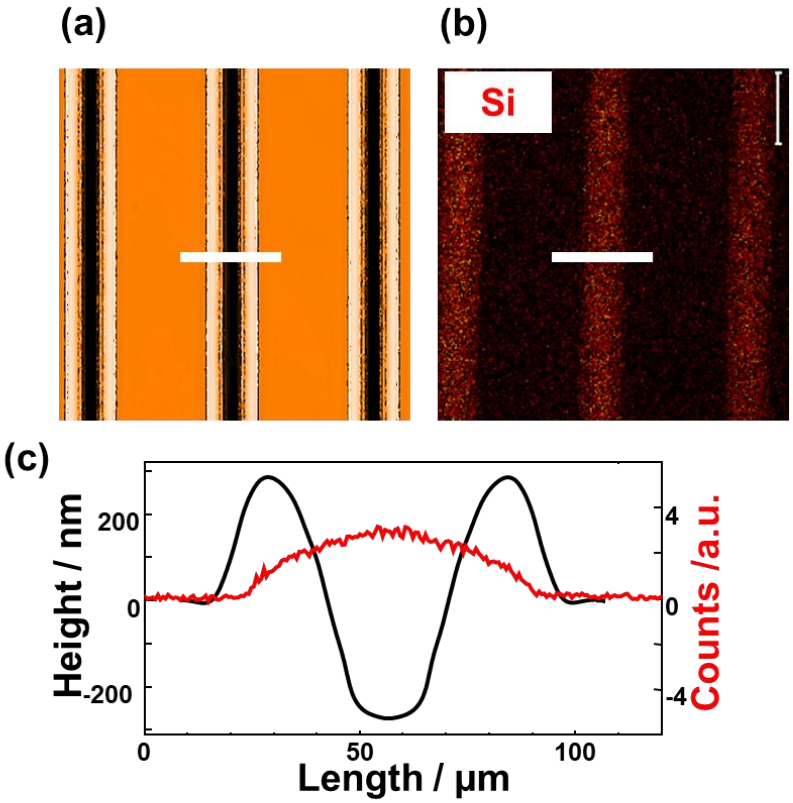

Figure 2-15. Observation of the distribution of the top of a printed line after mass transfer. (a) Topographical WLIM image for a PAz film surface after UV irradiation at 60 °C. (b) ToF-SIMS image exhibiting the distribution of Si ions. (c) compares the surface morphology outline (black) and the corresponding Si ion distribution profile (red) along the white lines of the upper figures.

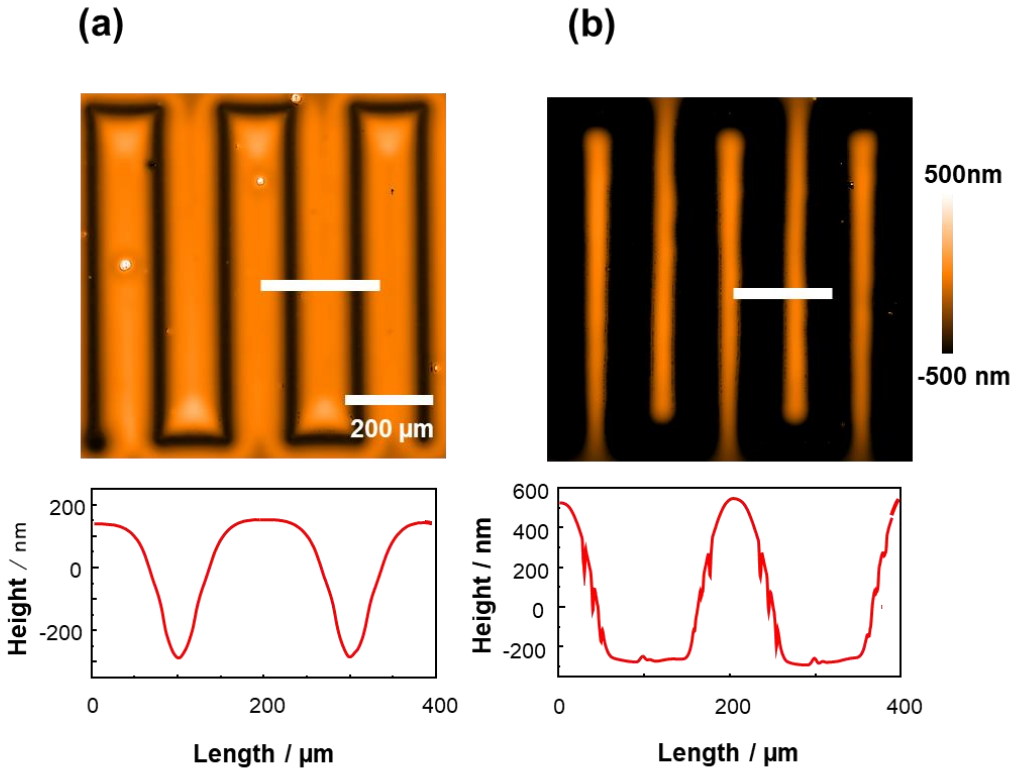

Figure 2-16. UV-initiated mass transfer behavior of a PAz film induced by different amounts of polymer ink. (a) WLIM images of an as-printed PAz film (upper) and that after UV light irradiation (1 mW cm^{-2}) for 12 h from the printed line with 70 nm. (b) The same procedures from the printed line with 300 nm height..

the effect of the transition from a smectic A to isotropic phase on the mass migration was enormous.

In the thermal transition, the reduction in viscosity was precisely evaluated. The shear viscosity measurements at 90 °C (smectic A state) and 130 °C (isotropic state) revealed that the viscosity of the PAz was reduced up one to three orders of magnitude by the thermal phase transition to the isotropic state (Fig. 2-7). As mentioned previously, the quantitative estimation of viscosity change by the photoinduced phase transition was difficult due to the measurement problem. However, considering the fast mass migration observed, it is anticipated that the viscosity reduction is of the same magnitude.

2-3-6. Discussion: Revisiting amorphous SRG systems by patterned light irradiation

Since 1995, the optical generation of surface relief gratings (SRGs) on azobenzene-containing polymer films has been a subject of extensive study and discussion[31–43]. A unified explanation of the mass transfer behavior has not yet been given[33]. At least, little attention has been paid to the non-uniformity of the surface tension of the top layer. In this regard, the work by Viswanathan et al.[34] at an early stage of photoinduced SRG study (just a few years later than the discovery of SRG phenomena) is to be noted. They showed the significant role of the free surface side in the SRG generation. When an azobenzene-containing amorphous polymer is covered with a molecular-level film by the layer-by-layer (LbL) electrostatic deposition on the top, the SRG formation is abruptly hindered. It has been explained that the disruption of surface topographical change by the overlaid LbL layer is the reason for hindrance of the mass transfer. Additionally, it seems reasonable to consider the effect of a surface tension modulation due to an uneven distribution of trans/cis azobenzene isomers in the

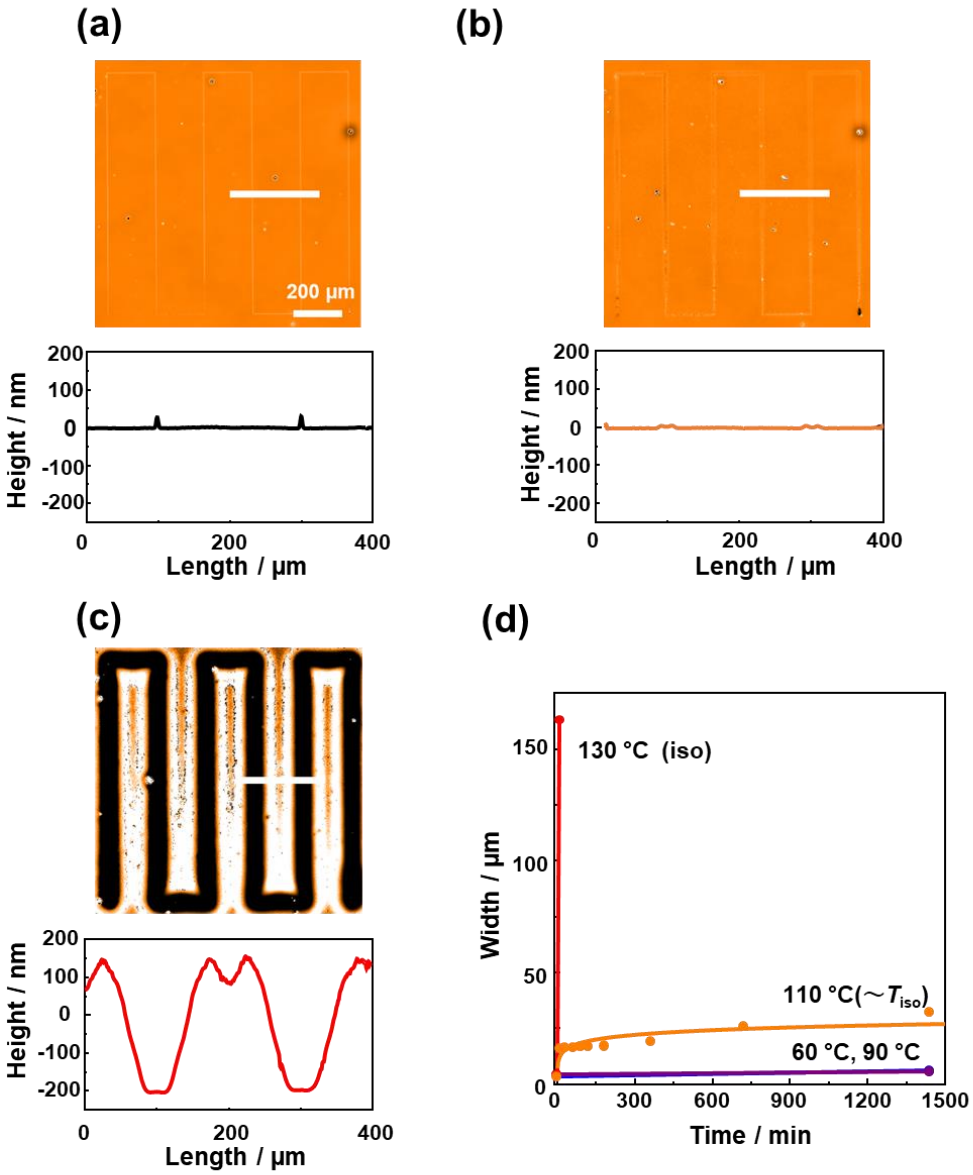

Figure 2-17. Thermally induced mass migration from a printed line. (a) A WLIM topographical image (upper) of an as-printed PAz film and cross-sectional height profile showing the height of the printed PBMA-b-PAz along the white line (lower). (b) The same measurement after annealing at 110 °C for 24 h. (c) The same measurement after annealing at 130 °C (isotropic state) for 10 min. (d) Time-course profiles of linewidth at 60 or 90 °C, 110 °C, and 130 °C.

uncovered azobenzene polymer film. Actually, Kim et al.[15] have discussed the mass migration process of an azobenzene-containing polymer film induced by the Marangoni effect. However, it is also evident that the surface-tension driven motion alone cannot explain the polarization effect of light, e. g., the mass transfer occurs along the electric vector of LPL[31–36]. Anisotropic photoinduced fluidity can also affect the migration[44]. The SRG formation in amorphous polymer films requires careful interpretations, but it seems necessary to consider the contribution of Marangoni flow effect.

2-3-7. Discussion: Implication for SRG formation in liquid crystalline polymer films

The mechanism of SRG formation in SCLCP films upon patterned irradiation[27,37,38,41–43,45] should be closely related to the present system. The motions involved in the previous studies are associated with the photochemical phase transition of azobenzene polymers[21,28–30]. The difference is whether the irradiation is achieved with patterned light (former SRG work) or overall exposure (this work). In conclusion, we assume that the Marangoni effect also plays the important role in the previous SRG formation systems for the following reasons. First, the migration motion occurs most efficiently at the boundary edge of the photomask patterns[40,43,45], which is consistent with the observations by Kim et al[15]. Second, the mass migration does not exhibit a dependence on the polarization of the irradiating light[46]. The mass migration behavior is very similar to the present investigation in terms of the effect of light exposure dose, an insensitivity to polarization, the surface shape possessing a receded trench with ridges along the edges. Possibly, the former SRG systems are driven in large part by the surface tension gradient formed by the patterned light. In patterned irradiation, the trans/cis isomerization ratio patterns are formed by patterned irradiation, thereby, both the surface tension and

rheological properties of interior parts are changed simultaneously. In contrast, in our present approach by inkjet printing, only the surface tension modification is obtained under uniform UV irradiation. Therefore, our approach is more favorable to precisely evaluate the Marangoni effects.

2-4. Conclusion

In conclusion, we newly demonstrate the photoinduction of surface morphology spatially directed using a sub-femto-liter inkjet printing technique. Using a lower-surface-tension polymer as the ink, the mass migration of a liquid crystalline photoresponsive base polymer film is initiated by irradiation with UV light. This action results in a crater or trench formation accompanied by an isotropic isothermal phase transition of the liquid crystal. The mass transfer behavior of the polymer material is reasonably explained by the Marangoni effect. The inkjet printing technique is extensively utilized and is in development in the field of 2D patterning on substrates, especially for printed electronics with high spatial accuracy. Therefore, we anticipate that the proposed strategy will provide a new type of platform possessing a large potential to be comparable with other widely known microfabrication methods such as photolithography, soft lithography[47], block copolymer lithography[48], photoinduced surface relief grating[31–43], surface wrinkling[49] etc. On the other hand, much attention has already been paid to azobenzene-containing SCLCPs. They show intriguing photoresponsive effects and functions[50] such as holographic optical recording, surface photoalignment of liquid crystals, photoinduced phase transitions, surface relief grating formations, and photoinduced deformations that allow macroscopic optical actuators. This phototriggered Marangoni effect can be recognized as an intriguing new optical effect in addition to the above widely recognized

photoprocesses.

References

[1] L. E. Scriven, C. V. Sternling, *Nature* **1960**, 187, 186–188.

[2] P. G. De Gennes, F. Brochard-Wyart, D. Quere, D. Capillarity and Wetting Phenomena: Drops, bubbles, pearls, waves, Springer, **2004**.

[3] S. Kumar, *Langmuir* **2003**, 19, 2473–2478 (2003).

[4] P. L. Evans, L. W. Schwartz, R. V. Roy, *J. Coll. Interf. Sci.* **2000**, 227, 191–205.

[5] L. O. Kornum, H. K. R. Nielsen, *Prog. Org. Coat.* **1980**, 8, 275-324.

[6] H. L. Bloomfield, H. Y. Nie, *Surf. Interface Anal.* **2017**, 49, 1379-1386.

[7] D. P. A. Birnie, *Langmuir* **2013**, 29, 9072–9078.

[8] T. Kajiya, W. Kobayashi, T. Okuzono, M. Doi, *J. Phys. Chem. B* **2009**, 113, 15460-15466.

[9] B. J. de Gans, U. S. Schubert, *Langmuir* **2004**, 20, 7789–7793.

[10] G. Li, K. Graf, E. Bonaccurso, D. S. Golovko, A. Best, H.-J. Butt, *Macromol. Chem. Phys* **2007**, 208, 2134–2144.

[11] J. Sun, B. Bao, M. He, H. Zhou, Y. Song, *ACS Appl. Mater. Interfaces* 2015, 7 28086–28099.

[12] J. M. Katzenstein, D. W. Janes, J. D. Cushen, N. B. Hira, D. L. McGuffin, N. A. Prisco, C. J. Ellison, *ACS Macro Lett.* **2012**, 1, 1150–1154.

[13] D. W. Janes, J. M. Katzenstein, K. Shanmuganathan, C. J. Ellison, *J. Polym. Sci., Part B: Polym. Phys*. **2013**, 51, 535–545.

[14] T. A. Arshad, C. B. Kim, N. A. Prisco, J. M. Katzenstein, D. W. Janes, R. T. Bonnecaze, C. J. Ellison, *Soft Matter* **2014**, 10, 8043–8050.

[15] C. B. Kim, J. C. Wistrom, H. Ha, S. X. Zhou, R. Katsumata, A. R. Jones, D. W. Janes, K. M. Miller, C. J. Ellison, *Macromolecules* **2016**, 49, 7069–7076.

[16] A. R. Jones, C. B. Kim, S. X. Zhou, H. Ha, R. Katsumata, G. Blachut, R. T. Bonnecaze, C. J. Ellison, *Macromolecules* **2017**, 50, 4588–4596.

[17] J. P. Singer, P.-T. Lin, S. E. Kooi, L. C. Kimerling, J. Michel, E. L. Thomas, *Adv. Mater.* **2013**, 25, 6100–6105.

[18] J. P. Singer, S. E. Kooi, E. L. Thomas, *J. Polym. Sci., Part B: Polym. Phys*. **2016, 54,** 225–236.

[19] R. Elashnikov, P. Fitl, V. Svorcik, O. Lyutakov, *Appl. Surf. Sci.* **2017**, 394, 562–568.

[20] T. Ubukata, Y. Moriya, Y. Yokoyama, *Polym. J.* **2012**, 44, 966–972.

[21] T. Ikeda, *J. Mater. Chem.* **2003**, 13, 2037–2057.

[22] K. Fukuhara, Y. Fujii, Y. Nagashima, M. Hara, S. Nagano, T. Seki, *Angew. Chem. Int. Ed*. **2013**, 52, 5988–5991.

[23] S. Nagano, Y. Koizuka, T. Murase, M. Sano, Y. Shinohara, Y. Amemiya, T. Seki, *Angew. Chem. Int. Ed.* **2012**, 51, 5884–5888.

[24] K. Fukuhara, S. Nagano, M. Hara, T. Seki, *Nat. Commun.* **2014**, 5, 3320.

[25] D. Tanaka, Y. Nagashima, M. Hara, S. Nagano, T. Seki, Langmuir **2015**, 31, 11379–11383.

[26] K. Aoki, T. Iwata, S. Nagano, T. Seki, *Macromol. Chem. Phys.* **2010**, 211, 2484–2489.

[27] N. Zettsu, T. Ogasawara, R. Arakawa, S. Nagano, T. Ubukata, T. Seki,. *Macromolecules* **2007**, 40, 4607–4613.

[28] S. Ito, A. Yamashita, H. Akiyama, H. Kihara, M. Yoshida, *Macromolecules* **2018**,

51, 3243–3253.

[29] H. Zhou, C. Xue, P. Weis, Y. Suzuki, S. Huang, K. Koynov, G. K. Auernhammer, R. Berger, H.-J. Butt, S. Wu, *Nat. Chem.* **2017**, 9, 145–151.

[30] H. Finkelmann, E. Nishikawa, G. G. Pereira, M. A. Warner, *Phys. Rev. Lett.* **2001**, 87, 015501.

[31] P. Rochon, E. Batalla, A. Natansohn, *Appl. Phys. Lett*. **1995**, 66, 136-138.

[32] D. Y. Kim, S. K. Tripathy, L. Li, J. Kumar, *Appl. Phys. Lett*. **1995**, 66, 1166-1168.

[33] K. G. Yager, C. J. Barrett, *Curr. Opin. Solid State Mater. Sci*. **2001**, 5, 487–494.

[34] N. K. Viswanathan, S. Balasubramanian, L. Li, J. Kumar, S. K. Tripathy, *J. Phys. Chem. B* **1998**, 102, 6064–6070.

[35] N. K. Viswanathan, D. Y. Kim, S. Bian, J. Williams, W. Liu, L. Li, L. Samuelson, J. Kumar and S. K. Tripathy. *J. Mater. Chem.* **1999**, 9 1941–1955.

[36] A. Natansohn, P. Rochon, *Chem. Rev*. 2002, 102, 4139–4175. 37.

[37] T. Ubukata, T. Seki, K. Ichimura, *Adv. Mater.* **2000**, 12, 1675–1678.

[38] T. Ubukata, M. Hara, K. Ichimura, T. Seki, *Adv. Mater*. **2004**, 16, 220–223.

[39] T. Ubukata, M. Nakayama, T. Sonoda, Y. Yokoyama, H. Kihara, *ACS Appl. Mater. interfaces* **2016**, 8, 21974–21978.

[40] J. Isayama, S. Nagano, T. Seki, *Macromolecules* **2010**, 43, 4105–4112.

[41] T. Seki, *Bull. Chem. Soc. Jpn*. **2018**, 91, 1026–1057.

[42] T. Seki, *Curr. Opin. Solid State Mater. Sci.* **2006**, 10 241–248.

[43] T. Seki, *Macromol. Rapid Commun*. **2014**, 35, 271–290.

[44] P. Karageorgiev, D. Neher, B. Schulz, B. Stiller, U. Pietsch, M. Giersig, L. Brehmer, *Nat. Mater.* **2005**, 4, 699–703.

[45] T. Ubukata, T. Higuchi, N. Zettsu, T. Seki, M. Hara, *Colloid. Surf. A:*

Physicochem. Eng. Asp. **2005**, 257–258, 123–126.

[46] N. Zettsu, T. Fukuda, H. Matsuda, T. Seki, *Appl. Phys. Lett*. **2003**, 83, 4960–4962.

[47] Y. Xia, G. M. Whitesides, *Annu. Rev. Mater. Sci.* **1998**, 28, 153–184.

[48] C. M. Bates, M. J. Maher, D. W. Janes, C. J. Ellison, C. G. Willson, *Macromolecules* **2014***,* 47 2–12.

[49] J. Y. Chung, A. J. Nolte, C. M. Stafford, *Adv. Mater.* **2011**, 23 349–368.

[50] H. Zeng, P. Wasylczyk, D. S. Wiersma, A. Priimagi, *Adv. Mater.* **2018**, 30, 1703554.

Chapter III

Photo-triggered large mass transport driven only by a photoresponsive surface skin layer

3-1. Introduction

In chapter II, photo-triggered mass migration are demonstrated by the Marangoni effect driven by the inkjet patterns. The plausible mechanism of this mass migration was the surface tension difference introduced by inkjet printings.

The research exploration on azobenzene (Az) polymers from the viewpoint of mass transfer can be traced back to the surface relief gratings (SRGs) by interference irradiation of two laser beams in amorphous polymer films, which was first reported in 1995. Since then, photoinduced SRG processes have been reported using various photofunctional materials such as amorphous polymers[1-20], side chain liquid crystalline polymers (SCLCPs)[21-27], supramolecular systems[24,27-29], amorphous molecular materials[30]. Additionally, SRG formation can be realized using other photoresponsive units[31-35].

Various mechanistic models for mass transfer have been proposed: isomerization pressure due to volume change[7,8], gradient force[9-11], mean-field model[12], directed softening or fluidization[13-15], molecular diffusion[16-18], molecular orientation force[19,20], etc. With regard to Az-containing side chain liquid crystalline polymers (SCLCPs)[21-27], UV light irradiation leads to a photochemical phase transition between the liquid crystal (LC) and isotropic phases. This phase change plays an important role in highly efficient SRG formation[23,25,26], which requires an overall dose of much less than 1 J cm^{-2}. Typically mass transport depends on the light irradiation conditions and physicochemical properties.

Consequently, a universal explanation about the mechanism has yet to be provided.

Recent studies have noted the importance of the surface effect on the mass transfer process. Ambrosio et al.[17,18] proposed an anisotropic light-driven molecular diffusion model for spiral morphology induction under vortex-beam illumination. Their model stressed enhanced molecular diffusion in proximity of the free surface. Ellison et al.[36-39] have proposed microfabrications via the Marangoni flow by photochemical reactions. Similarly, the author reported UV light-induced mass transfer of an Az-containing SCLCP film at the inkjet-printed lines of another polymer (Chapter II)[40]. In this case, mass transfer could be explained by the Marangoni flow occurring at the inkjet-printed areas. Related to the molecular orientation in SCLCP films, an Az-containing command layer at the free surface or inkjet-printed patterns could control the orientation of the majority of the mesogens of the base film[41-45].Kawatsuki et al. also controlled of mesogen orientation from free surfaces using different types of photoreactive units[46,47].

The above knowledge inspired us to examine light-driven mass transport for "light-inert" SCLCP films with only a photoresponsive layer at the free surface and a photoresponsive SCLCP films covered with a light-inert molecular layer. Such a study should provide decisive evidence to extract the effect of the topmost surface. Figure 1 schematically depicts the materials and systems used in this work. This study demonstrates that the existence of a nm-thick photoresponsive skin layer on the surface can induce mass transfer. Conversely, the existence of 1–2-nm-thick layer of the octadecyl side chain polymer on the top of the film almost fully hinders transport motions. These observations highlight the critical role of the topmost surface in the macroscopic mass transfer of polymer films. Moreover, they suggest that previous arguments in SRGs studies should be reconsidered. Finally, this work demonstrates the technological

importance in the microfabrication of materials without photoreactive units.

3-2. Experimental

3-2-1. Materials and monomer and polymer synthesis

3-2-1-1. Synthesis of 4-cyanophenyl-4'-(6-acryloxyhexyloxy) benzoate (CPBz) monomer

4-Cyanophenyl-4'-(6-acryloxyhexyloxy) benzoate (CPBz) was synthesized as described in a previous paper[48] as shown in Fig. 3-1.

Synthesis of Methyl-4-(6-hydroxyhexyloxy) benzoate

Potassium carbonate (28.6 g, 0.21 mol) was added to a dry N,N'-dimethylformamide (DMF) solution containing methyl-4-(6-hydroxyhexyloxy) (20.9 g, 0.14 mol) under N_2 gas. 6-Bromo-1-hexanol (22.6 mg, 0.17 mol) in dry DMF was then added dropwise under stirring. The solution was stirred for 8 h at 80 °C. After this procedure, the solution was dissolved in water, and extracted with ethyl acetate and water. The precipitate was recrystallized from ethyl acetate to give white powdery crystals. Yield: 30.5 g (87.6%).

1H-NMR (400 MHz, CDCl3): δ (ppm) = 1.36-1.44 (6H, m, -CH2-), 1.71-1.75 (2H, m, -CH2-), 3.75 (3H, s, -O-CH3), 4.01-4.05 (2H, t, -CH2-OH), 4.35-4.38 (2H, q, -O-CH2-), 6.99-7.01 (2H, d, Ar-H), 7.86-7.89 (2H, d, Ar-H)

Synthesis of 4-(6-hydroxyhexyloxy) benzoic acid

3 M Sodium hydroxide aqueous solution (140 mL) was add to a mixed solution of purified tetrahydrofuran (THF) and ethanol containing 4-(6-hydroxyhexyloxy)benzoic acid (30.5 g, 0.12 mol). The solution was stirred for 24 h at 25 °C. After this procedure, the solution was dissolved in water, and extracted with THF and water. The precipitate was recrystallized from THF to give white powdery crystals. Yield: 23.1 g (70.2%). 1H-

NMR (400 MHz, CDCl3): δ (ppm) = 1.36-1.44 (6H, m, -CH2-), 1.71-1.75 (2H, m, -CH2-), 4.01-4.05 (2H, t, -CH2-OH), 4.35-4.38 (2H, q, -O-CH2-), 6.99-7.01 (2H, d, Ar-H), 7.86-7.89 (2H, d, Ar-H), 12.6 (-C(=O)O-H)

Synthesis of 4-(6-acryloxyhexyloxy) benzoic acid

Triethylamine (26.9 mL, 0.19 mol) was added to a purified THF solution containing 4-(6-hydroxyhexyloxy) benzoic acid (23.1 g, 0.097 mol) under N_2 gas. A purified THF solution of acryloyl chloride (11.7 mL, 0.15 mol) was added dropwise to the solution at 5 ^{o}C. The mixture was stirred for 24 h at 25 °C. After this procedure, the solution was dissolved in chloroform and water, and extracted with ethyl acetate and water. The precipitate was recrystallized from ethyl acetate and hexane to give white powdery crystals. Yield: 19.7 g (69.5%). 1H-NMR (400 MHz, CDCl3): δ (ppm) = 1.41 (6H, m, -CH2-), 1.62-1.74 (2H, m, -CH2-), 4.02-4.05 (2H, t, -CH2-O-C(=O)-), 4.09-4.13 (2H, q, -O-CH2-), 5.92-5.95, 6.29-6.34 (CH=CH2), 6.14-6.20 (CH=CH2), 6.98-7.01 (2H, d, Ar-H), 7.86-7.88 (2H, d, Ar-H), 12.5 (-C(=O)O-H)

Synthesis of 4-cyanophenyl-4'-(6-acryloxyhexyloxy) benzoate (CPBz)

1-(3-Dimethylaminopropyl)-3-ethylcarbodiimide (EDC, 24.0 mL, 0.14 mol) in purified THF was added dropwise to a mixed solution of THF and DMF containing 4-(6-acryloxyhexyloxy) benzoic acid and 4-hydroxybenzonitrile under N_2 gas. The mixture was stirred for 7 days at 25 °C. After this procedure, the solution was dissolved in chloroform and water, and the crude product was extracted with chloroform and water. The precipitate was recrystallized from ethyl acetate to give white powdery crystals. Yield: 11.5 g (42.9%).

1H-NMR (400 MHz, CDCl3): δ (ppm) = 1.47-1.87 (8H, m, -CH2-), 4.04-4.08 (2H, t, -CH2-O-C(=O)-), 4.17-4.20 (2H, q, -O-CH2-), 5.81-5.84, 6.39-6.43 (CH=CH2), 6.09-6.16

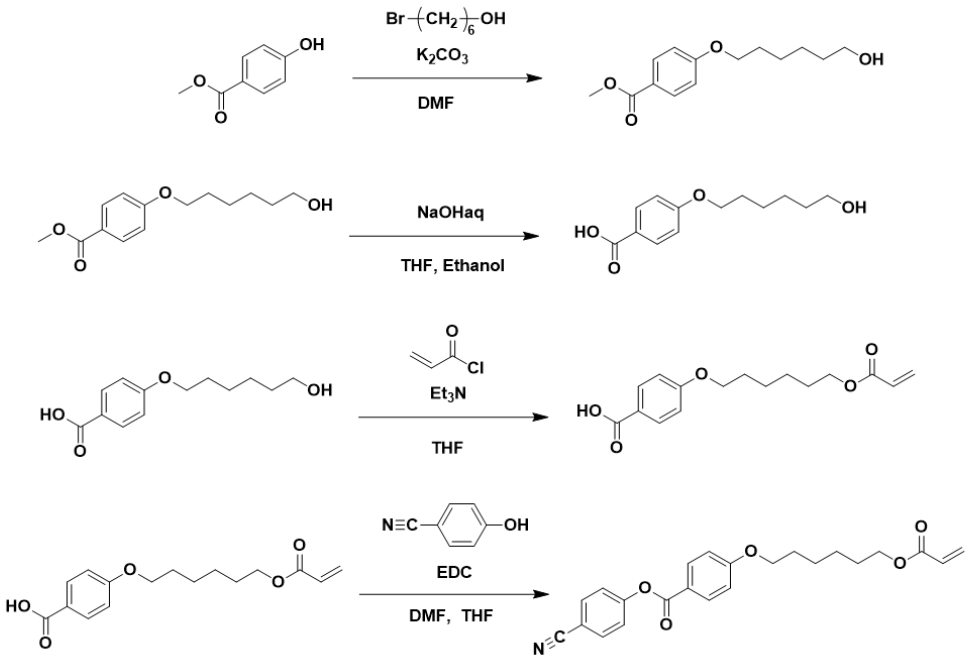

Figure 3-1. Synthesis of CPBz monomer.

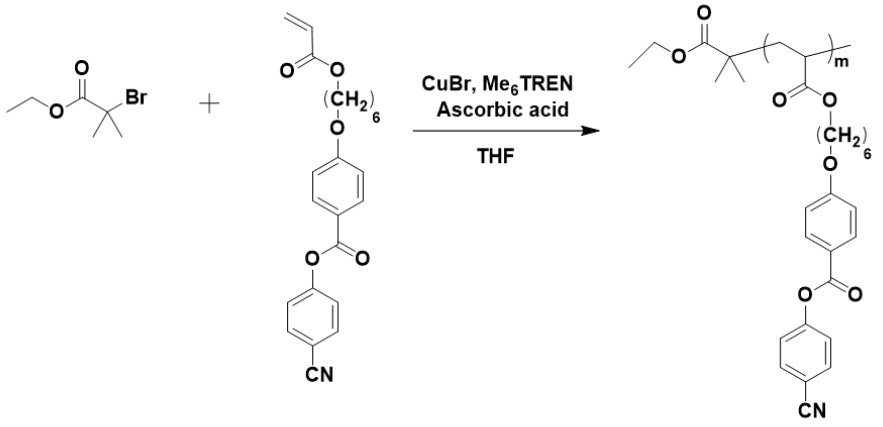

Figure 3-2. Polymerization of PCPBz via atomic transfer living radical polymerization.

(CH=CH2), 6.97-6.99 (2H, d, Ar-H), 7.26-7.37 (2H, d, Ar-H), 7.73-7.75 (2H, d, Ar-H), 8.12-8.14 (2H, d, Ar-H)

3-2-1-2 Polymerization

Polymerization of cyanophenyl-benzoate containing acrylate (PCPBz) was achieved by the atom transfer radical polymerization (ATRP) method as shown in Fig. 3-2.

Cu(I)Br (1.5 mg, 0.01 mmol), Me6TREN (3.3 mg, 0.01 mmol), ascorbic acid (9.0mg, 0.05 mmol) and CPBz monomer 1000 mg, 2.5 mmol) were put into a 15 mL pressure tube and purged with a N_2 gas. In a glove box, dry THF (1.32 mL, 2mol dm-3 for CPBz monomer) was added to the tube and stirred for 5 min. Polymerization started by injection of a initiator, ethyl-2-bromoisobutyrate (EBB) (1.3 μL, 0.01 mmol), and the sealed tube was moved from the glove box to a personal synthesizer (ChemiStation, EYELA, Japan) and stirred for 24 h at 70 °C. The polymerization was quenched by exposure the reaction solution to air. The solution was pass through an activated neutral alumina column to remove the Cu catalyst with chloroform as the eluent. The solution was concentrated by evaporation, and the product was precipitated by pouring into methanol.

Az-containing and octadecyl methacrylate polymers (PAz[40,42] and PC18[49], Fig. 3-3) were synthesized from their corresponding monomers by atom transfer radical polymerization (ATRP). Chemical structures of all polymers used in this study are displayed in Fig. 3-3 and the characterization data are listed in Table 3-1.

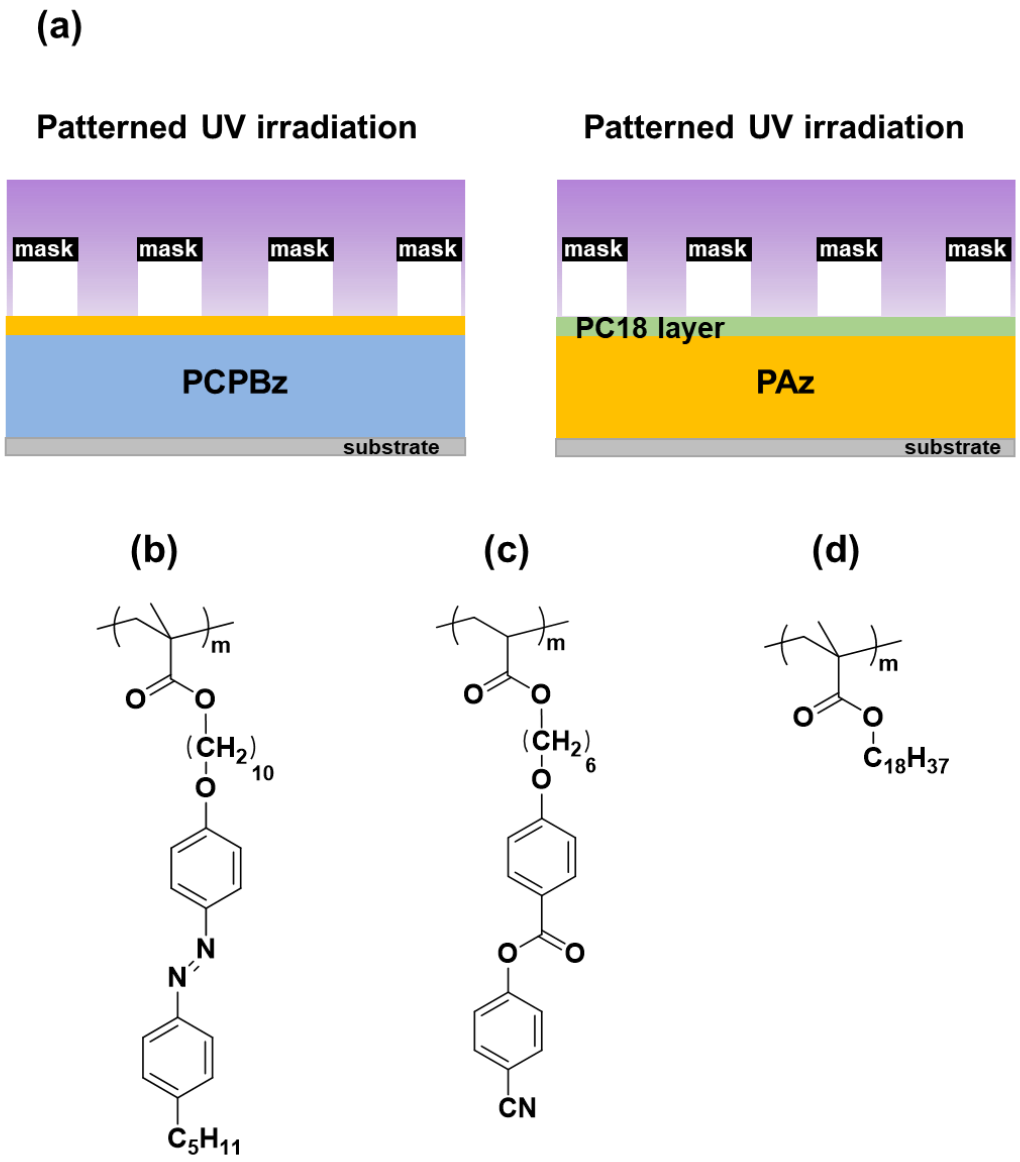

Figure 3-3. Schematic of photo-triggered morphology system (a) and chemical structures of PAz (b), PCPBz (c) and PC18 (d).

Table 3-1. Characterizations of the polymers used in this study.

Polymer	M_n (M_w/M_n)	Degree of polymerization	Thermophysical Properties / ° C	Contact angle of glycerol (θgly) / deg	
				25 ° C	90 ° C
PAz	1.3×10^4 (1.08)	26	g (45) sm C (87) sm A (110) iso	102.5±0.9	103.2±0.7
PAz (UV)				89.1±1.8	85.1±1.6
PCPBz	5.1×10^4 (1.19)	129	g (23) nematic (114) iso	76.1±1.0	80.1±1.5
PAz/PCPBz blend				99.2±1.6	98.4±1.4
PAz/PCPBz blend (UV)				89.4±0.9	85.3±0.9
PC18	3.0×10^4 (1.14)	88	g (ca. -100) cryst (27) iso		

UV: under UV light irradiation, g: glass, sm: smectic, iso: isotropic, csryst:crystal

3-2-2. Film preparation

PCPBz films were prepared by spin coating (2000 rpm, 60 s) (Mikasa, Japan) from Chloroform solutions (typically 3.0 or 4.5 wt% in toluene) onto clean quartz substrate (typical film thickness: approximately 200 or 430 nm).

Surface segregated films of PAz layer/PCPBz were prepared from a 3 wt% mixed solution of chloroform containing 5% of PAz to PCPBz by weight. The films were subsequently annealed at 90 °C for 10 min.

Polymer films for static contact angle measurement were prepared from 3 wt% solution chloroform.

3-2-3. Langmuir-Schaefer deposition

The PAz solution (ca. 1.0×10^{-3} mol dm^{-3} per Az monomer unit) in chloroform was prepared. The spreading behaviour of the PAz monolayer was characterized by a Lauda film balance (FW-1, Germany) filled with pure water at 20 °C. The sliding barrier was compressed at a speed of 30 cm^2 min^{-1}. The floating PAz monolayer obtained on the water surface was transferred onto a PCPBz film by the Langmuir-Schaefer (LS) method at a surface pressure of 15 mN m^{-1} as shown in Fig. 3-4. The same procedure was used to transfer the PC18 monolayer on water onto the PAz film. π-*A* isotherms of PAz and PC18 on pure water at 20 °C are shown in Fig. 3-5.

3-2-4. Light irradiation

UV-light irradiation (365 nm) was performed with a mercury-xenon lamp (Sanei Electronics Supercure 203S, Japan) at 1.0 mW cm^{-2} (365 nm) at 90 °C. Patterned UV irradiation was achieved through a photomask, which typically had a 20-μm line-and-

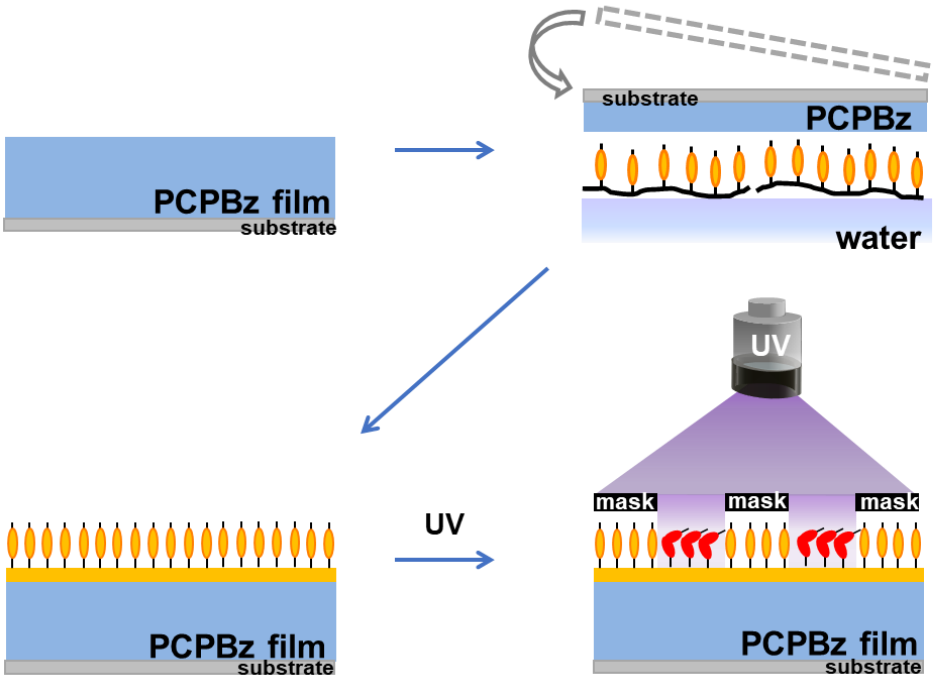

Figure 3-4. Schematic of procedure adopted in this work; spin coating, Langmuir-Schaefer process and patterned UV light irradiation.

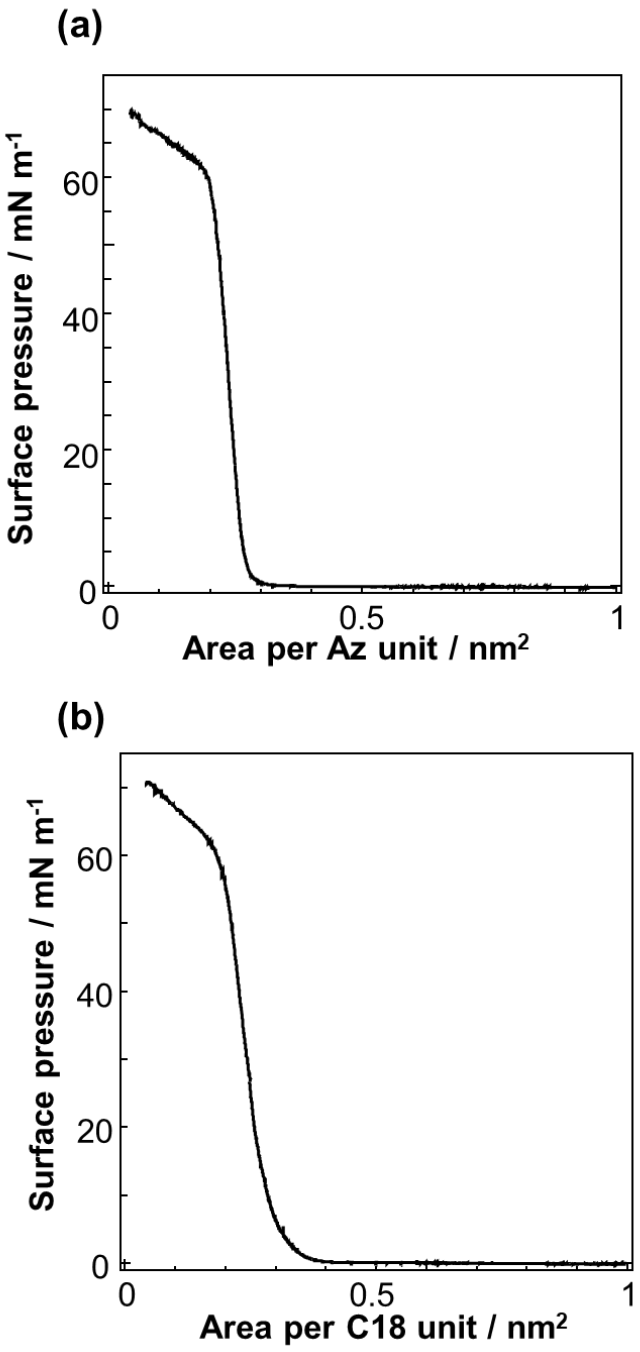

Figure 3-5. π-A isotherms of PAz (a) and PC18 (b) on pure water at 20 °C.

stripe pitch and “I” shape pattern (Edmond Optics, USA). The 365-nm line was selected by passing through combinations of glass filters of UV-35/UV35D (Toshiba, Japan).

3-2-5. Measurement

The gel permeation chromatography (GPC) measurement, differential Scanning Calorimeter (DSC) measurement, polarized optical microscope (POM) observation, static contact angle measurement, white-light interferometric microscope (WLIM) observation, atomic force microscopy (AFM) observation and UV-Vis absorption spectral measurement were performed by same set-up in previous chapters.

Static contact angles of water (θ_w, surface tension, $\gamma_w = 72$ mN m^{-1} at 25 °C) and glycerol (θ_{gly}, $\gamma_{gly} = 63$ mN m^{-1} at 25 °C) droplets on these polymer films were obtained by a contact angle meter (CA-XP, Kyowa Interface Science, Japan). The contact angle values were the average of at least five repeated measurements. Glycerol was used for the requirement of measurements at high temperatures such as 90 °C.

The X-ray scattering (XRS) measurements were performed by using an FR-E (Rigaku) with CuKα radiation ($\lambda = 0.154$ nm). The scattering images were captured with two-dimensional imaging plate detector R-AXIS IV (Rigaku). The camera length was 300 mm. The sample substrate was set on hot-stage (CHUO Precision Industrial ATS-C316-EM / ALV-300-HM).

3-3. Results and discussions

3-3-1. Characterization of PCPBz

The optical properties of PCPBz in bulk state was examined using POM at controlled temperature. Figure 3-6a shows the POM images at 100 °C and 120 °C,

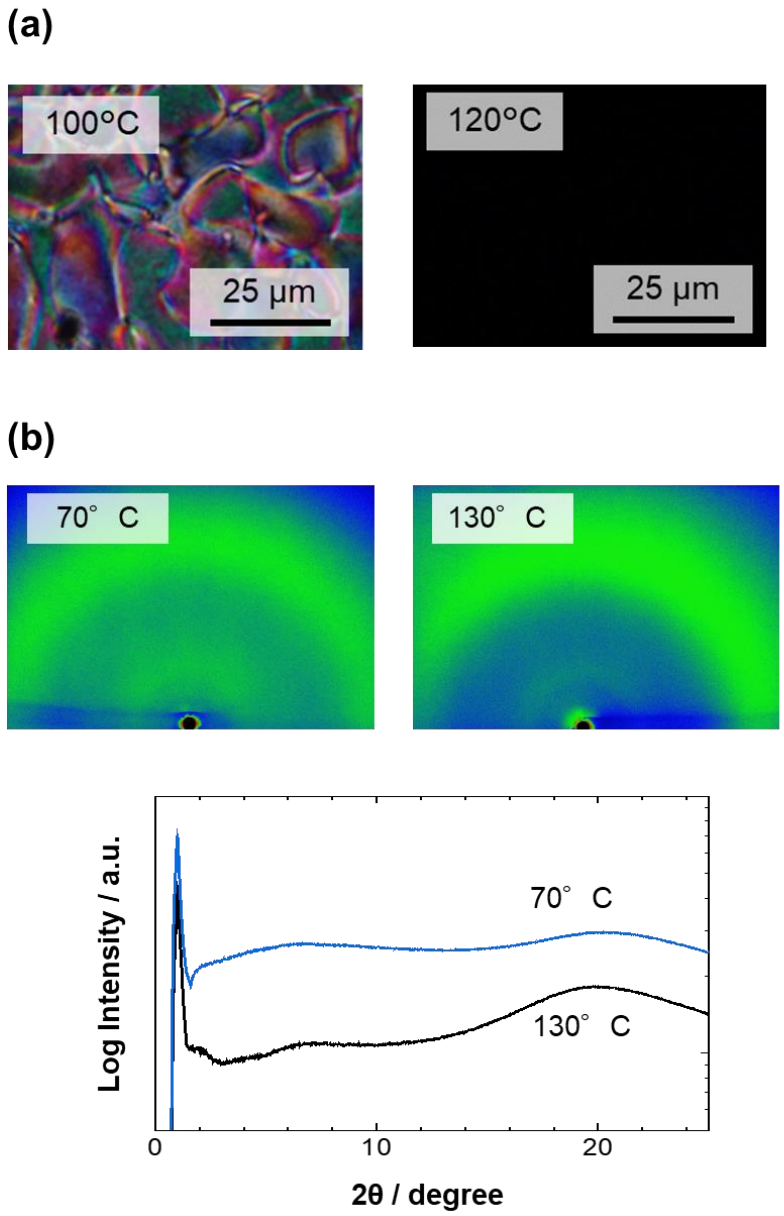

Figure 3-6. Characterizations of PCPBz. POM observations (a) and X-ray scattering profiles (b). Schlieren texture at 100 °C in POM image and absence of peaks in small angle regions of X-ray scattering profiles indicate that this polymer exhibits a nematic phase.

respectively under crossed polarizers. PCPBz indicated Schlieren texture at 100 °C. On the other hand, a uniform black field image was observed at 130 °C.

PCPBz in bulk state were evaluated by XRS measurement (Fig. 3-6b). No scattering peak were observed at all temperature. These data suggest that PCPBz shows nematic LC feature.

3-3-2. Contact angle measurement

Table 3-1 lists the θ_{gly} values. For reference, θ_w on the polymer films at 25 °C are shown in Fig. 3-7. The θ_{gly} values on PAz were 102.5 ± 0.9° (25 °C) and 103.2 ± 0.7° (90 °C), but decreased to 89.1±1.8° (25 °C) and 85.1±1.6° (90 °C) under UV irradiation, respectively. For all temperatures, the θ_{gly} values of unirradiated PAz were larger than those under UV light irradiation, indicating that UV irradiation induces a higher surface tension on the PAz surface as the cis-isomers of Az increases[50,51]. Moreover, the θ_{gly} values for light-inert PCPBz were 76.1 ±1.0° (25 °C) and 80.1 ±1.6° (90 °C), demonstrating that the light-inert PCPBz has a substantially higher surface tension. On the other hand, the surface tension of PC18 was low as θ_{gly} = 107.1 ± 0.9° at 25 °C. These values were used to characterize the topmost surfaces.

3-3-3. Photoinduced mass migration in PCPBz films with a PAz LS layer

Figure 3-3 shows the light-inert SCLCP film covered with a photoactive layer. Repeated deposition of a PAz floating monolayer by the LS method realized a molecularly controlled coating onto the surface of PCPBz films (Fig. 3-4). Figure 3-5 shows the pressure-surface area isotherm (π-*A* curve) of PAz on the water surface at 20 °C. Based on the steep uprise in the π-*A* curve, the estimated molecular occupied area of the Az

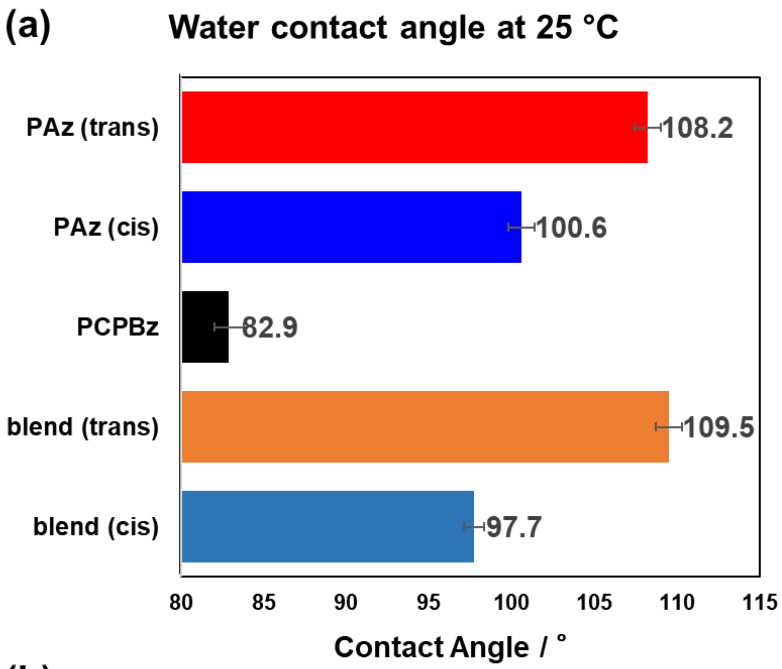

(b)

Droplet	γ / mN · m^{-1}	b.p. / °C
Glycerol	63.4	290

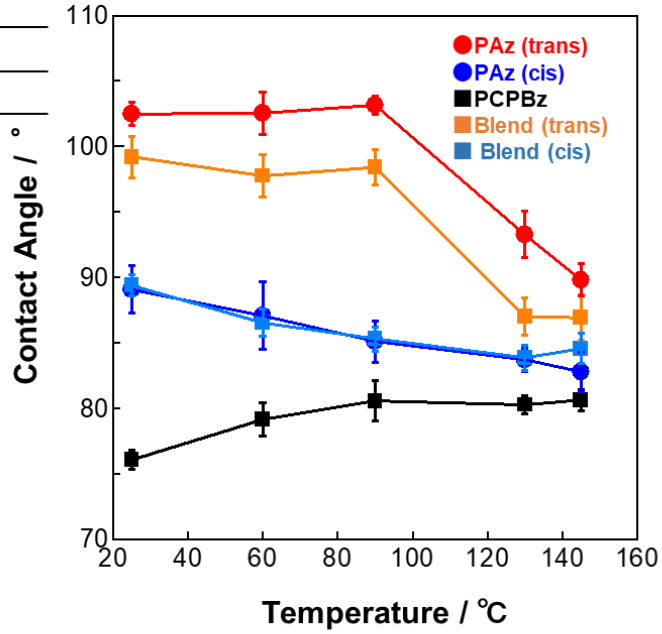

Figure 3-7. Contact angle measurements. (a) The contact angle of a water droplet on various polymer film surface. (b) The contact angle of glycerol (θ_{gly}) on polymers at various temperatures.

monomer unit was 0.3 nm^2. This value agrees well with that previously reported for a similarly occupied area of mesogenic Az polymers[52, 53], suggesting that PAz forms a stable monolayer film on a water surface.

The PAz monolayer was transferred onto a quartz substrate at a pressure of 15 mN m^{-1}. Figure 3-8 shows the topographical AFM image (3-8a, left) and a height profile (3-8a, right) of PAz monolayer on a hydrophobized Si wafer with 1,1,1,3,3,3-hexamethydisilazane. The estimated thickness of the PAz monolayered film at a defect area was 2 nm. Figure 3-8c,d displays the UV-visible absorption spectra of the PAz layers as a function of the number of deposition layers on the PCPBz film after subtracting the spectrum of the pure PCPBz film. There were two absorption bands at 246 nm (ϕ-ϕ* transition) and 348 nm (π-π* transition) of the Az unit. The ϕ-ϕ* absorption at 246 nm increased proportionally with the deposition number, indicating that the PAz layer is accurately deposited onto the PCPBz film. This band was chosen to check the deposition state because the transition moment is independent of the Az orientation.

Next, AFM topographical images were acquired for 200-nm thick PCPBz films covered with the PAz LS layer. Figure 3-9 displays the height profiles after UV light irradiation (1 mW cm^{-2} for 300 s) at various temperature through a line and space photomask (20-μm pitch). The temperature control is an important factor in the SCLCP systems*, and the most efficient mass migration occurred at 90 °C in the present case (Fig. 3-9). A pure PCPBz film had a flat surface, and UV irradiation did not induce a topological change (Fig. 3-10a). However, depositing a PAz LS layer on the PCPBz film caused obvious surface undulations. Even a 2-nm-thick PAz monolayer deformed the PCPBz film surface. The height difference between the peak and valley induced by the PAz monolayer was 41 nm (Fig. 3-10b), demonstrating that a 2-nm-thick PAz monolayer on

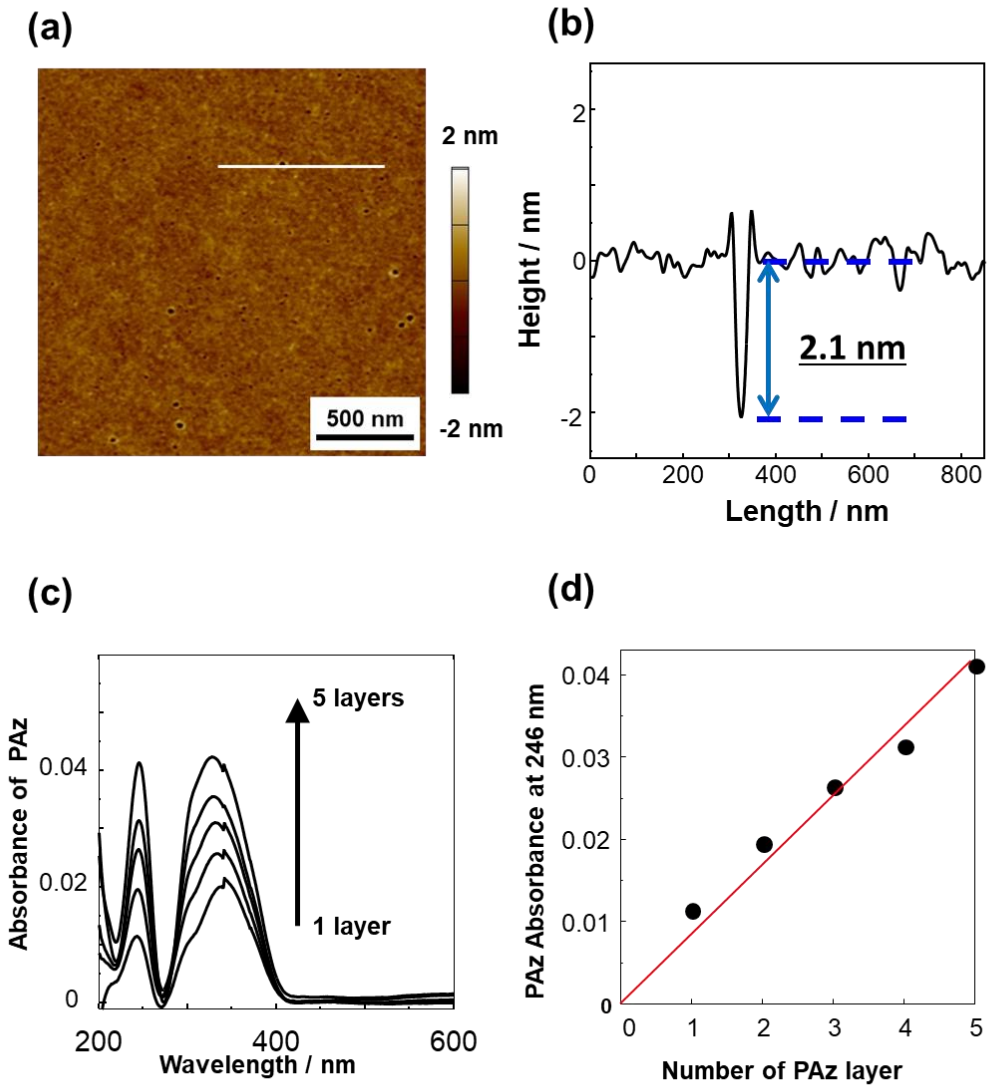

Figure 3-8. Topographical AFM images of a PAz monolayer film on Si wafer (a) and cross-sectional profile obtained from the AFM data (b). UV–visible absorption spectra for different deposition numbers of PAz layers (1–5 layers) on the PCPBz film (c) and the absorbance of PAz at 246 nm as a function of the deposition number of PAz monolayers (d)

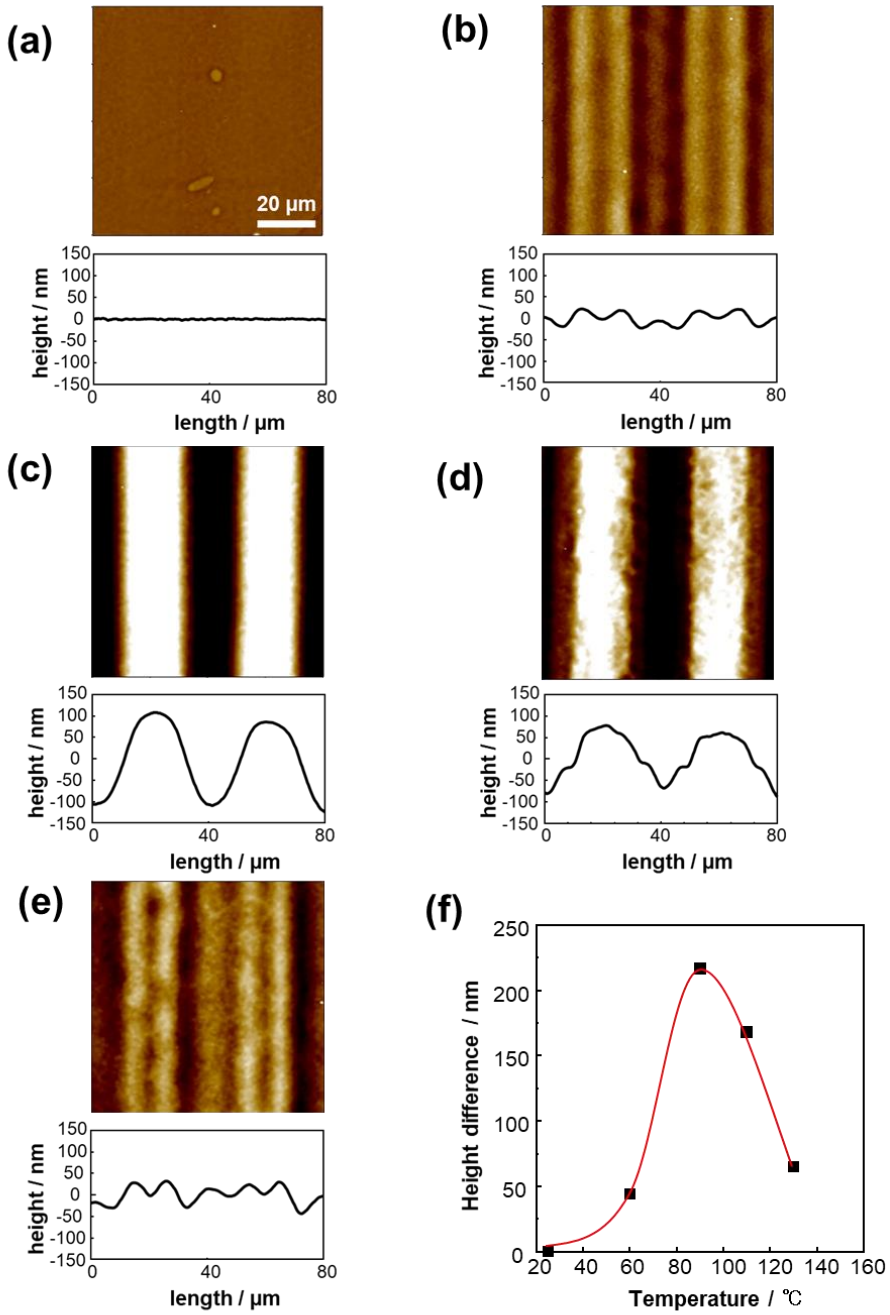

Figure 3-9. Photoinduced mass transport of 5-layerd PAz film on PCPBz film. UV irradiation is performed through a stripe photomask (20 μm pitch) at 25 °C (a), 60 °C (b), 90 °C (c), 110 °C (d), 130 °C (e). Top-to-bottom height difference of the SRG structure for 5-layerd PAz LS film on PCPBz films with various UV irradiation temperature (f).

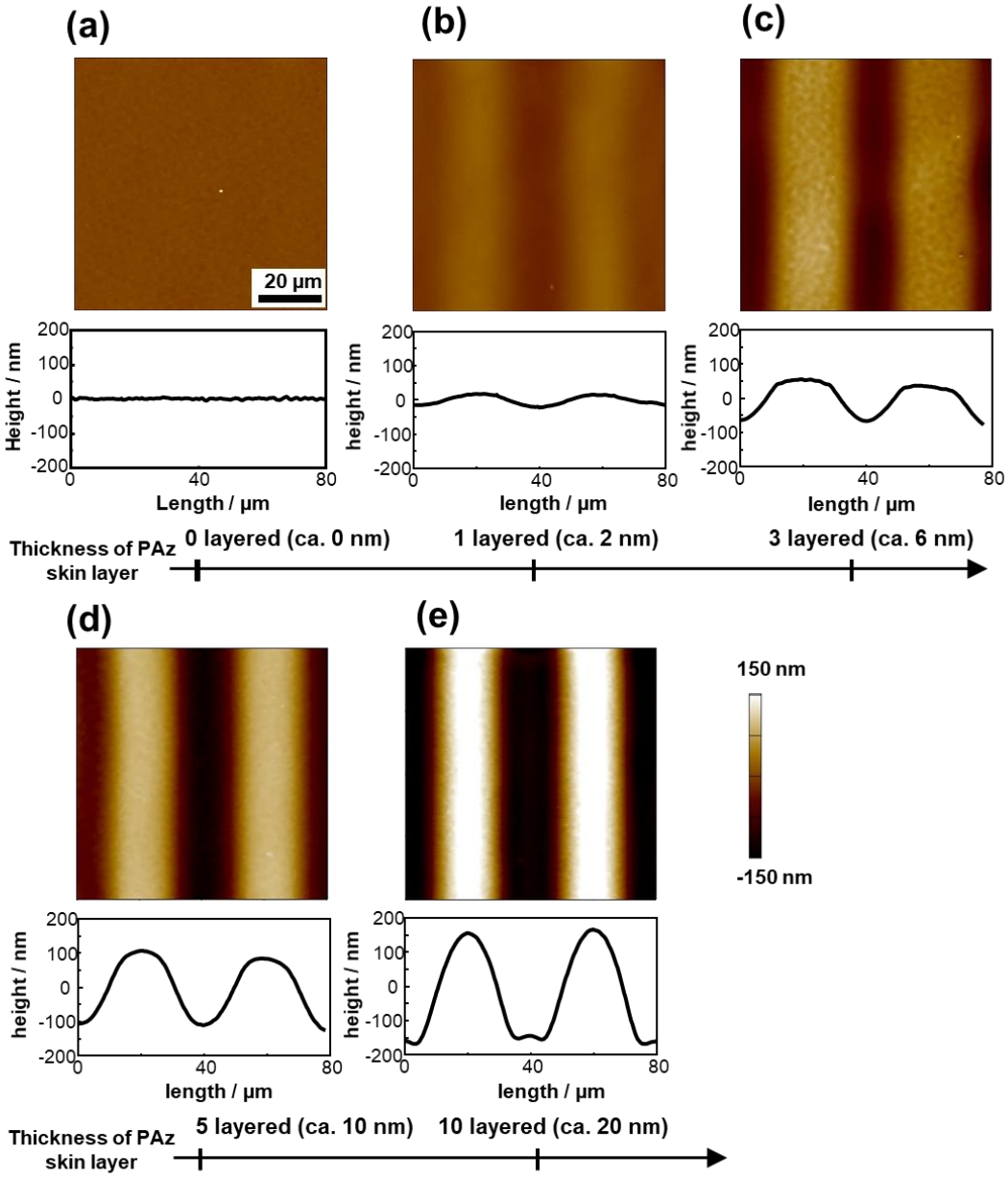

Figure 3-10. Photoinduced mass migration behavior of PCPBz films with the LS layer of PAz. Topographical AFM images (upper) and cross-sectional height profiles (lower) after stripe-patterned UV irradiation at 90 °C on PCPBz films (a) without a PAz layer, (b) with a 1-layered, and (c) 3-layered, (d) 5-layeredand (e) 10-layered LS film of PAz on the surface of 200-nm-thick PCPBz film.

the surface can generate a SRG with ca. 20-times larger surface undulation. The 10-layered PAz resulted in a top-to-bottom difference of 334 nm (Fig. 3-10e). Hence, a thicker top-coated PAz layer resulted in a larger deformation. For the 10-layered PAz film, the mass motion became saturated where the substrate surface was almost exposed.

Since the protrusions and the trenches preserves the polymer volume, this surface topography originates from a mass transfer. To evaluate the mass flow direction, we adopted a photomask with an "I"-shaped transparent window. Figure 3-11 shows the surface topographical image and height profile extracted along the line for a five-layered PAz/PCPBz film observed with a WLIM. Mass transfer occurred at the boundary region between the UV light irradiated and the non-irradiated areas. The height positions of UV-exposed and shaded areas were higher and lower, respectively. Hence, lateral mass flow occurred from the trans-Az area to the cis-rich-Az one of the PAz skin layer at the surface. The cis-Az surface had a larger wettability for polar solvents[50,51] as confirmed by the smaller values of θ_{gly} throughout the examined temperature range (Fig. 3-7). Thus, PAz in the cis-rich state has a higher surface tension than that in the trans state. These results agree with the reports by Ellison et al. for the surface fabrication by photopatterening onto an Az polymer[36] and observations in inkjet printed system[40]. The effect of linear UV light polarization was examined. As shown in Fig. 3-12, a polarization dependence was not observed. This fact also suggest that the observed mass transport is attributed to the Marangoni flow mechanism.

Figure 3-13 shows the top-to-bottom height difference as a function of the LS layer thickness of PAz. As the PAz layer thickness increased, the height difference was enhanced almost linearly. The PAz skin layer triggered mass motion of PCPBz in an amplified manner. Roughly 20 times larger thickness of PCPBz is affected from the PAz

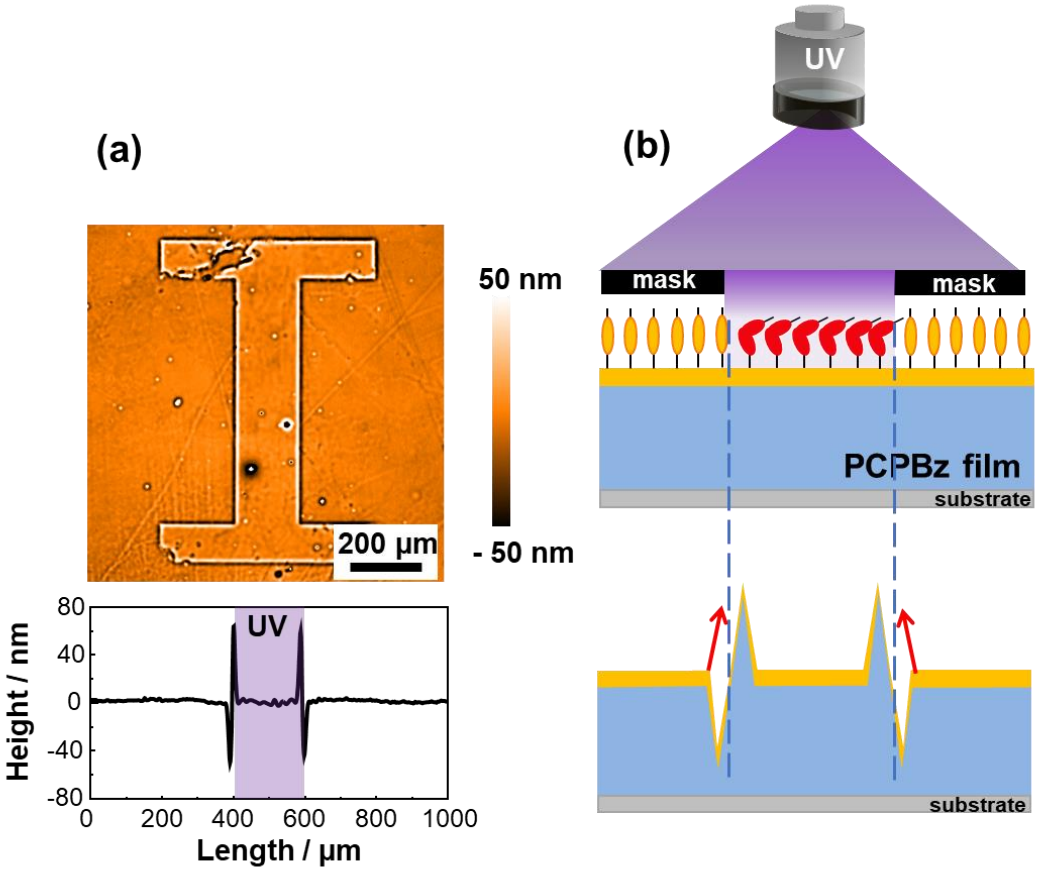

Figure 3-11. Direction of mass migration. (a) Topographical WLIM image (upper) cross-sectional height profile (lower) of a PCPBz film with a 5-layered PAz LS film at the surface after UV irradiation through a masked shaped like the letter "I". (b) Schematic illustration of the direction of mass migration.

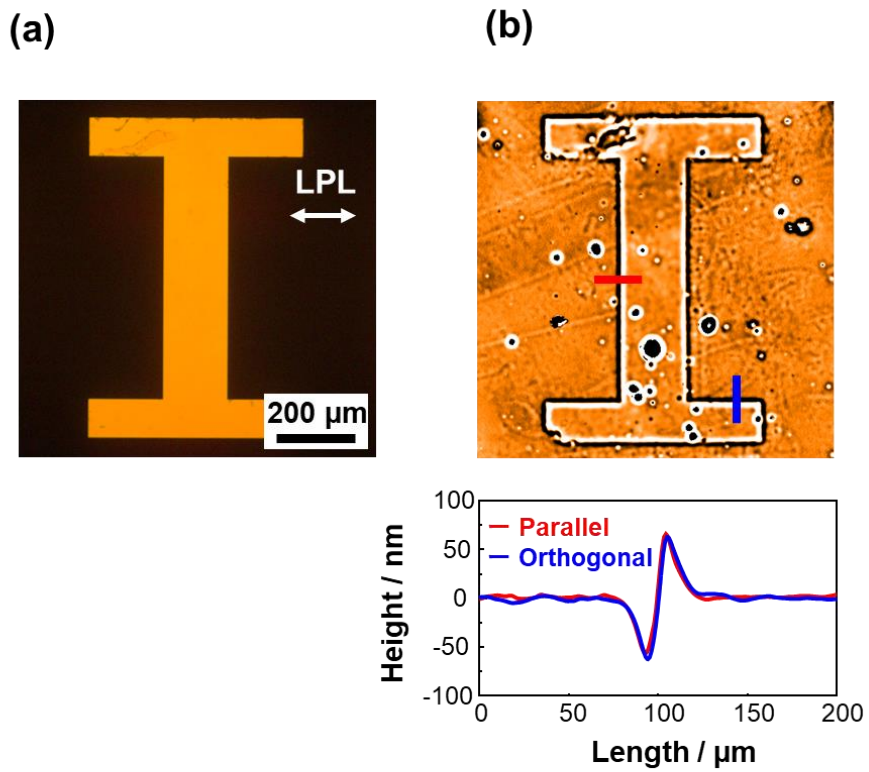

Figure 3-12. Polarization dependence. The surface morphology of PCPBz film (200 nm) covered with a 5-layered PAz LS film (10 nm) after linearly polarized UV light for 100 s at 90 °C. (a) Photomask and (b) resulting relief structure.

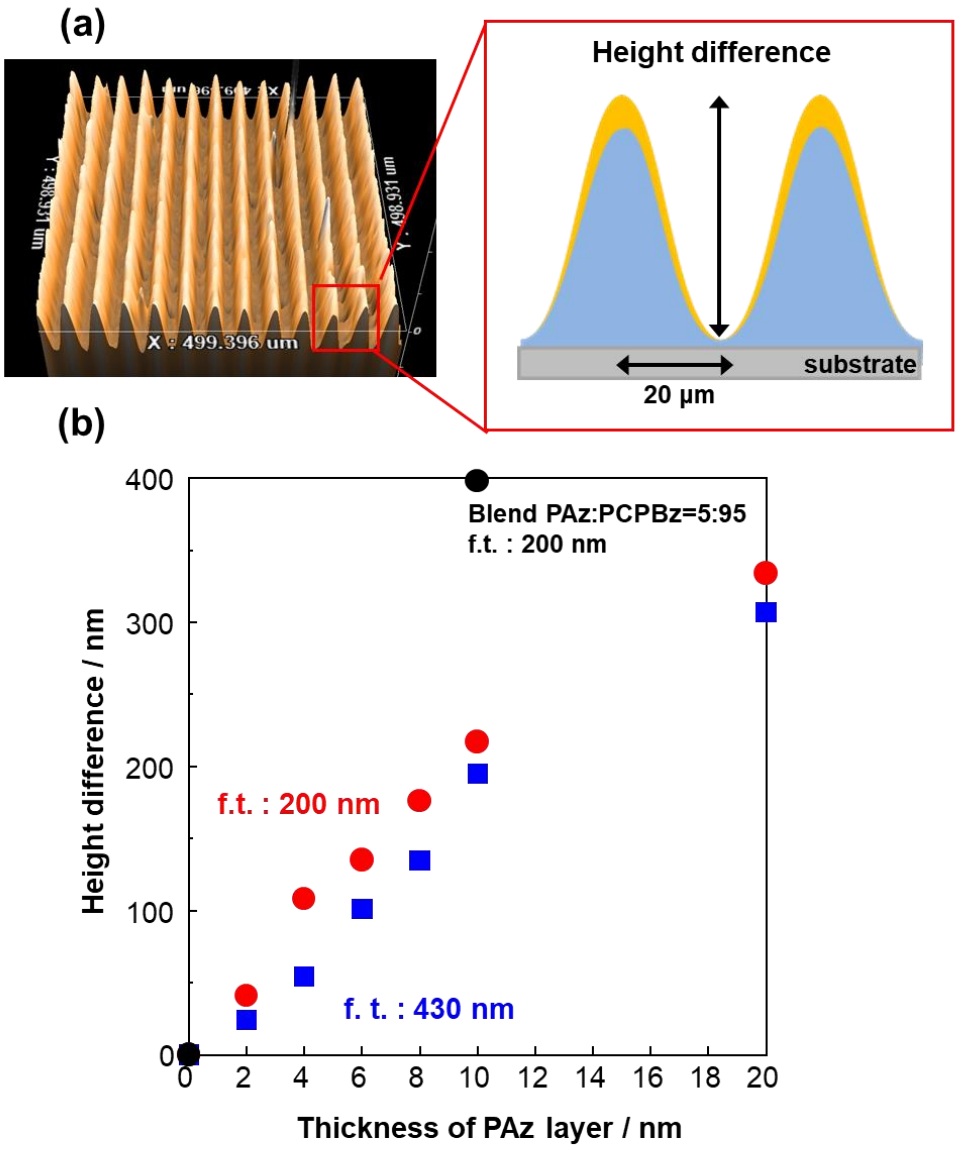

Figure 3-13. (a) Schematic illustration of the Top-to-bottom height difference induced by mass migration. (b) Top-to-bottom height difference of the SRG structure for PCPBz films with various deposition numbers of the PAz LS layer (layer thickness). Red and blue correspond to data for PCPBz films with initial thicknesses of 200 and 430 nm, respectively. Black square indicates data obtained for a 200-nm-thick surface segregated blended film (PAz:PCPBz = 5:95) film.

surface layer at each thickness. Our previous inkjet-printing study[40] revealed that a larger amount of surface ink results in a larger flow motion. The observed thickness dependence herein could be explained in the same manner. As the PCPBz base film thickness increased to 430 nm (blue symbols), the protrusion-trench height difference systematically became smaller compared to the case with a 200-nm thickness. It seems that the convection flow is more favorable for a thicker film, allowing back flow in the bottom region.

To monitor the dynamics of mass migration, the surface morphology was observed at different periods of UV light irradiation time for the 5-layerd PAz film on PCPBz film. Efficient mass migration comparable to that of PAz homopolymer[25] was observed in PAz/ PCPBz bilayer system within 200 s patterned UV light irradiation (Fig. 3-14). SRGs structure was erasable by uniform UV light irradiation at LC temperature of PAz and PCPBz. Then, SRGs was re-writable after second patterned UV light irradiation. Using above feature of SRGs formation, overwriting was demonstrated. The first patterning was performed with line-and-space photomask in the vertical position of polymer film. Subsequently, the second patterning was performed with parallel position of polymer films. In this way, overwriting microfabrication was successfully achieved with multiple UV light irradiation (Fig. 3-15).

A SCLCP with a cyanobiphenyl mesogene (PCB)[42] was covered with five-layered PAz LS film and photoirradiated using the same procedure (Fig. 3-16). A smectic A phase appeared at 90 °C. In this case, mass transport only appeared in the surface layer of PAz, and the base film of PCB was not transported. This drastically different behavior is attributed to the viscosity difference between the nematic (PCPBz) and smectic A (PCB) phases. For SCLCPs, an appreciable viscosity change between the nematic and

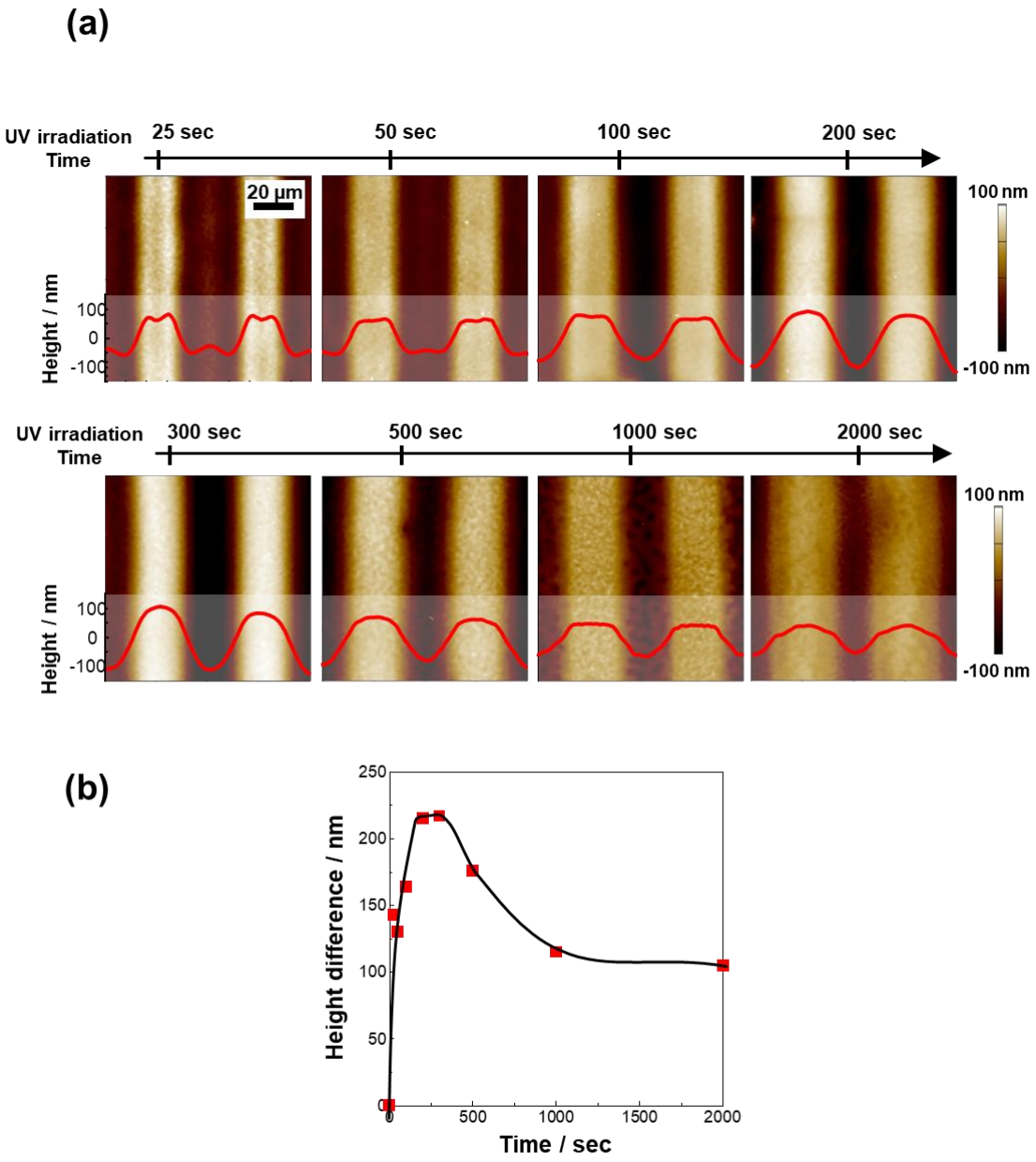

Figure 3-14. Photoinduced mass migration for a 5-layerd PAz film on PCPBz film at various periods of irradiation time. (a). UV light irradiation is performed through a stripe photomask (20 μm pitch) at 90 °C for 25-2000 s and (b) time-course profile of the resulting height difference.

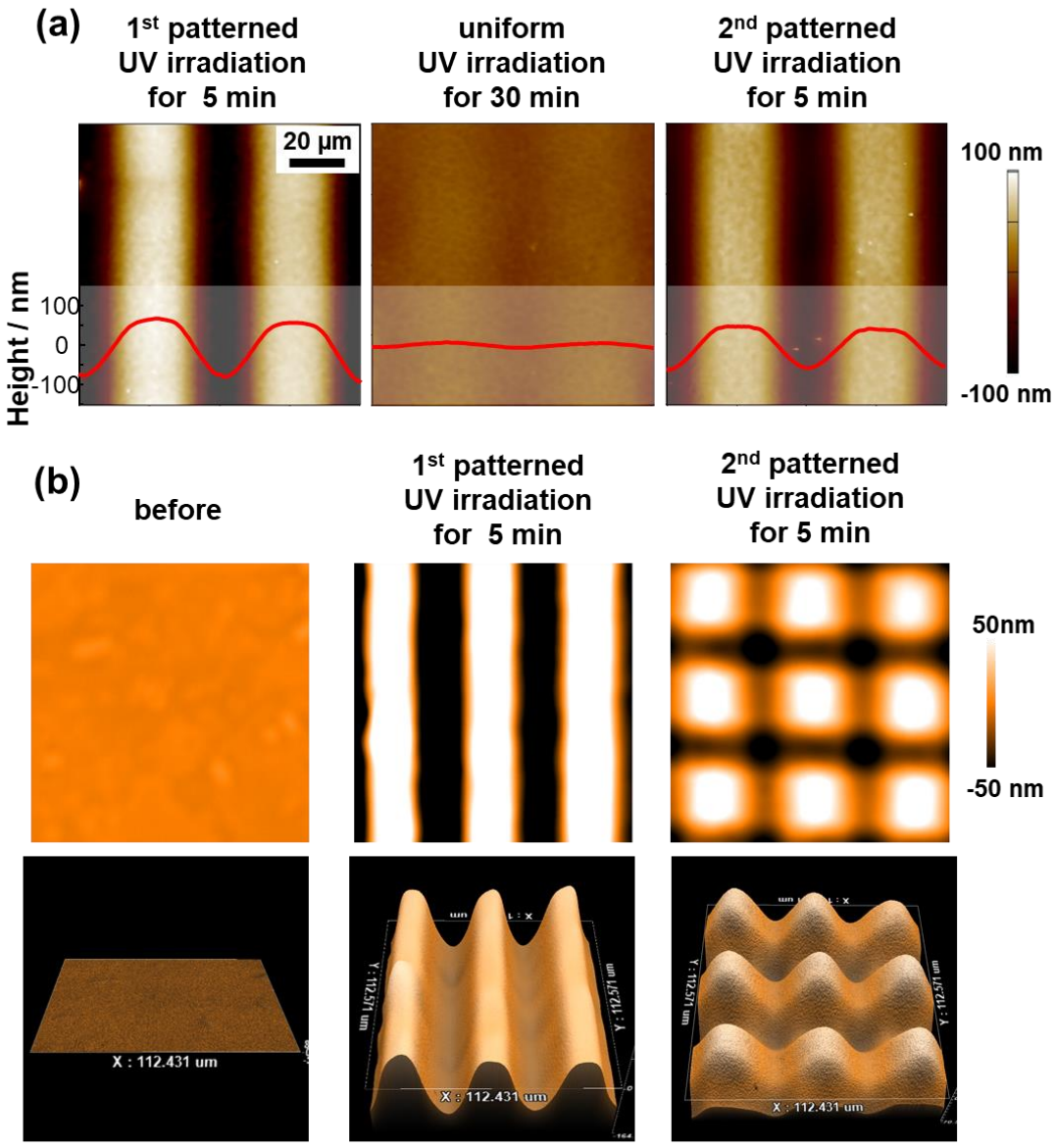

Figure 3-15. Re-writability and Over-writability of SRGs structure in a 5-layerd PAz film on PCPBz film at 90 °C. (a) AFM topographical images after 1st patterned irradiation, uniform irradiation and 2nd patterned irradiation. (b) WLIM topographical images and 3D images before irradiation, after 1st patterned irradiation and 2nd patterned irradiation.

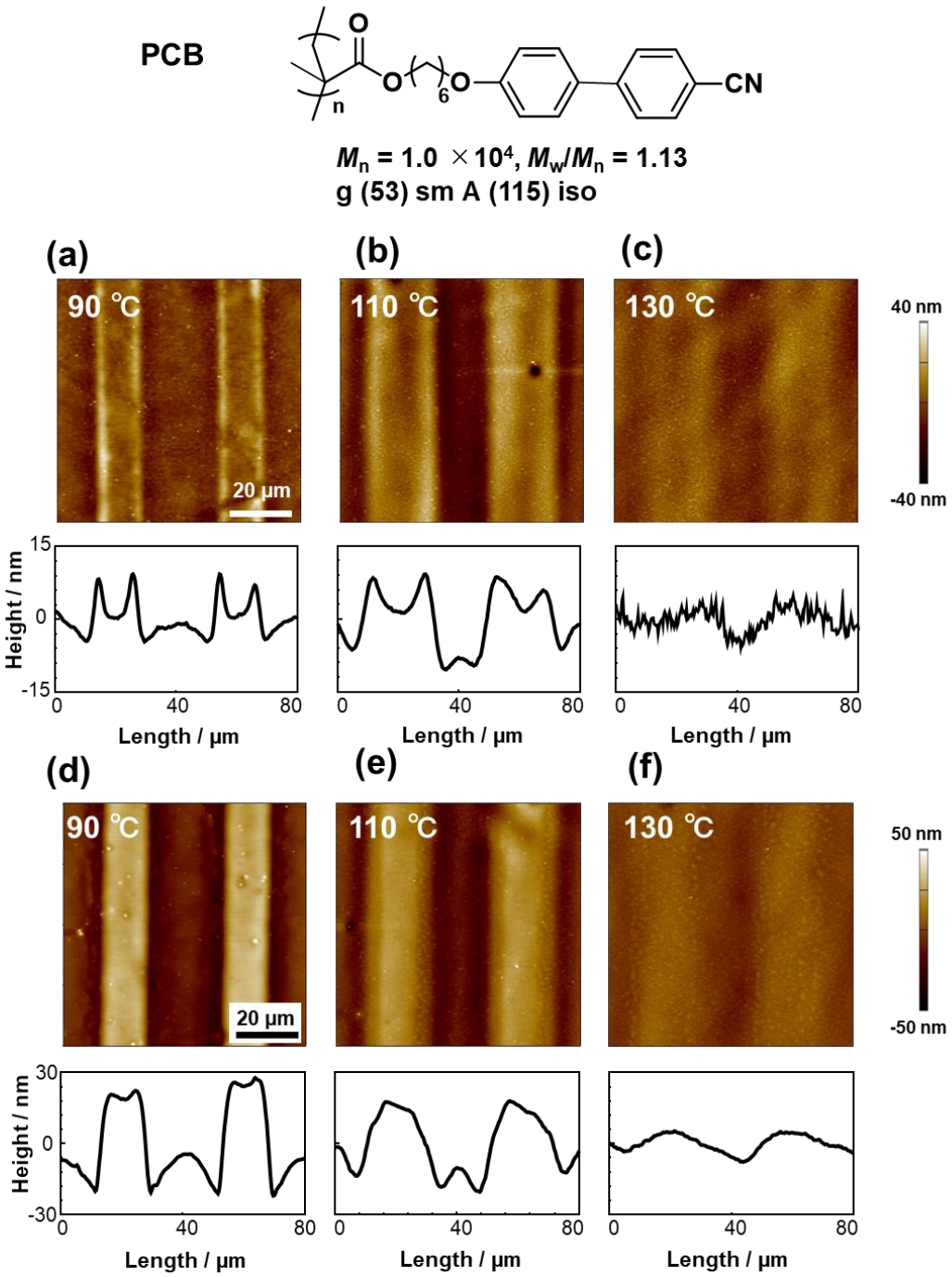

Figure 3-16. Photoinduced mass transport of PAz LS layer on PCB film. UV irradiation is performed through a stripe photomask (20 μm pitch). The layer numbers of PAz are 5 (a - c) and 10 (d - f).

isotropic thermal transition was not observed[55]. In contrast, the viscosity discontinuously changed with different orders of magnitude between the smectic and isotropic phases[40,55]. Our previous SRG systems of SCLCPs demonstrated that mass transport occurs from the trans-Az side (smectic A) area toward the cis-Az rich (isotropic) one[21-26]. Hence, a photoinduced phase transition to the isotropic state is necessary to reduce the film viscosity, and the previously observed SRG generation seems to be due to the Marangoni flow.

3-3-4. Photoinduced mass migration in PCPBz films with a surface segregated PAz layer

The surface segregation procedure is simple and very practical to set a photoresponsive skin layer. A 200-nm-thick mixed film of PAz and PCPBz (5:95 by weight) was annealed at 90 °C for 10 min. The θ_{gly} values of a mixture of PAz and PCPBz (5:95 by weight) after annealing at 90 °C for 10 min before and after UV irradiation were 99.2 ± 1.6° and 89.4 ± 1.6° at 25 °C, which agree well with those of the pure PAz film (Table 3-1). These results indicate that annealing selectively segregates the PAz component to the free surface[41-43].

UV light irradiation was performed onto this surface segregated film through a photomask (stripe pitch: 20 μm) for 300 s at 90 °C. Photoirradiation efficiently generated SRG patterns corresponding to the photomask stripe pattern (Fig. 3-17). The observed pattern was more efficient than that of the LS transferred one. The surface segregated skin layer of PAz should correspond to that of 10-nm-thick five-layered LS film. The black square in Fig. 3-13 indicates the height difference obtained in this procedure. The significantly larger transport motion is attributed to the stronger molecular interactions

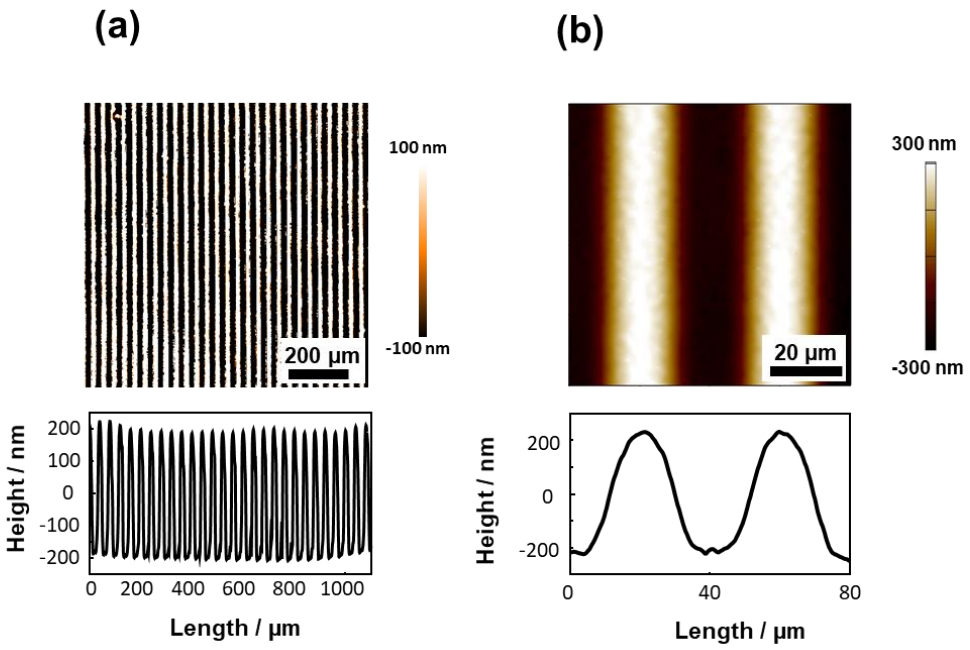

Figure 3-17. Photoinduced mass transport of surface segregated blended (PAz:PCPBz (5:95)) film. Topographical WLIM images (a) and AFM images (b) after UV irradiation at 90 °C through a stripe photomask (20 µm pitch).

between the top skin layer and the inner mesogens. The surface segregated PAz should have more significant interactions between the different mesogens with the concentration gradient at the boundary region of the two polymers. In contrast, the films were separately prepared and physically transferred in the LS deposition system, resulting in inefficient mesogen interactions between the layers.

3-3-5. Photoinduced mass migration in PAz films with a PC18 LS layer

Next, the system of a photoresponsive film covered with a photo-inert surface was explored (Fig. 3-3). A photo-inert long-chain side-chain polymer (PC18) layer was transferred by the LS method onto a PAz film, Then UV light was irradiated through a photomask. PC18 monolayer deposition was carried out under the same conditions used to form a monolayer spreading film of PAz on water (Fig. 3-3, 3-5). The PC18 layer was selected because LS deposition is readily performed and does not absorb light in the UV wavelength region. Expectedly, the PC18 molecular layer inhibited the surface tension difference of the inner PAz film due to UV light irradiation.

As a control experiment, a pure 200-nm-thick PAz film was first exposed to patterned UV irradiation (conventional system). As previously confirmed[25], the SRG structure was generated efficiently and the top-to-bottom height reached to 335 nm (Fig. 3-18a). When a PC18 monolayer was transferred to the PAz film by the LS method, the transport motion was greatly hindered, and the height difference was only 30 nm (Fig. 3-18b). Therefore, the PC18 monolayer approximately 1–2-nm thick[56] strongly suppressed the formation of SRG, although more than 99% of the film component was composed of PAz. The surface of the PAz film covered with PC18 monolayer gave θ_{gly} of 106.9 ± 0.6° and 106.8 ± 0.6° before and after UV irradiation, respectively, at 25 °C. These results

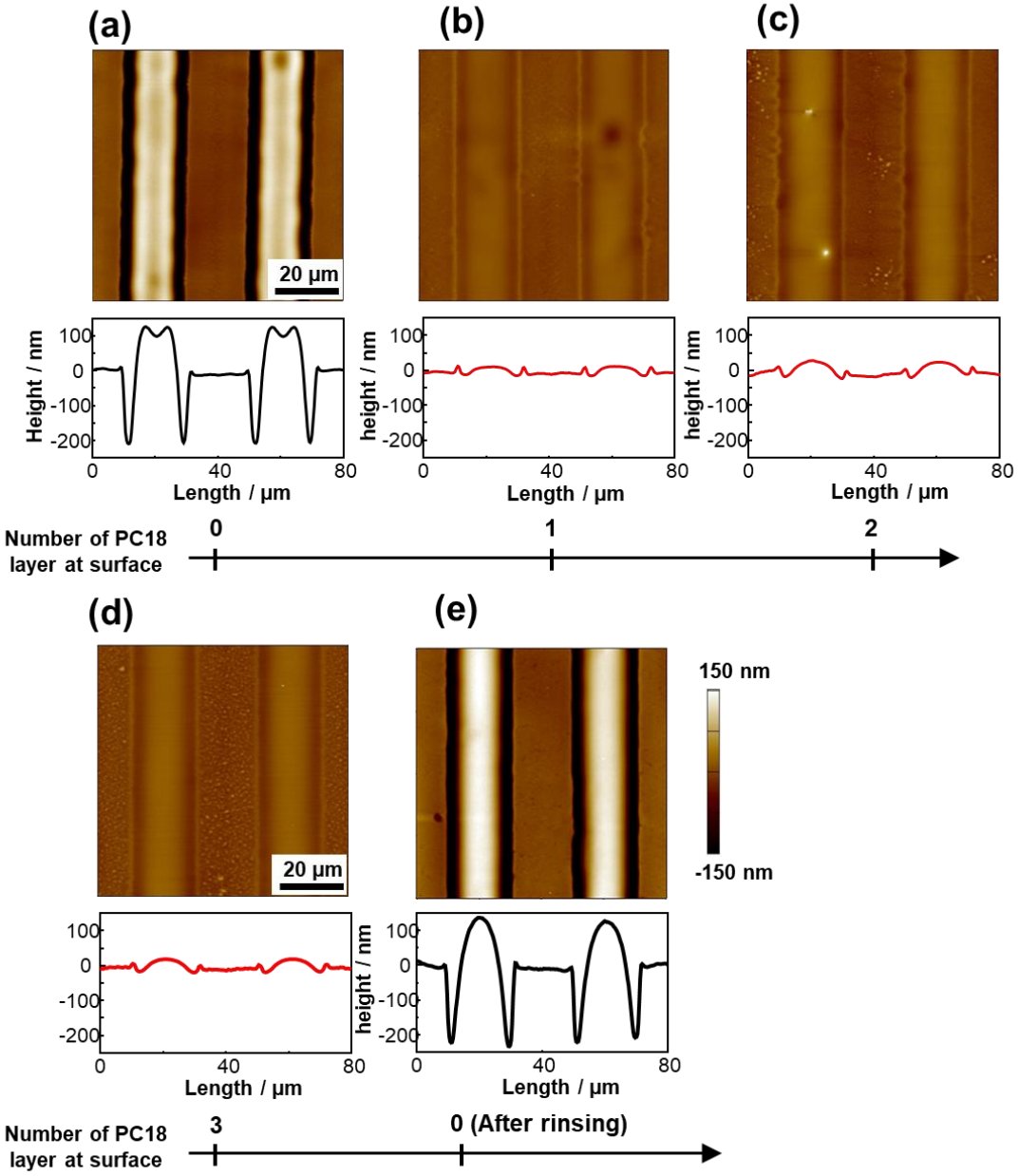

Figure 3-18. Suppression of mass transport of a 200-nm-thick PAz film by a PC18 top layer. Topographical AFM images (upper) after cross-sectional height profile (lower) stripe-patterned UV irradiation at 90 °C on a (a) pure PAz film and those (b) with a 1-layered, (c) 2-layered and (d) 3-layered PC18 LS films on the surface. In (d), the same data is shown after removal of the PC18 LS monolayer.

agree precisely with the pure PC18 film surface without changes upon UV light irradiation. Thus, one monolayer can prevent a photoinduced surface tension change. Further deposition of three layers of PC18 did not enhance the effect (Fig. 3-18d). Figure 3-19 shows the above situation. To prevent mass transfer motion, one monolayer coverage is sufficient regardless of the initial film thickness. The minor motions leading to 30 nm undulations may be attributed to the effect of the large viscosity alternation formed at the boundary between the smectic A and isotropic phases[40]. In this UV irradiation condition, photoisomerization to the cis-rich photostationary state fully proceeded. To confirm the role of the surface, the PC18 monolayer was successively removed by rinsing the film in cyclohexane at 20 °C (Fig. 3-20). When the monolayer was detached, the large transport motion was recovered (Fig. 3-18e).

Viswanathan et al.[57] demonstrated that the deposition of layer-by-layer polyelectrolyte ultrathin film on an amorphous Az polymer significantly impeded the mass transport motions. Later, Ober's group[58] showed that films of Az SCLCPs with semifluorinated tails at the Az mesogen displayed a similar restriction. However, these investigations did not mention the surface tension change upon irradiation. Since the hinderance of the migration motion is similar with our results and our PC18 monolayer hardly has a steric constraint, the contribution of the surface tension changes must be considered, even for the former studies[57,58].

3-3-6. SRGs film essentially without color

The SRG systems based on Az polymers are colored in yellow or red. The Az unit is essential for the photoinduced mass migration, but the existence of this strongly light absorbing chromophore can be a drawback after relief formation for many optical

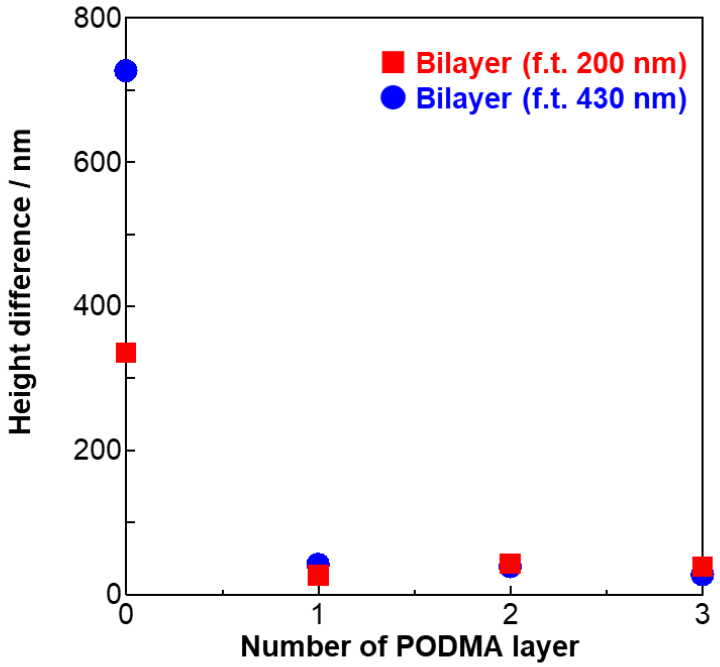

Figure 3-19. Top-to-bottom height difference of the SRG structure of PAz films with various deposition numbers of the PC18 LS layers. Patterned irradiation was performed at 90 °C. Red and blue correspond to data for PAz films with initial thicknesses of 200 and 430 nm, respectively.

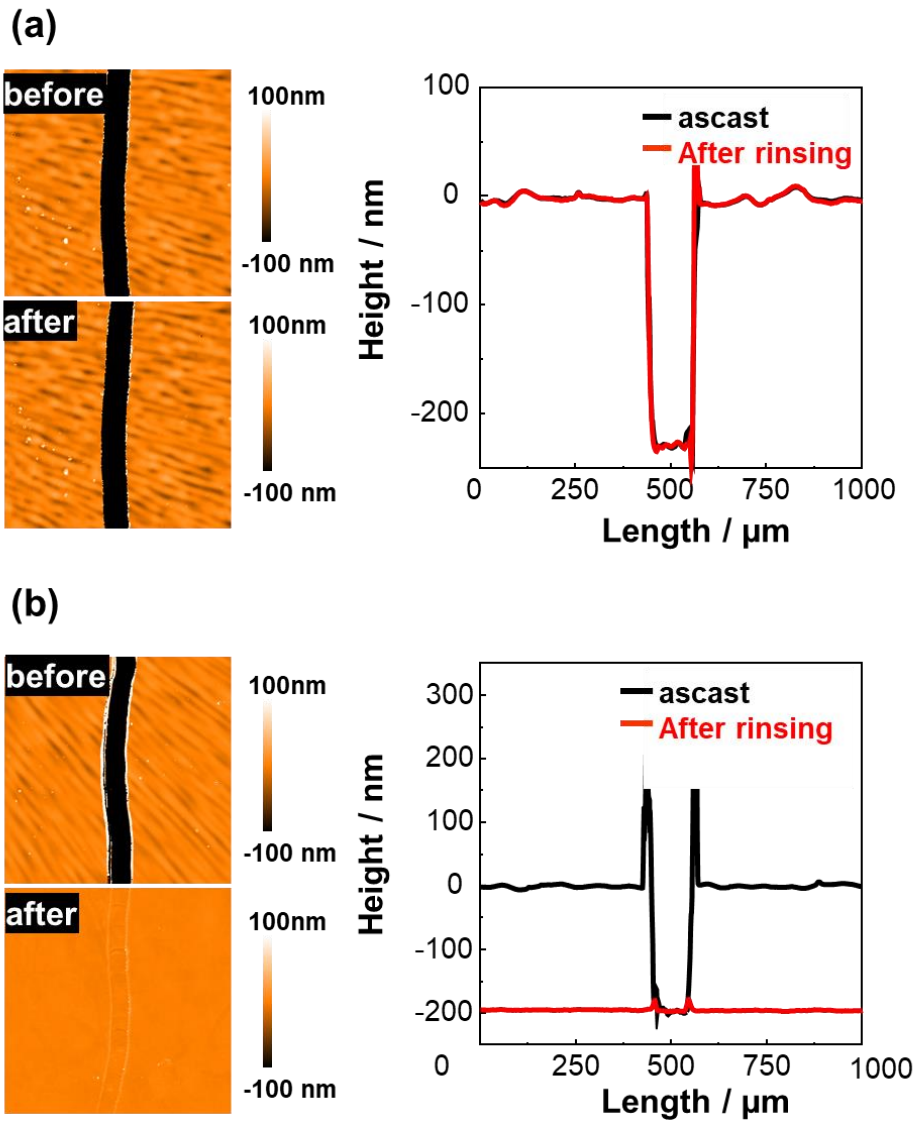

Figure 3-20. Selected removal of the printed polymer ink and the morphology change. (a) Solubility tests showing that PAz is not dissolved in cyclohexane (b) while PC18 fill was fully dissolved in this solvent as revealed with scratched film of PAz and PC18 films.

applications such as optical storage, waveguide couplers, liquid crystal alignment layers, etc. Therefore, SRG systems without color are favored. So far, post-decoloration of Az polymer films have been attempted by detaching the Az unit via solvent extraction from supramolecular polymers[24, 55] or by heat-cleavage of the chemical bond[60].

This study offers another strategy to provide colorless SRG films. Figure 3-21 displays photos of pure PAz, PAz-PCPBz blend (5:95) and pure PCPBz films after irradiation with patterned UV light. The pure PAz (Fig. 3-21a, left) and PCPBz (Fig. 3-21a, right) films were yellowish and colorless as recognized by the naked eye, respectively. Similar to the PCPBz film (right), the surface segregated PAz/PCPBz film (Fig. 3-21a, middle) was almost colorless. The difference was obvious in the UV-visible absorption spectra. For the surface segregated blended film, the large π–π^* absorption band peaking at 348 nm was significantly reduced in the blend film, generating a spectrum similar to that of pure PCPBz film. In this way, the selective introduction of Az unit at the surface can be a facile and useful strategy to fabricate colorless SRG films.

3-3-7. Discussion: Revisiting previous reported SRG studies

Although the suppression of SRG formation by the surface layer has been reported[57,58], this chapter demonstrates, for the first time, photoinduction of the surface morphology for photo-inert polymer films by the photoactive surface layer. To date, SRG studies have been conducted for films with photoreactive units existing in the entire film. For these films, photoirradiation induces multiple changes simultaneously such as a viscosity change, molecular order and orientation change, and surface tension change. Kim et al.[36] showed the surface fabrication of an Az polymer via the Marangoni flow, but these other factors may also be involved.

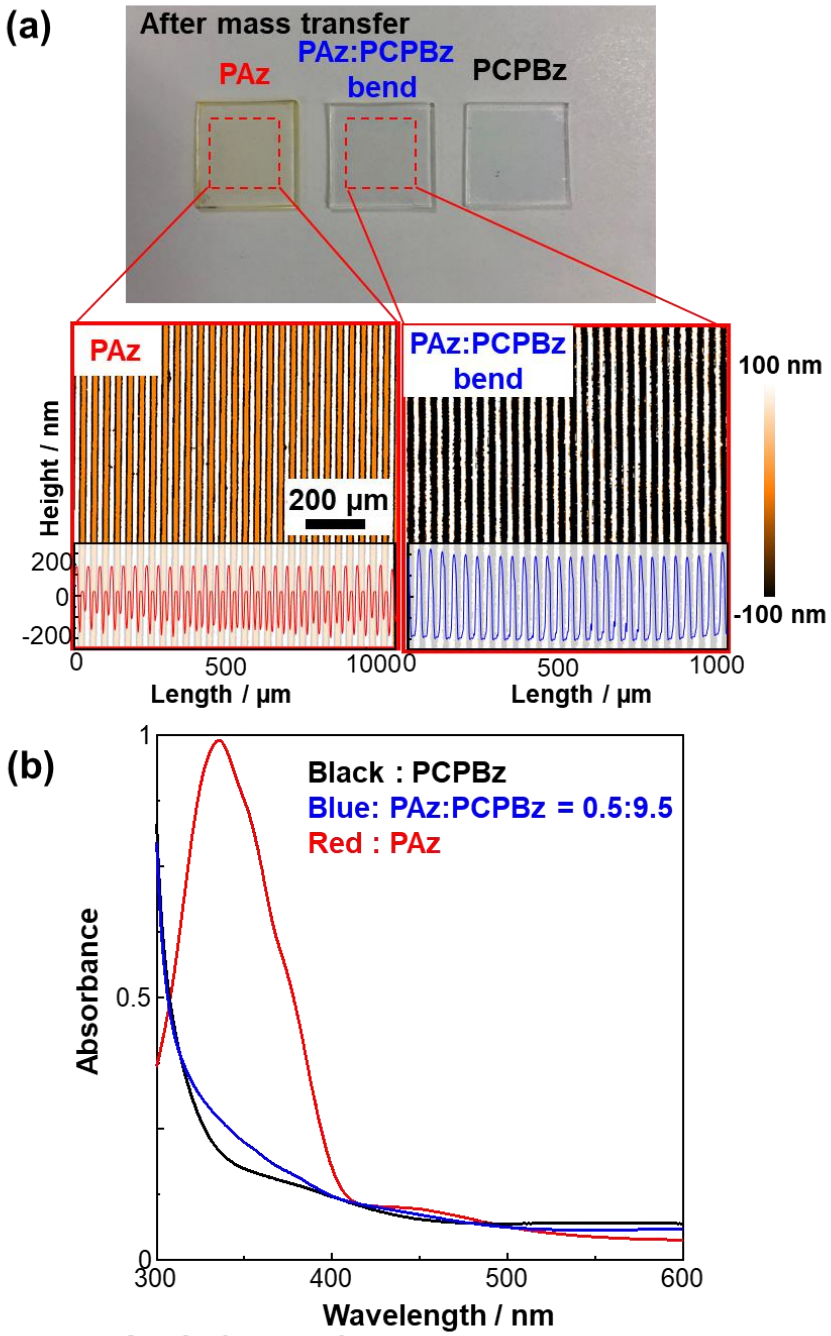

Figure 3-21. SRG films after patterned irradiation at 90 °C. Photos of SRG films of a pure PAz film (a, left), surface segregated blended (PAz:PCPBz (5:95)) film (a, middle), and pure PCPBz film (a, right). UV–visible absorption spectra before light irradiation (b). All samples are 200-nm thick.

Our strategy of preparing a surface skin layer provides a system that allows arguments purely based on the surface effect. It is confirmed that the surface tension gradient should be the primary factor, and the other physical changes inside the film are negligible in our system. A small change in the surface tension can cause large mass convection in polymer films[39]. Hence, the surface tension gradient should be taken into more consideration in SRG studies. For example, Koskela et al.[28] reported interesting data where only 1–2% introduction of an Az chromophore into a polymer via a supramolecular framework can induce SRG structures. It is possible that the surface segregation of more hydrophobic Az molecules to the surface facilitates the mass transport process.

In our SCLCP films, the transport direction was independent of linear light polarization[54] (Fig. 3-12), strongly suggesting that the Marangoni effect is the plausible mechanism. In most of SRG studies using amorphous Az polymers, a strong polarization dependence has been observed. Such a polarization dependence cannot be explained by the surface tension gradient. Angular selective excitation and orientation effects are involved in such systems. Hence, complex factors should be involved to precisely understand morphology induction.

3-4. Conclusions

In conclusion, this chapter demonstrated the essential contribution of the topmost surface to the macroscopic mass transport process in SCLCP films. The presence of only a molecular level skin layer at the free surface is sufficient to promote or terminate a large-scale surface deformation. These results are well understood by the Marangoni flow driven by the light-triggered surface tension instability. Although only a few previous reports mentioned the significance of the surface effect[57,58], several recent studies

emphasized the importance of surface proximities for both LC[40,58] and amorphous[17,18,36,57] polymers. To precisely understand the behavior, the driving mechanism, including the surface effect, should be reconsidered.

In the surface photoalignment of LC systems, a small amount of photoreactive molecules on a solid substrate can control the alignment of a large number of non-photorsponsive LC molecules. Such a surface is called the command layer[45,52,61] Recent investigations have revealed that a photoactive command layer can be placed at the free surface in SCLCP films[41-47]. Similarly, the present work offers another command layer scenario where large molecular amplification is reflected in macroscopic surface morphing. This strategy should realize light-assisted microfabrications for light-inert polymer films.

References

[1] P. Rochon, E. Batalla, A. Natansohn, *Appl. Phys. Lett.* **1995**, 66, 136-138.

[2] D. Y. Kim, S. K. Tripathy, L. Li, J. Kumar, *Appl. Phys. Lett.* **1995**, 66, 1166-1168.

[3] N. K. Viswanathan, D. Y. Kim, S. Bian, J. Williams, W. Liu, L. Li, L. Samuelson, J. Kumar and S. K. Tripathy. *J. Mater. Chem.* **1999**, 9 1941–1955.

[4] A. Natansohn, P. Rochon, *Chem. Rev*. **2002**, 102, 4139–4175.

[5] K. G. Yager, C. J. Barrett, *Curr. Opin. Solid State Mater. Sci*. **2001**, 5, 487–494.

[6] K. G. Yager, C. J. Barrett, *J. Photochem. Photobiol. A* **2006**, 182, 250–261.

[7] C. J. Barrett, A. Natansohn, P. L. Rochon, *J. Phys. Chem.* **1996**, 100, 8836–8842.

[8] C. J. Barrett, P. L. Rochon, A. Natansohn, *J. Chem. Phys.* **1998**, 109, 1505–1516.

[9] J. Kumar, L. Li, X. L. Jiang, D. Y. Kim, T. S. Lee, S. Tripathy, *Appl. Phys. Lett*. **1998**, 72, 2096–2098.

[10] O. Baldus, S. J. Zilker, *Appl. Phys. B: Laser Opt*. **2001**, 72, 425–427.

[11] K. Sumaru, T. Fukuda, T. Kimura, H. Matsuda, T. Yamanaka, *J. Appl. Phys*. **2002**, 91, 3421–3430.

[12] T. G. Pedersen, P. M. Johansen, N. C. R. Holme, P. S. Ramanujam, S. Hvilsted, *Phys. Rev. Lett*. **1998**, 80, 89–92.

[13] P. Karageorgiev, D. Neher, B. Schulz, B. Stiller, U. Pietsch, M. Giersig, L. Brehmer, *Nat. Mater.* **2005**, 4, 699–703.

[14] S. Lee, H. S. Kang, J. K. Park, *Adv. Mater.* **2012**, 24, 2069–2103.

[15] N. Hurduc, B. C. Donose, A. Macovei, C. Paius, C. Ibanescu, D. Scutaru, M. Hamel, N. Branza-Nichita, L. Rocha, *Soft Matter* **2014**, 10, 4640–4647.

[16] N. Mechau, D. Neher, V. Börger, H. Menzel, K. Urayama, *Appl. Phys. Lett*. **2003**, 81, 4715–4717.

[17] A. Ambrosio, L. Marrucci, F. Borbone, A. Roviello, P. Maddalena, *Nat. Commun*. **2012**, 3, 989.

[18] A. Ambrosio, P. Maddalena, L. Marrucci, *Phys. Rev. Lett.* **2013**, 110, 146102.

[19] M. Saphiannikova, V. Toshchevikov, *J. Soc. Inf. Disp*. **2015**, 23, 146–153.

[20] V. Toshchevikov, J. Ilnytskyi, M. Saphiannikova, *J. Phys. Chem. Lett.* **2017**, 8, 1094–1098.

[21] T. Ubukata, T. Seki, K. Ichimura, *Adv. Mater.* **2000**, 12, 1675–1678.

[22] T. Ubukata, M. Hara, K. Ichimura, T. Seki, *Adv. Mater.* **2004**, 16, 220–223.

[23] N. Zettsu, T. Ogasawara, R. Arakawa, S. Nagano, T. Ubukata, T. Seki,. *Macromolecules* **2007**, 40, 4607–4613.

[24] N. Zettsu, T. Ogasawara, N. Mizoshita, S. Nagano, T. Seki, *Adv. Mater.* **2008**, 20, 516–521.

[25] J. Isayama, S. Nagano, T. Seki, *Macromolecules* **2010**, 43, 4105–4112.

[26] T. Seki, *Macromol. Rapid Commun*. **2014**, 35, 271–290.

[27] J. Gao, Y. He, F. Liu, X. Zhang, Z. Wang, X. Wang, *Chem. Mater*. **2007**, 19, 3877–3881.

[28] J. E. Koskela, J. Vapaavuori, R. H. A. Ras, A. Priimagi, *ACS Macro Lett*. **2014**, 3, 1196–1200.

[29] X. Wang, J. Vapaavuori, X. Wang, R. G. Sabat, C. Pellerin, C. G. Bazuin, *Macromolecules* **2016**, 49 4923- 4934.

[30] H. Nakano, T. Takahashi, T. Kadota, Y. Shirota, *Adv. Mater.* **2002**, 14, 1157–1160.

[31] T. Ubukata, Y. Moriya, Y. Yokoyama, *Polym. J*. **2012**, 44, 966–972.

[32] T. Ubukata, M. Nakayama, T. Sonoda, Y. Yokoyama, H. Kihara, *ACS Appl. Mater. interfaces* **2016**, 8, 21974–21978.

[33] T. Ubukata, S. Fujii, Y. Yokoyama, *J. Mater. Chem*. **2009**, 19, 3373-3377.

[34] A. Kikuchi, Y. Harada, M. Yagi, T. Ubukata, Y. Yokoyama, J. Abe, *Chem. Commun*. **2010**, 46, 2262–2264.

[35] J. W. Park, S. Nagano, S.-J. Yoon, T. Dohi, J. Seo, T. Seki, S. Y. Park, *Adv. Mater*. **2013**, 25, 1354-1359.

[36] C. B. Kim, J. C. Wistrom, H. Ha, S. X. Zhou, R. Katsumata, A. R. Jones, D. W. Janes, K. M. Miller, C. J. Ellison, *Macromolecules* **2016**, 49, 7069–7076.

[37] J. M. Katzenstein, D. W. Janes, J. D. Cushen, N. B. Hira, D. L. McGuffin, N. A. Prisco, C. J. Ellison, *ACS Macro Lett.* **2012**, 1, 1150–1154.

[38] A. R. Jones, C. B. Kim, S. X. Zhou, H. Ha, R. Katsumata, G. Blachut, R. T. Bonnecaze, C. J. Ellison, *Macromolecules* **2017**, 50, 4588–4596.

[39] T. A. Arshad, C. B. Kim, N. A. Prisco, J. M. Katzenstein, D. W. Janes, R. T.

Bonnecaze, C. J. Ellison, *Soft Matter* **2014**, 10, 8043–8050.

[40] I. Kitamura, K. Oishi, M. Hara, S. Nagano, T. Seki, *Sci. Rep*. **2019**, 9, 2256.

[41] K. Fukuhara, Y. Fujii, Y. Nagashima, M. Hara, S. Nagano, T. Seki, *Angew. Chem. Int. Ed*. **2013**, 52, 5988–5991.

[42] K. Fukuhara, S. Nagano, M. Hara, T. Seki, *Nat. Commun.* **2014**, 5, 3320.

[43] T. Nakai, D. Tanaka, M. Hara, S. Nagano, T. Seki, *Langmuir* **2016**, 32, 909–914.

[44] S. Nagano, *Langmuir* **2019**, 35, 5673–5683.

[45] T. Seki, *Bull. Chem. Soc. Jpn*. **2018**, 91, 1026–1057.

[46] N. Kawatsuki, K. Miyake, M. Kondo, *ACS Macro Lett.* **2015**, 4, 764–768.

[47] K. Miyake, H. Ikoma, M. Okada, S. Matsui, M. Kondo, N. Kawatsuki, *ACS Macro Lett*. **2016**, 5, 761–765.

[48] C. Noël, C. Friedrich, V. Leonard, P. L. Barny, G. Ravaux, J. C. Dubois, *Makromol. Chem. Macromol. Symp*. **1989**, 24, 283-301.

[49] M. Sano, T. Murase, M.Hara, S. Nagano, Y. Shinohara, Y. Amemiya, T. Seki, *Mol. Cryst. Liq. Cryst*. **2015**, 617, 5-13.

[50] G. Möller, M. Harke, H. Motschmann, D. Prescher, *Langmuir* **1998**, 14, 4955-4957.

[51] C. L. Feng, Y. J. Zhang, J. Jin, Y. L. Song, L. Y. Xie, G. R. Qu, L. Jiang, D. B. Zhu, *Langmuir* **2001**, 17, 4593-4597.

[52] T. Seki, M. Sakuragi, Y. Kawanishi, Y. Suzuki, T. Tamaki, R. Fukuda, K. Ichimura, *Langmuir* **1993**, 9, 211–218.

[53] K. Aoki, T. Iwata, S. Nagano, T. Seki, *Macromol. Chem. Phys.* **2010**, 211, 2484–2489.

[54] N. Zettsu, T. Fukuda, H. Matsuda, T. Seki, *Appl. Phys. Lett*. **2003**, 83, 4960–

4962.

[55] K. M. Lee, C. D. Han, *Macromolecules* **2003**, 36, 8796-8810

[56] T. Arndt, A. J. Schouten, G. F. Schmidt, G. Wegner, *Makromol. Chem*. **1991**, 92, 2215-2229.

[57] N. K. Viswanathan, S. Balasubramanian, L. Li, J. Kumar, S. K. Tripathy, *J. Phys. Chem. B* **1998**, 102, 6064–6070.

[58] F. You, M. Y. Paik, M. Häckel, L. Kador, D. Kropp, H. W. Schmidt, C. K. Ober, *Adv. Funct. Mater*. **2006**, 16, 1577-1581.

[59] S. Mitsui, S. Nagano, M. Hara, T. Seki, *Crystals* **2017**, 7, 52.

[60] L. M. Goldenberg, L. Kulikovsky, O. Kulikovska, J. Stumpe, *J. Mater. Chem*. **2009**, 19, 8068–8071.

[61] K. Ichimura, Y. Suzuki, T. Seki, A. Hosoki, K. Aoki,. *Langmuir* **1988**, 4, 1214–1216.

Chapter IV

Photo-triggered surface relief formation of polystyrene films based on the Marangoni flow driven by a surface photoresponsive skin layer

4-1. Introduction

Surface relief gratings (SRGs) are widely investigated in azobenzene (Az)-containing polymer films such as amorphous polymers[1-16], side-chain liquid crystal polymers (SCLCP)[17-25], supramolecular systems[20,24-27] and low molecular weight amorphous materials[28]. Key aspects of these SRG processes have been recapitulated as the action of photoisomerization of Az units distributed in the entire films. In chapter III, the author have demonstrated that a photoresponsive azobenzene layer existing only at the surface of a non-photoresponsive liquid crystalline polymer film can induce mass migration by patterned UV light irradiation, resulting in the SRG structure[29]. This process is explained by the Marangoni flow triggered by the photoinduced surface tension change of the surface layer[30-35].

SRGs can be applied to rewritable holographic optical memory storage[36], alignment of colloidal nano-particles[18], directing self-assembly of block copolymer[37,38], distributed feedback laser[39,40] and photonic crystals[41]. For these potentials towards optical applications, an efficient SRGs formation in colorless polymer films is required. To fulfill this demand, some attempts have already been proposed: detachable Az molecular systems[20,24-27] and other photochromic molecular systems[43-45] exhibiting no strong absorption in the visible light region. The author have developed a simple SRGs formation system of surface modified films composed of non-photoreactive colorless nematic-SCLCP films covered with a very thin Az polymer (PAz) skin layer[29].

In this chapter, we explored the SRGs formation for widely commercially available polystyrene (PS) films covered with a thin photoresponsive SCLC-PAz skin layer at the free surface (Fig. 4-1a). Careful explorations of the PAz/PS systems showed that the Marangoni effect is the adequate mechanism, which has not been considered in previous studies[1-16]. Photoinduced surface morphing of PS films based on the photochemical reactions of PS has previously been demonstrated by Ellison's[30] and Ubukata's[46] groups. We expect that our strategy is not limited to PS systems, and that SRGs formation in commercially available general polymer films such as various amorphous poly(meth)acrylates can be also used.

4-2. Experimental

4-2-1. Materials and polymer synthesis

Az-containing polymers[35] (PAz, Fig. 4-1b) were synthesized from the corresponding monomer by atom transfer radical polymerization (ATRP). Polystyrenes with three different molecular weights (PS10, PS20 and PS30, Fig. 4-1c) were purchased from Toyo Soda Manufacturing Co., Ltd, Japan (PS10) and Sigma-Aldrich, USA (PS20 and PS30), respectively and were used without further purification. Chemical structures of all polymers used in this study are displayed in Fig. 4-1 and the characterization data are listed in Table 4-1.

4-2-2. Film preparation

PS10 films were prepared by spin coating (2000 rpm, 60 s) (Mikasa, Japan) from toluen solutions (typically 5.5 wt% in toluene) onto clean quartz substrate (typical film thickness: approximately 200 nm).

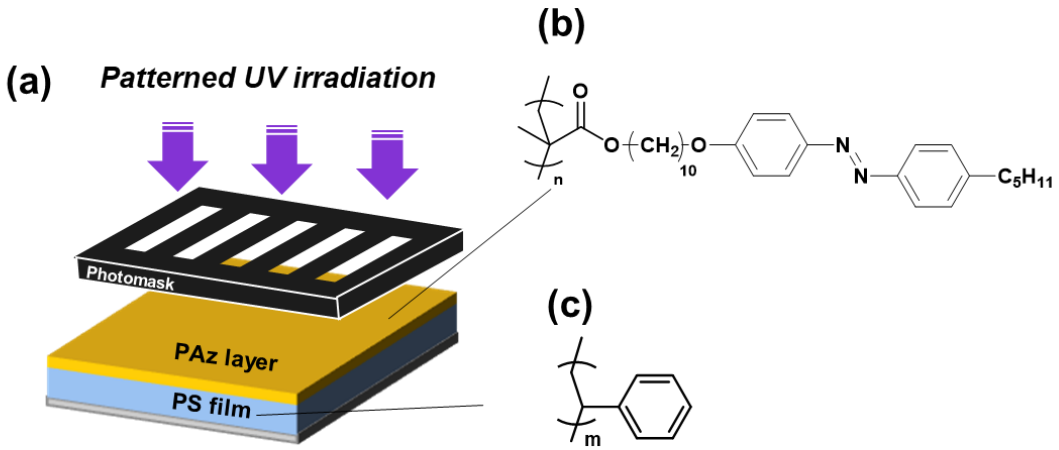

Figure 4-1. Schematic of photo-triggered morphology system (a) and chemical structures of PAz (b) and PS (c).

Table 4-1. Characterizations of the polymers used in this study.

Polymer	M_w (M_w/M_n)	Degree of polymerization	Thermophysical Properties / ° C	Water contact angle θ / deg
PAz	1.4×10^4 (1.08)	26	g (45) sm C (87) sm A (110) iso	108.2±0.8
PAz (UV)				100.6±0.8
PS10	1.0×10^3 (1.01)	10	g (15) rubber	102.7±1.1
PS20	1.8×10^3 (1.05)	18	g (61) rubber	101.8±0.7
PS30	3.5×10^3 (1.05)	34	g (82) rubber	101.5±0.8

UV: under UV light irradiation, g: glass, sm: smectic, iso: isotropic

Surface segregated films of PAz layer/PS10, PS20 and PS30 were prepared from a 5.5

wt% mixed solution of chloroform containing 5, 10 % of PAz to PS (10, 20 and 30) by weight. The films were subsequently annealed at 90 °C for 1 min before photoirradiation, allowing the surface segregation of PAz on the PS film.

Polymer films for static contact angle measurement were prepared from 5.5 wt% solution chloroform.

4-2-3. Langmuir-Schaefer deposition

PAz monolayer deposition onto PS10 film were performed by Langmuir-Schaefer (LS) method by same set-up in previous chapters.

4-2-4. Light irradiation

UV-light irradiation (365 nm) was performed with a same set-up in previous chapters.

Schematic illustrations of sample preparations (spincoating, LS method and light irradiation) are shown in Fig. 4-2a.

4-2-5. Measurement

The gel permeation chromatography (GPC) measurement, differential Scanning Calorimeter (DSC) measurement, polarized optical microscope (POM) observation, static contact angle measurement, white-light interferometric microscope (WLIM) observation, atomic force microscopy (AFM) observation and UV-Vis absorption spectral measurement were performed by same set-up in previous chapters.

Static contact angles of water (θ_w, surface tension, $\gamma_w = 72$ mN m^{-1} at 25 °C) droplets on these polymer films were obtained by a contact angle meter (CA-XP, Kyowa

Interface Science, Japan).

X-ray measurements using the CuK$_\alpha$ line (0.154 nm) were made with a FR-E equipped with a R-AXIS IV 2D detector (Rigaku). The camera length was 300 mm.

4-3. Results and discussions

4-3-1. Contact angles of polymer films

Table 1 lists the θ_w values at 25 °C. The θ_w values on PAz were 108.2 ± 0.8°, and decreased to 100.6 ± 0.8° under UV irradiation. The θ_w values of PAz before UV irradiation were larger than that under UV light irradiation, indicating that UV irradiation induces a higher surface tension of the PAz surface layer due to the enhancement of the content of cis-Az isomer. The θ_w values for non-photoreactive PS10, PS20 and PS30 were 102.7±1.1°, 101.8 ± 0.7° and 101.5 ± 0.8°, respectively, indicating essentially the same surface tension, and have a substantially higher surface tension than that of PAz before UV irradiation.

4-3-2. Photoinduced mass migration in PS films with a PAz LS layer

Figure 4-2a shows schematic illustration for patterned UV light irradiation on PS10 film covered with photoresponsive PAz layer. Repeated LS deposition of a PAz floating monolayer on water onto PS10 films was achieved in the same manner as previously reported[47]. The thickness of PAz monolayer on a solid substrate was estimated to be 2 nm[29,47,48].

Figure 4-2b shows the UV-visible absorption spectra of PAz layers as a function of the deposition number on the PS10 film after subtracting the absorption of the pure PS10 film. The ϕ-ϕ* absorption at 246 nm increased proportionally with the deposition

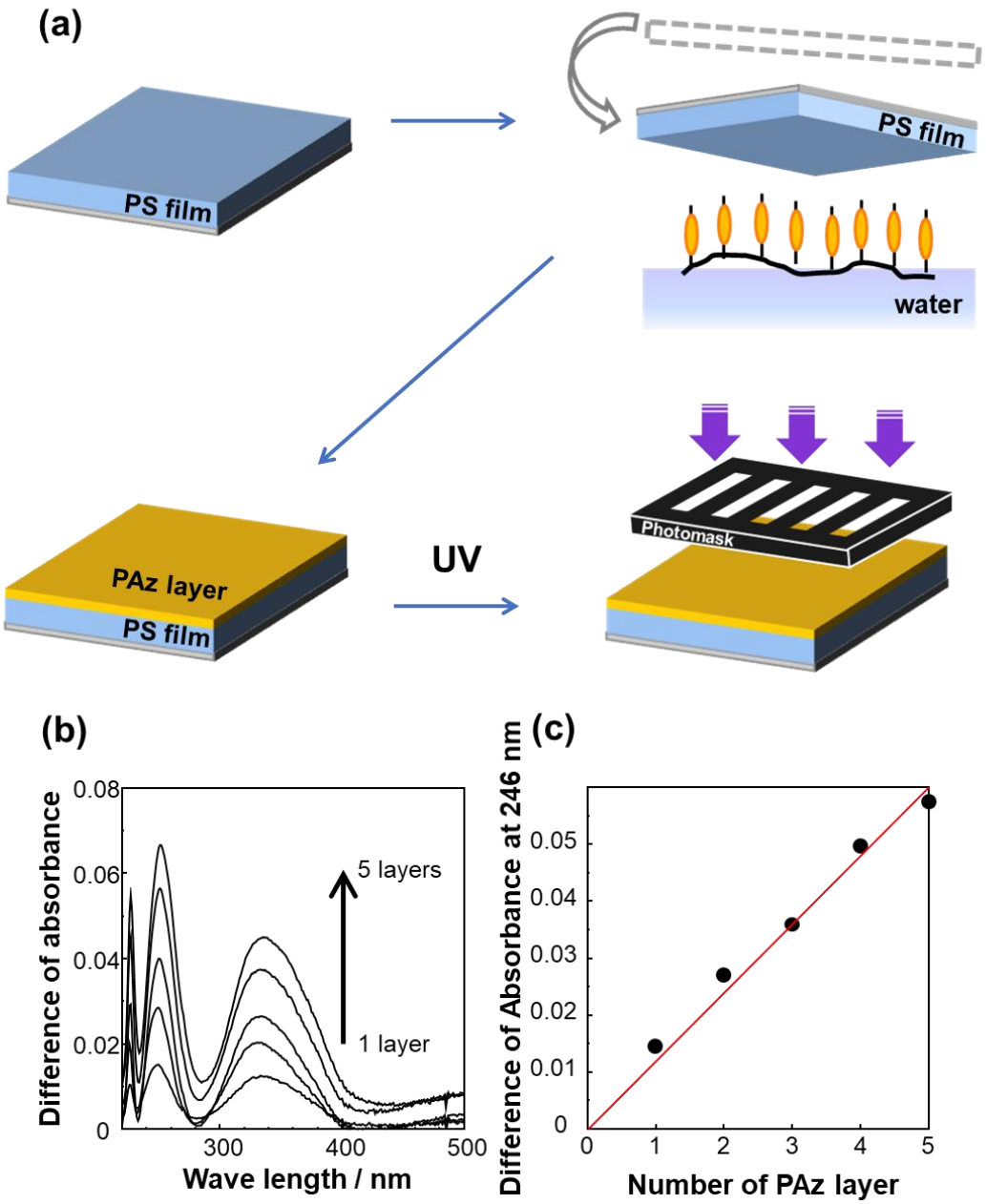

Figure 4-2. Schematic of LS deposition of a PAz layer on a PS10 film and successive UV irradiation through a stripe mask (pitch: 20 μm) (a). UV-visible absorption spectra at different deposition numbers of PAz layers (1–5 layers) on the PS10 film (b), and the absorbance of PAz at 246 nm as a function of deposition number of PAz monolayer (c).

number, indicating that the PAz layer is accurately deposited onto the PS10 film repeatedly (Fig. 4-2c).

Figures 4-3 display AFM topographical images and height profiles after UV light irradiation (1.0 mW cm^{-2} for 300 s) at 90 °C through 20-μm line-and-space photomask. A pure PS10 film provided smooth surface after patterned UV irradiation and no mass transfer was induced (Fig. 4-3a). On the other hand, the PS10 film covered with a PAz LS monolayer exhibited an obvious modulation of the surface. The PS10 film covered with a PAz monolayer only created smooth 3-dimensional topography reflecting the light irradiation pattern. The peak-to-valley height difference formed by the PAz monolayer was 18 nm (Fig. 4-3b), indicating that PAz monolayer (thickness: 2 nm) at the topmost surface provided SRG with 9-times larger undulation. This result suggests that the SRG formation is originated from the spatially patterned Az photoisomerization at the topmost surface, and mass transfer generated at the surface is propagated to the PS10 film underneath. For a 10-layered PAz LS layer system, the peak-to-valley height difference reached 185 nm (Fig. 4-3c). Hence, the thicker surface PAz layer induced the larger mass motion.

To evaluate the direction of mass transfer and linearly polarized light dependence, we performed an additional experiment. Irradiation with linearly polarized UV light through 250-μm diameter circle photomask was performed onto a PS10 film with 5-layered PAz LS film. Figure 4-3d shows a WLIM topographical image and height profiles after linearly polarized UV light irradiation. Mass motion occurred at the boundary area between the UV light exposed and non-exposed areas. The height of UV-irradiated areas (outside circle) became larger than that of non-irradiated ones (inside circle), indicating that the mass migration motion occurred from trans-Az areas toward

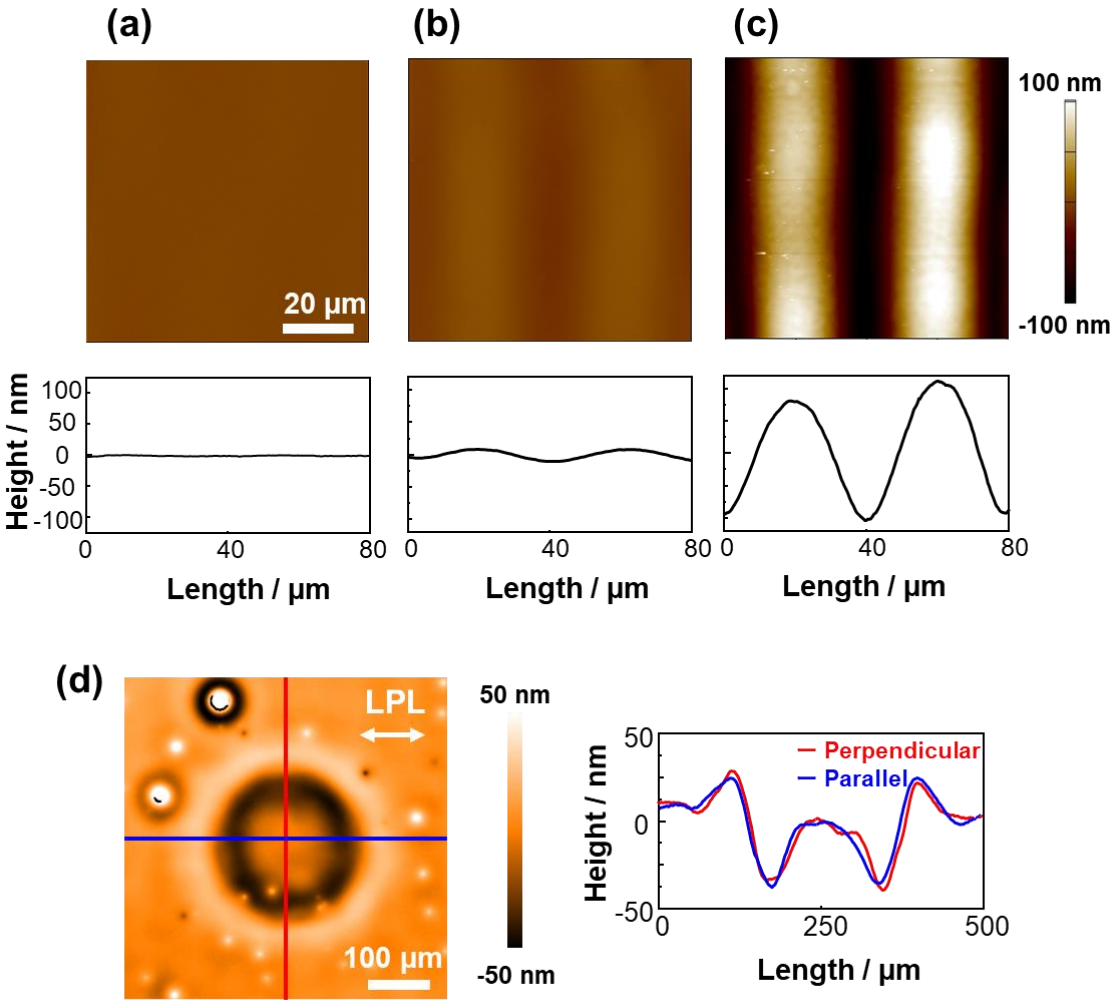

Figure 4-3. Photoinduced mass migration behavior of PS10 films with the PAz LS layer at the surface. Topographical AFM images (upper) and cross-sectional height profiles (lower) after 20 μm-pitch stripe-patterned UV light irradiation at 90 °C on PS films without a PAz layer (a), with a 1-layered (b), and 10-layered (c) PAz LS film on the surface of 200-nm-thick PS10 film. (d) Topographical WLIM image (upper) cross-sectional height profile (lower) of a PS film with a 5-layered PAz LS film at the surface after linearly polarized UV light irradiation through a circle-shaped (center) mask.

cis-rich-Az ones of the topmost PAz skin layer. The cis-Az surface has the higher wettability[49,50] and higher polarity than that of trans-Az. The θ_w of cis-PAz was lower than that of trans-PAz (Table 4-1). Therefore, PAz in the cis-rich state has a higher surface tension than that in the trans state. The direction of mass transfer is in agreement with the effect of the Marangoni flow[29-35]. As shown in Fig. 4-3d, this mass motion is independent of the direction of linear UV light polarization. These results agree with our previous data reported in previous chapter. This mass flow is not reflective of the transition moment of Az unit, therefore this motion is not attributed to the gradient force[7-9] and orientation force[15,16]. These two facts regarding the mass flow direction and light polarization dependence indicate that the Marangoni flow should be the plausible mechanism for the SRG formation.

Figure 4-4 shows the peak-to-valley height difference as a function of thickness of the surface LS layer of PAz. The height difference increased almost linearly with the thickness of the PAz layer. The PAz skin layer propagated its mass motion to the underlying PS10 in an amplified manner. Approximately 9-10 times thicker PS10 is transferred by the topmost PAz skin layer at each PAz thickness. In chapter II, amplified mass transfer was observed in nematic-SCLCP film covered with the PAz LS layer, and roughly 20 times larger thickness of nematic-SCLCP was affected from the PAz surface layer[29]. Probably, more efficient SRG formation in the previous system is explained by stronger interactions between nematic SCLCP and SCLC PAz due to cooperative behavior of liquid crystalline nature. On the other hand, in this study, the molecular interaction between amorphous PS10 and SCLC-PAz should be inadequate, resulting in the less efficient SRG formation.

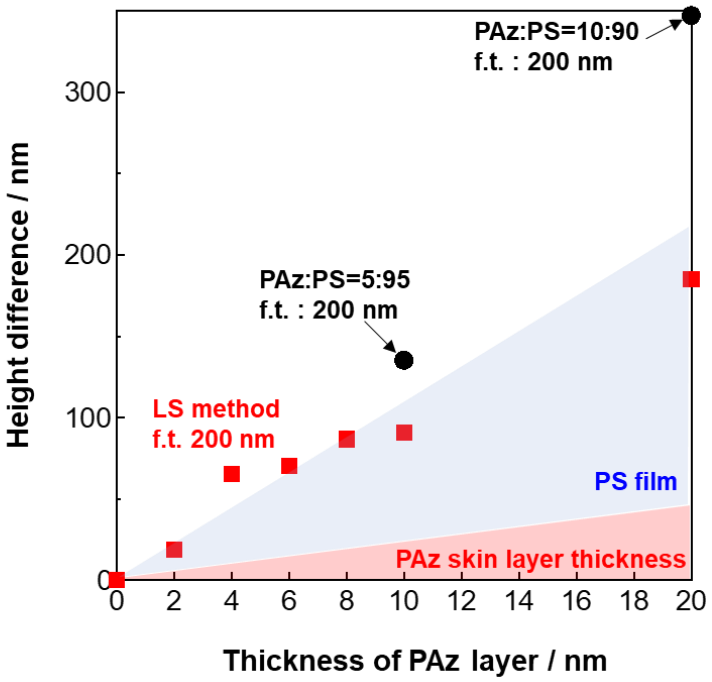

Figure 4-4. Peak-to-valley height difference of the SRG structure for PS films at various deposition numbers of PAz LS layer (layer thickness). Square symbols correspond to data for 200 nm-thick LS film. Filled circles indicate data obtained for a 200-nm-thick surface segregated blended film (PAz:PS=5:95, 10:90) film.

4-3-3. Photoinduced mass migration in PAz/PS blended films

The surface segregation process allows for simple, low-cost and reliable surface modification to rest a photoresponsive layer[51-55]. Blended films (200-nm thickness) composed of PAz and PS10 (5:95 and 10:90 by weight) were annealed at 90 °C for 1 min. After the annealing process, the θ_w values of PAz/PS10 (10:90) blended film was 115.3±0.4 °, which is close to that of pure PAz. We reported PAz-containing polymer segregated to surface in PS blended film due to PAz lower free surface energy[53-55]. The wettability experiments indicate that most of the PAz component segregates to the free surface on the low molecular weight PS (M_w=1.0×10^3) blended film. UV-visible absorption measurements showed a reduction of the absorption intensity of the π-π* band in the transmission mode after annealing, indicative of induction of the homeotropic orientation of Az side chains at the free surface. Further, the smectic layer structure of PAz (layer spacing, d=3.2 nm) in the out-of-plane direction was induced after annealing as indicated by X-ray measurements, which indicates an induction of phase separation between PS and PAz with Az layer being oriented horizontal with the substrate plane. All these data including the surface wettability of water droplet show that the annealing procedure promotes the clear surface segregation of PAz component, thereby, the thickness of the surface segregated PAz layer can be roughly estimated by the weight ratio of the mixture.

Figures 4-5a, b display AFM and WLIM topographical images and height profiles after UV light irradiation (1.0 mW cm^{-2} for 300 s) at 90 °C through 20-μm line-and-space photomask onto the two PAz/PS10 blended films of 5:95 respectively. Efficient mass transfer was observed in both blended polymer films. The thickness of the surface segregated PAz layer in the blended films (PAz/PS10 (5:95 and 10:90)) was

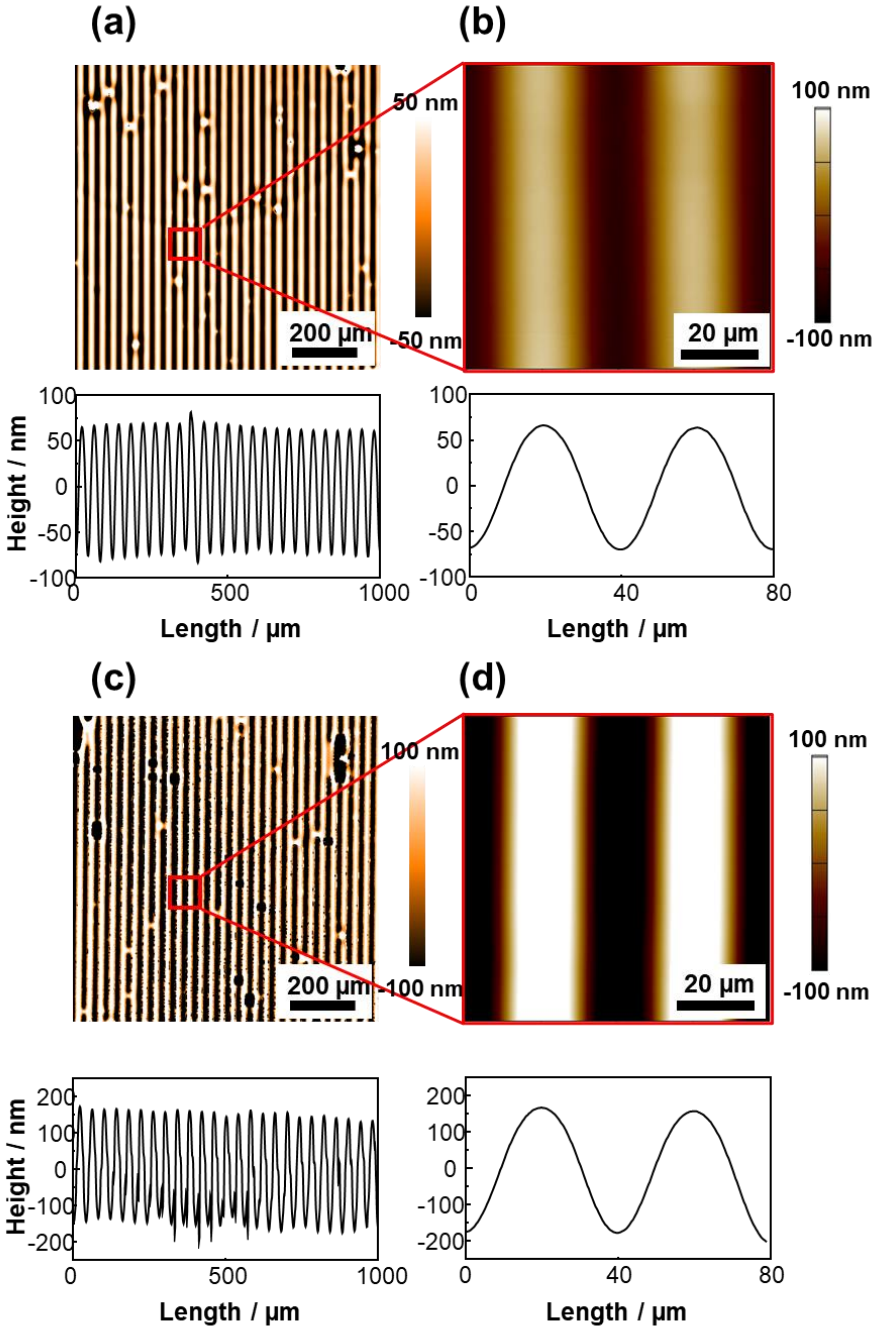

Figure 4-5. Photoinduced mass migration in blended (PAz:PS10=5:95;(a), (b), 10:90; (c), (d)) film. WLIM (a), (c) and AFM (b), (d) images after UV light irradiation is performed through a stripe photomask (20 μm pitch) at 90 °C for 300 s.

estimated to be 10 nm (corresponding to 5-layered LS film) and 20 nm (corresponding to 10-layered LS film). The filled circles in Fig. 4-4 show the peak-to-valley height difference obtained in the surface segregation system. The SRG structures were larger than that of LS skin layered PS film. Blended polymer film resulted in more efficient mass transfer, which is explained by the stronger molecular interaction and mutual diffusion between segregated PAz layer and PS10 at the interface. On the other hand, the surface layers prepared by the physical deposition of LS method results in the less strong molecular interaction with no mutual diffusion.

4-3-4. Optimization of the SRG formation in PAz/PS blended films

To monitor the dynamic process of mass transfer, the surface morphology was observed at different periods of UV light irradiation time for the PAz/PS10 (10:90) blended film (Fig. 4-6). The peak-to-valley height difference obtained at 25 and 300 s irradiation were 127 and 337 nm, respectively. This significantly efficient mass transfer is comparable to the case of SRG formation observed in the pure PAz homopolymer film[21]. After longer irradiation time of 500 s, SRG structure was deteriorated to 206 nm due to the capillary force[56]. We suppose that the capillary force can be the only factor of the leveling and decomposition or ablation by light is not involved in consideration of the small dose of total light irradiation.

The dynamics of the mass transfer strongly depends on the temperature during UV light irradiation[21,29]. Hence, we performed UV light irradiation at various temperatures for PAz/PS10 (10:90) blended film (Fig. 4-7). Efficient mass transfers were observed after UV light irradiation at a wide range of temperature of 60-110 °C, and the maximum peak-to-valley height difference was obtained at 90 °C. On the other hand, no

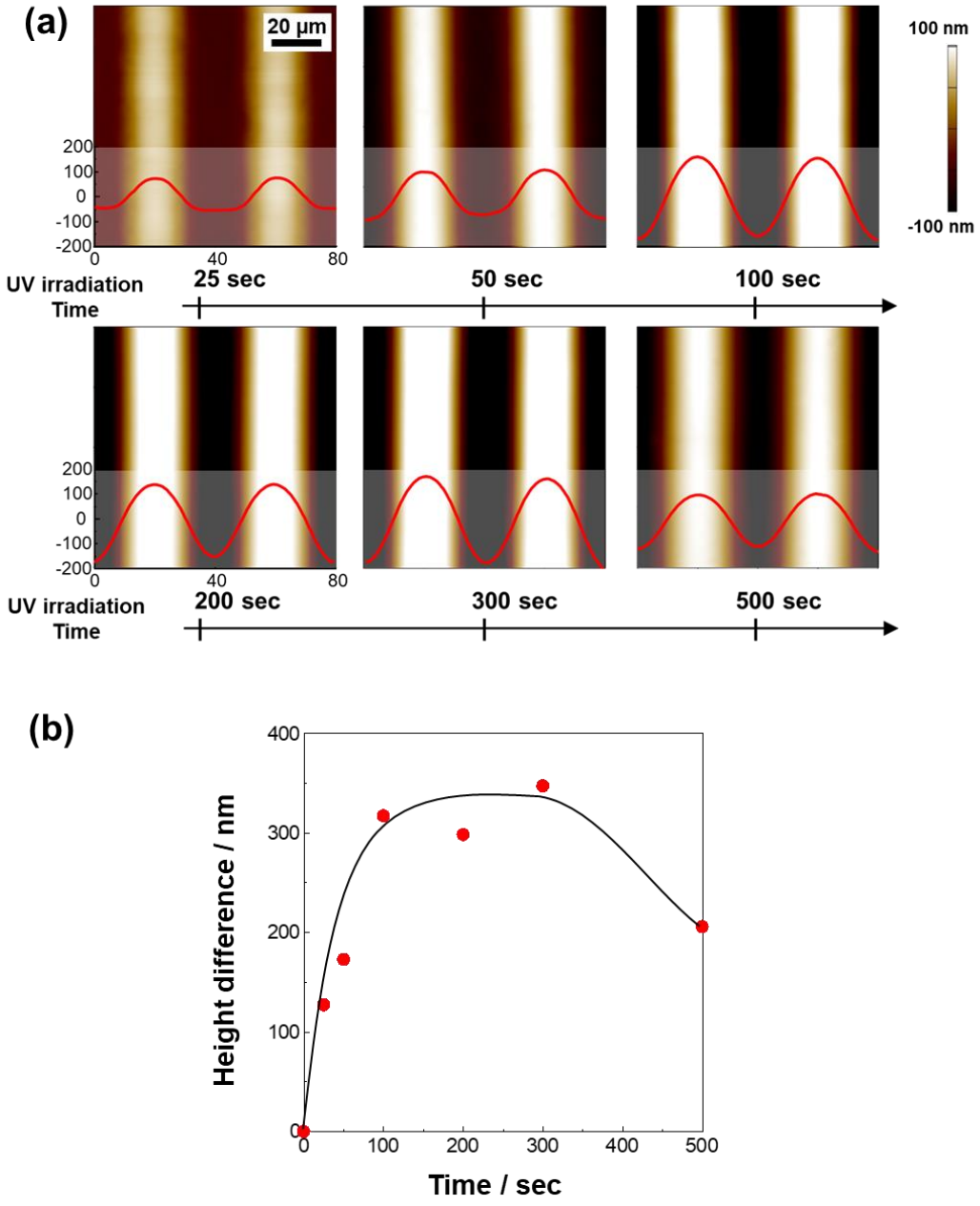

Figure 4-6. Photoinduced mass migration for a blended (PAz:PS10=10:90) film at various periods of irradiation time. UV light irradiation is performed through a stripe photomask (20 μm pitch) at 90 °C for 25-500 s (a) and time-course profile of the resulting height difference (b).

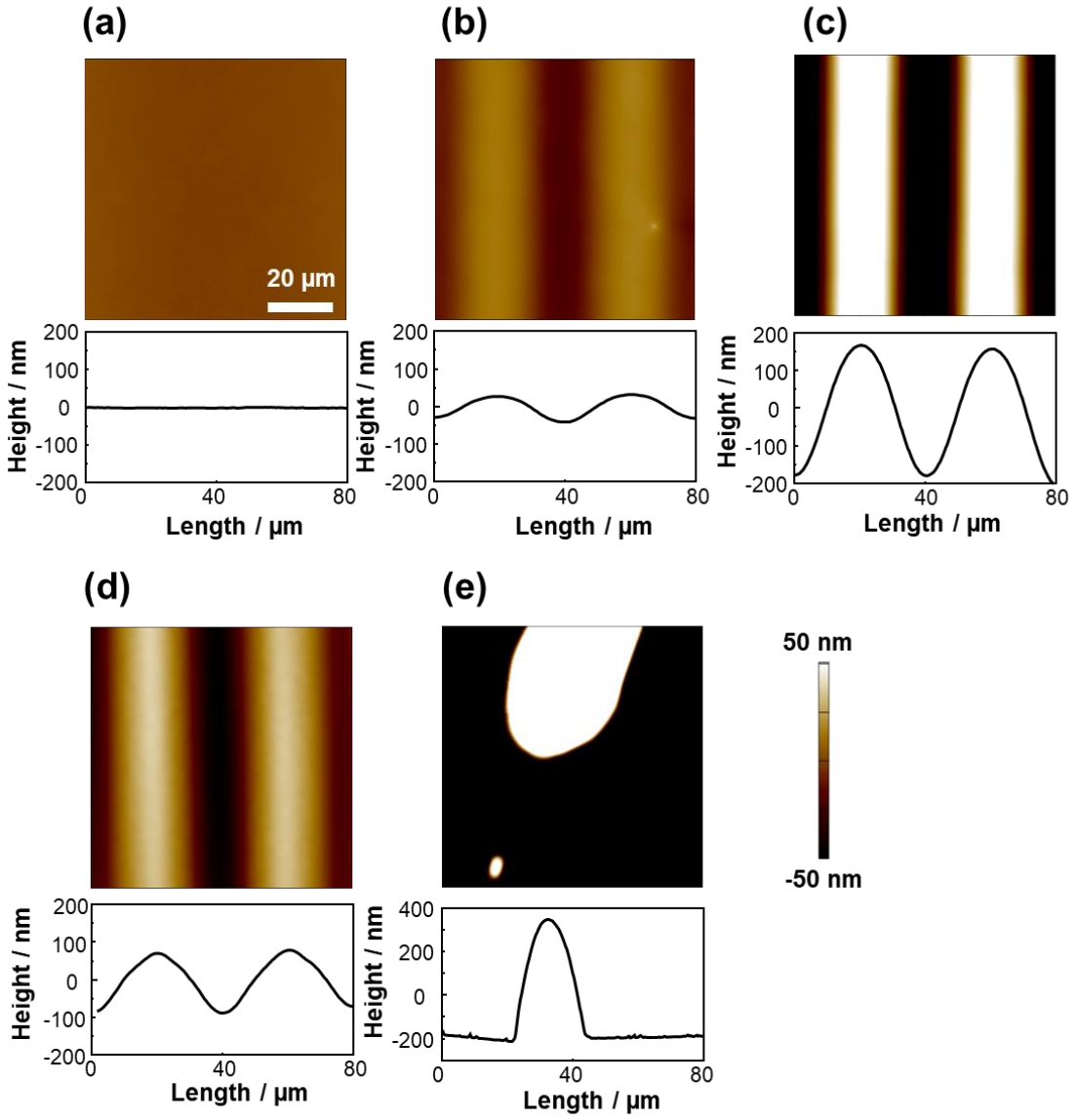

Figure 4-7. Photoinduced mass migration blended film (PS10:PAz=10:90) film. AFM topographical images and height profile after UV irradiation performed through a stripe photomask (20 μm pitch) at 25 °C (a), 60 °C (b), 90 °C (c), 110 °C (d), 130 °C (e).

mass transfer was observed at 25 °C, and dewetting occurred at 130 °C. Increasing temperature reduces the viscosity of PS10 film and increases its diffusivity. Lowered viscosity promotes the efficiency of mass transfer, but higher diffusivity prevents from retention of SRG structure. The temperature dependence is explained by the competition between molecular mobility and leveling effect.

Next, the molecular weight dependence of PS was examined. UV light was irradiated at various temperatures with PAz/PS10, PAz/PS20 and PAz/PS30 (10:90 by weight) blended films(Fig 4-8, 9). Figure 4-10 shows AFM topographical images and height profiles after UV light irradiation (1.0 mW cm^{-2} for 300 s) at 90 °C for three blended films. PAz/PS10 blended film formed regular sinusoidal surface modulation. In contrast, very small relief structures were observed corresponding to the mass transfer of segregated PAz skin layer in PAz/PS20 and PAz/PS30 blended films. Figure 4-11 summarizes the peak-to-valley height difference as a function of temperature under UV irradiation. No mass transfer was observed in PAz/PS20 and PAz/PS30 blended films in the range of 25-60 °C. The SRG structure was generated at 90-130 °C, and their maximum peak-to-valley height differences were 140 nm (PAz/PS20 at 130 °C) and 127 nm (PAz/PS30 at 110 °C). In these cases, only approximately 4 times height changes of the PAz layer thickness were observed. Such inefficient mass transfers should be attributed to the higher viscosity of the PS films with higher molecular weight PS possessing the higher viscosity[57-59].

4-3-5. Discussion: SRG formation in PS films

Ubukata et al. reported the SRG formation in pure PS films driven by the diffusivity difference generated by photocrosslinking or/and photodegradation[46]. Further,

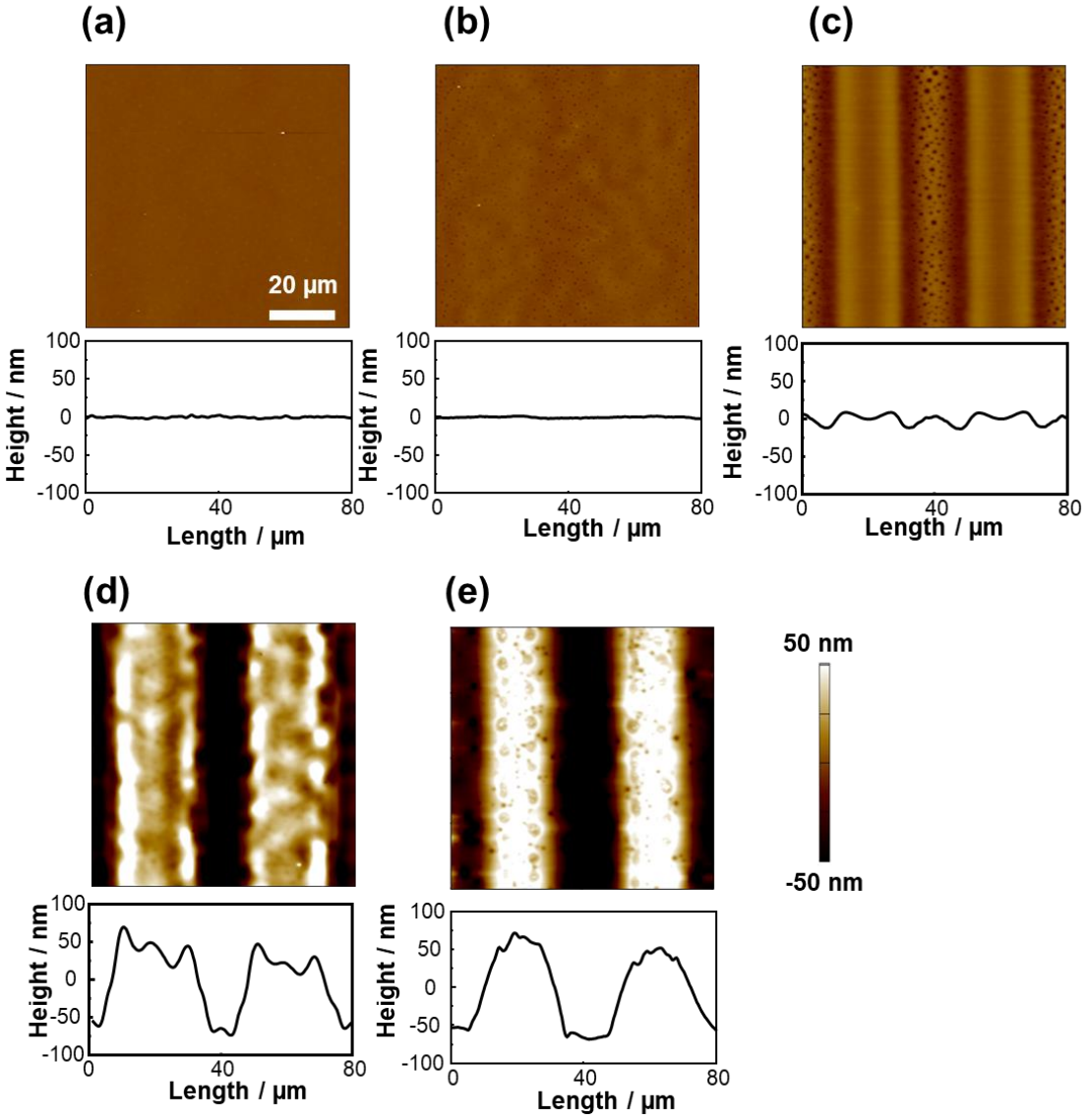

Figure 4-8. Photoinduced mass migration blended film (PS20:PAz=10:90) film. AFM topographical images and height profile after UV irradiation performed through a stripe photomask (20 μm pitch) at 25 °C (a), 60 °C (b), 90 °C (c), 110 °C (d), 130 °C (e).

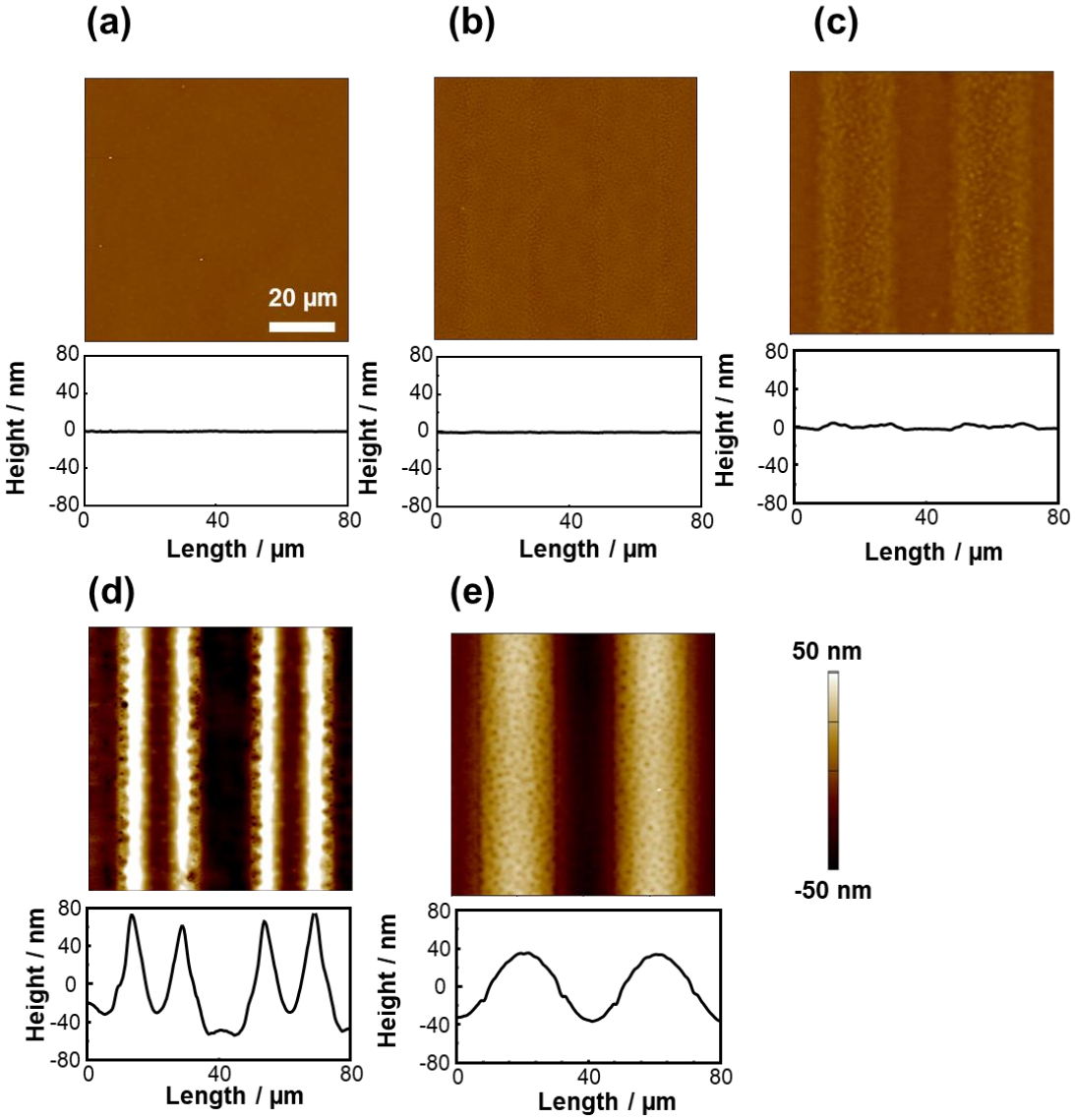

Figure 4-9. Photoinduced mass migration blended film (PS30:PAz=10:90) film. AFM topographical images and height profile after UV irradiation performed through a stripe photomask (20 μm pitch) at 25 °C (a), 60 °C (b), 90 °C (c), 110 °C (d), 130 °C (e).

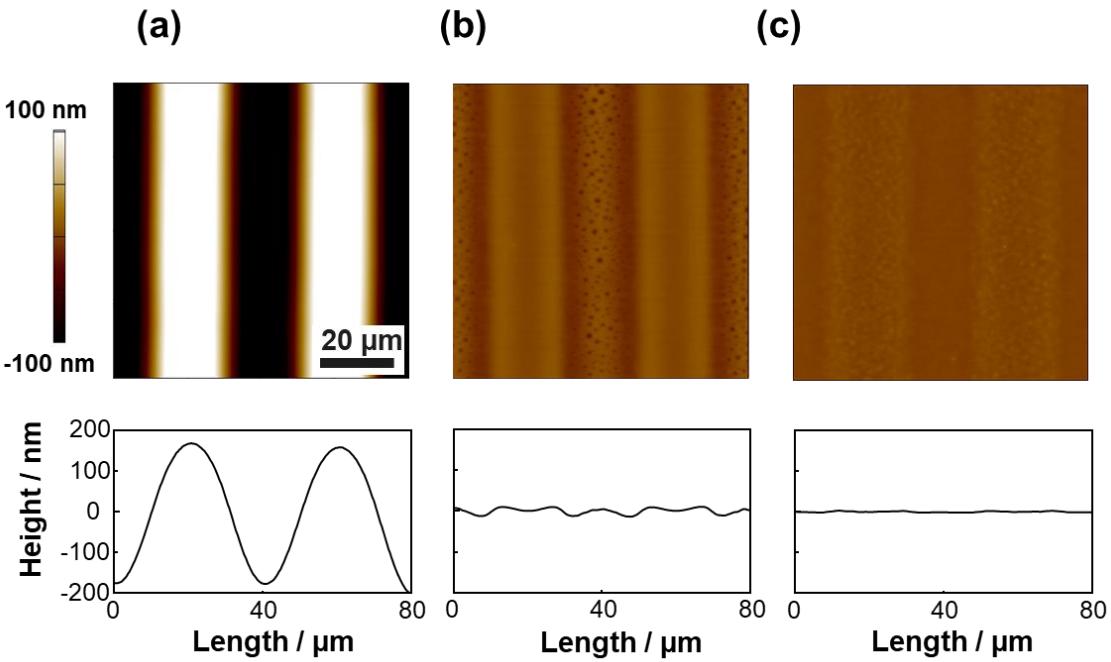

Figure 4-10. Photoinduced mass migration in blended (PAz:PS10=5:95) film. WLIM (a) and AFM (b) images after UV light irradiation is performed through a stripe photomask (20 μm pitch) at 90 °C for 300 s.

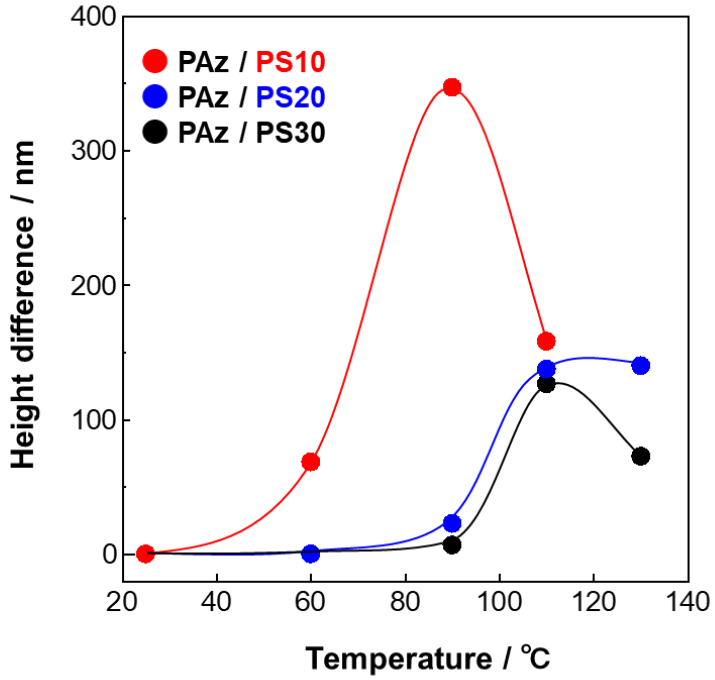

Figure 4-11. Peak-to-valley height difference of the SRG structure for blended (PAz:PS (10:90)) films changing the molecular weight of PS and temperature under UV light irradiation. red, blue and black symbols correspond to data for PAz/PS10, PAz/PS20 and PAz/PS30 blended films, respectively.

Ellison et al. developed surface patterning in pure PS films by the Marangoni flow formed by photoinduced dehydrogenation[29,30]. These previous studies are associated with photoreactions of PS itself by UV light irradiation (λ < 300 nm), which requires a large amount of light dose (typically 840 J cm^{-2})[29]. In contrast, in our present strategy, the photoreaction occurs only at surface PAz layer and not within the PS film. This situation enables highly efficient mass transfer with UV (365 nm) light irradiation with low light dose (1.0 mW cm^{-2}), which corresponds 10^5 – 10^6 times lower than those in the previous works)[29].

4-4. Conclusion

In this chapter, the author have successfully demonstrated the efficient SRG formation in PS films covered with a PAz photorespnsive skin layer. This mass motion is explained by the Marangoni flow driven by spatially patterned surface tension instability of PAz skin layer. Then, the lateral mass flow is propagated and amplified to the underlying PS film, resulting in a large SRG structure. Mass migration efficiency is affected by viscosity of PS that are controlled by temperature and molecular weight, and is well reflective of the Marangoni flow feature[60]. SRG formation systems so far investigated have Az units in the entire film[1-16]. Such films have a strong light absorption in the visible region, which limits applications for optical elements. In our strategy, essentially colorless SRG film can be used, and expectedly paves the way for next-generation optical applications of SRG structure. We assume that this approach is not limited to PS, and SRGs formation in many types of non-photoreactive polymers such as commercial poly(meth)acrylates may be used. Our approach should extend the applicability of polymer materials for the direct SRG photoprocessing.

References

[1] P. Rochon, E. Batalla, A. Natansohn, *Appl. Phys. Lett.* **1995**, 66, 136-138.

[2] D. Y. Kim, S. K. Tripathy, L. Li, J. Kumar, *Appl. Phys. Lett.* **1995**, 66, 1166-1168.

[3] N. K. Viswanathan, D. Y. Kim, S. Bian, J. Williams, W. Liu, L. Li, L. Samuelson, J. Kumar and S. K. Tripathy. *J. Mater. Chem.* **1999**, 9 1941–1955.

[4] A. Natansohn, P. Rochon, *Chem. Rev*. **2002**, 102, 4139–4175.

[5] C. J. Barrett, A. Natansohn, P. L. Rochon, *J. Phys. Chem.* **1996**, 100, 8836–8842.

[6] C. J. Barrett, P. L. Rochon, A. Natansohn, *J. Chem. Phys.* **1998**, 109, 1505–1516.

[7] J. Kumar, L. Li, X. L. Jiang, D. Y. Kim, T. S. Lee, S. Tripathy, *Appl. Phys. Lett*. **1998**, 72, 2096–2098.

[8] O. Baldus, S. J. Zilker, *Appl. Phys. B: Laser Opt*. **2001**, 72, 425–427.

[9] K. Sumaru, T. Fukuda, T. Kimura, H. Matsuda, T. Yamanaka, *J. Appl. Phys*. **2002**, 91, 3421–3430.

[10] T. G. Pedersen, P. M. Johansen, N. C. R. Holme, P. S. Ramanujam, S. Hvilsted, *Phys. Rev. Lett*. **1998**, 80, 89–92.

[11] P. Karageorgiev, D. Neher, B. Schulz, B. Stiller, U. Pietsch, M. Giersig, L. Brehmer, *Nat. Mater.* **2005**, 4, 699–703.

[12] S. Lee, H. S. Kang, J. K. Park, *Adv. Mater.* **2012**, 24, 2069–2103.

[13] N. Hurduc, B. C. Donose, A. Macovei, C. Paius, C. Ibanescu, D. Scutaru, M. Hamel, N. Branza-Nichita, L. Rocha, *Soft Matter* **2014**, 10, 4640–4647.

[14] A. Ambrosio, L. Marrucci, F. Borbone, A. Roviello, P. Maddalena, *Nat. Commun*. **2012**, 3, 989.

[15] V. Toshchevikov, J. Ilnytskyi, M. Saphiannikova, *J. Phys. Chem. Lett.* **2017**, 8, 1094–1098.

[16] M. Saphiannikova, V. Toshchevikov, *J. Soc. Inf. Disp*. **2015**, 23, 146–153.

[17] T. Ubukata, T. Seki, K. Ichimura, *Adv. Mater.* **2000**, 12, 1675–1678.

[18] T. Ubukata, M. Hara, K. Ichimura, T. Seki, *Adv. Mater.* **2004**, 16, 220–223.

[19] N. Zettsu, T. Ogasawara, R. Arakawa, S. Nagano, T. Ubukata, T. Seki,. *Macromolecules* **2007**, 40, 4607–4613.

[20] N. Zettsu, T. Ogasawara, N. Mizoshita, S. Nagano, T. Seki, *Adv. Mater.* **2008**, 20, 516–521.

[21] J. Isayama, S. Nagano, T. Seki, *Macromolecules* **2010**, 43, 4105–4112.

[22] T. Seki, *Macromol. Rapid Commun*. **2014**, 35, 271–290.

[23] N. Zettsu, T. Fukuda, H. Matsuda, T. Seki, *Appl. Phys. Lett*. **2003**, 83, 4960–4962.

[24] S. Mitsui, S. Nagano, M. Hara, T. Seki, *Crystals* **2017**, 7, 52.

[25] J. Gao, Y. He, F. Liu, X. Zhang, Z. Wang, X. Wang, *Chem. Mater*. **2007**, 19, 3877–3881.

[26] J. E. Koskela, J. Vapaavuori, R. H. A. Ras, A. Priimagi, *ACS Macro Lett*. **2014**, 3, 1196–1200.

[27] X. Wang, J. Vapaavuori, X. Wang, R. G. Sabat, C. Pellerin, C. G. Bazuin, *Macromolecules* **2016**, 49 4923- 4934.

[28] H. Nakano, T. Takahashi, T. Kadota, Y. Shirota, *Adv. Mater.* **2002**, 14, 1157–1160.

[29] I. Kitamura, K. Kato, R. B. Berk, T. Nakai, M. Hara, S. Nagano, T. Seki, *Sci. Rep*. **2020**, 10, 12664.

[30] J. M. Katzenstein, D. W. Janes, J. D. Cushen, N. B. Hira, D. L. McGuffin, N. A. Prisco, C. J. Ellison, *ACS Macro Lett.* **2012**, 1, 1150–1154.

[31] T. A. Arshad, C. B. Kim, N. A. Prisco, J. M. Katzenstein, D. W. Janes, R. T.

Bonnecaze, C. J. Ellison, *Soft Matter* **2014**, 10, 8043–8050.

[32] C. B. Kim, J. C. Wistrom, H. Ha, S. X. Zhou, R. Katsumata, A. R. Jones, D. W. Janes, K. M. Miller, C. J. Ellison, *Macromolecules* **2016**, 49, 7069–7076.

[33] A. R. Jones, C. B. Kim, S. X. Zhou, H. Ha, R. Katsumata, G. Blachut, R. T. Bonnecaze, C. J. Ellison, *Macromolecules* **2017**, 50, 4588–4596.

[34] A. Miniewicz, A. Sobolewska, W. Piotrowski, P. Karpinski, S. Bartkiewicz, E. Schab-Balcerzak, *Materials* **2020**, 13, 2464.

[35] I. Kitamura, K. Oishi, M. Hara, S. Nagano, T. Seki, *Sci. Rep*. **2019**, 9, 2256.

[36] E. Ishow, A. Brosseau, G. Clavier, K. Nakatani, R. B. Pansu, J. J. Vachon, P. Tauc, D. Chauvat, C. R. Mendonça, E. Piovesan, *J. Am. Chem. Soc.* **2007**, 129, 8970–8971.

[37] Y. Morikawa, S. Nagano, K. Watanabe, K. Kamata, T. Iyoda, T. Seki, *Adv. Mater*. **2006**, 18, 883–886.

[38] K. Aissou, J. Shaver, G. Fleury, G. Pécastaings, C. Brochon, C. Navarro, S. Grauby, J. M. Rampnoux, S. Dilhaire, G. Hadziioannou, *Adv. Mater.* **2013**, 25, 213-217.

[39] T. Ubukata, T. Isoshima, M. Hara. *Adv. Mater*. **2005**, 17, 1630-1633.

[40] L. M. Goldenberg, V. Lisinetskii, Y. Gritsai, J. Stumpe, S. Schrader *Adv. Mater*. **2012**, 24, 3339-3343.

[41] Y. Gritsai, L. M. Goldenberg, O. Kulikovska, J. Stumpe, *J. Opt. A: Pure Appl. Opt*. **2008**, 10, 125304.

[42] L. M. Goldenberg, L. Kulikovsky, O. Kulikovska, J. Stumpe, *J. Mater. Chem*., **2009**, 19, 8068-8071.

[43] A. Kikuchi, Y. Harada, M. Yagi, T. Ubukata, Y. Yokoyama, J. Abe, *Chem. Commun*. **2010**, 46, 2262–2264.

[44] T. Ubukata, S. Fujii, Y. Yokoyama, *J. Mater. Chem*. **2009**, 19, 3373-3377.

[45] T. Ubukata, M. Nakayama, T. Sonoda, Y. Yokoyama, H. Kihara, *ACS Appl. Mater. interfaces* **2016**, 8, 21974–21978.

[46] T. Ubukata, Y. Moriya, Y. Yokoyama, *Polym. J.* **2012**, 44, 966–972.

[47] T. Seki, M. Sakuragi, Y. Kawanishi, Y. Suzuki, T. Tamaki, R. Fukuda, K. Ichimura, *Langmuir* **1993**, 9, 211–218.

[48] K. Aoki, T. Iwata, S. Nagano, T. Seki, *Macromol. Chem. Phys.* **2010**, 211, 2484–2489.

[49] G. Möller, M. Harke, H. Motschmann, D. Prescher, *Langmuir* **1998**, 14, 4955-4957.

[50] C. L. Feng, Y. J. Zhang, J. Jin, Y. L. Song, L. Y. Xie, G. R. Qu, L. Jiang, D. B. Zhu, *Langmuir* **2001**, 17, 4593-4597.

[51] K. Fukuhara, Y. Fujii, Y. Nagashima, M. Hara, S. Nagano, T. Seki, *Angew. Chem. Int. Ed*. **2013**, 52, 5988–5991.

[52] T. Nakai, D. Tanaka, M. Hara, S. Nagano, T. Seki, *Langmuir* **2016**, 32, 909–914.

[53] K. Mukai, M. Hara, S. Nagano, T. Seki, *Angew. Chem. Int. Ed*. **2016**, 55, 14028-14032.

[54] S. Nagano, *Langmuir* **2019**, 35, 5673–5683.

[55] T. Seki, *Bull. Chem. Soc. Jpn*. **2018**, 91, 1026–1057.

[56] M. Backholm, M. Benzaquen, T. Salez, E. Raphaël, D. Dalnoki-Veress, *Soft Matter* **2014**, 10, 2550-2558.

[57] M. L. Williams, *J. Appl. Phys*. **1958**, 29, 1395-139.

[58] G. Fleischer, *Polym. Bull*. **1984**, 11, 75-80.

[59] T. Kajiyama, K. Tanaka, A. Takahara, *Macromolecules* **1997**, 30, 280-285.

[60] L. E. Scriven, C. V. Sternling, *Nature* **1960**, 187, 186–188.

Chapter V
Summary and Outlook

This thesis has presented a new motif for the study of polymer surface and interface, focusing on the super-inkjet printing method. This approach with inkjet printings, enables submicro-sized polymer printing on deformable polymer films, leading direct observations of polymer dynamics of lateral wetting and deformation in the film thickness direction. Observation of hetero-polymer interface fabricated by inkjet printing revealed that the photoinduced Marangoni flow was driven by the surface tension difference on azobenzene polymer films (PAz). The Marangoni flow can be applied to the Surface Relief Gratings (SRGs) process in PAz film. Based on the dynamic Marangoni flow process, a new guideline for the creation of three-dimensional functions originating from the polymer film surface was presented by means of inkjet printing and Langmuir-Schaefer (LS) method. The summaries of each chapter are described as follows.

In Chapter II, the photoinduced Marangoni flow driven by the inkjet patterns of lower surface tension on azobenzene side chain liquid crystalline polymer (SCLCP) films is demonstrated. UV light irradiation onto Poly(butyl methacrylate)-*block*-PAz (PBMA-*b*-PAz) inkjet line on PAz film induced efficient mass migration triggered by the Marangoni effect. Surface elemental analysis of ToF-SIMS measurement elucidated that inkjet line was extended on PAz film surface during mass migration. Further, this photoinduced Marangoni flow can be tuned by the viscosity control of PAz film with alternative UV and visible light irradiation. This printing-aided photoprocess for surface inscription is expected to provide a new platform of dynamic microfabrication.

In Chapter III, the Marangoni flow is applied to SRGs formation in non-

photoresponsive nematic SCLCP films covered with azobenzene SCLCP skin layer. A PAz skin layer controlled at the molecular level thickness was introduced by LS method onto nematic SCLCP films. A negligible amount of PAz skin layer was found to induce large SRGs upon patterned UV light irradiation. Conversely, the motion of the SRG-forming azobenzene SCLCP was impeded by the existence of a LS monolayer of the octadecyl side chain polymer set on the topmost surface. These results are well understood by considering the Marangoni flow driven by the surface tension instability. Further, surface PAz skin layer induced the mass transfer also in a simple and very practical surface segregation procedure for blended films. This strategy should realize light-assisted microfabrications for light-inert polymer films.

In Chapter IV, the SRGs formation propagated from the photoresponsive skin layer was tailored to a general amorphous poly styrene (PS). SRGs formation was demonstrated by action of the topmost surface of photoresponsive layer on PS film through the control of the Marangoni flow. Tailored SRGs formation in PS film suggests the generality of mass transfer propagated from the topmost photoresponsive skin layer. This approach should pave the way toward in-situ inscription of the surface topography for non-photoresponsive materials, which eliminates the strong light absorption of PAz. This fact leads to great potential applications in recording media and optical materials such as diffraction gratings and liquid crystal alignment films.

As demonstrated in this thesis, a new photoinduced Marangoni flow induced from the inkjet patterns is suggested. The Marangoni flow is technically troublesome in the coating and printing fields because it causes film flaking. However, the present study paves the new way for the application of the Marangoni flow to industrially useful surface processing technology. Furthermore, based on the knowledge obtained in the research

with the inkjet printing, SRGs formation was developed by only topmost surface PAz skin layer by patterned UV light irradiation. Even 25 years after the first report of SRGs formation in 1995, universal explanation about the mechanism has not yet been provided. The work in this thesis experimentally elucidates that a highly plausible mechanism of SRGs formation is the Marangoni flow driven by the surface tension difference at topmost surface. These surface microfabrication for polymer films in this study can be applied, for the first time, to a various type of general non-photoresponsive polymer materials, which can lead to great potential applications especially in optical elements fields.

In accordance with the above knowledge, surface and interface strategy gives new aspects to develop varieties of performance and characteristics, such as patterning, surface dynamics, wettability, adhesion, friction, and biocompatibility. The continuous pursuit and development in this research field should largely expand the possibilities in polymer material processing and surface-mediated functionalities.

Publications

1. Issei Kitamura, Kazuak Oishi, Mitsuo Hara, Shusaku Nagano, Takahiro Seki, “Photoinitiated Marangoni flow morphing in a liquid crystalline polymer film directed by superinkjet printing patterns”, *Scientific Reports*, **9**, 2256 (2019).

2. Issei Kitamura, Keisuke. Kato, Rafael. Benjamin Berk, Takashi. Nakai, Mitsuo. Hara, Shusaku. Nagano, Takahiro Seki, “Photo-triggered large mass transport driven only by a photoresponsive surface skin layer”, *Scientific Reports*, **10**, 12664 (2020).

3. Issei Kitamura, Mitsuo Hara, Shusaku Nagano, Takahiro Seki, “Photo-triggered surface relief formation of polystyrene films based on the Marangoni flow driven by a surface photoresponsive skin layer”, *Molecular Crystals and Liquid Crystals*, in press.

Other Related Publications

1. Ayae Sugawara-Narutaki, Sawako Yasunaga, Yusuke Sugioka, Duc H. T. Le, Issei Kitamura, Jin Nakamura, Chikara. Ohtsuki, “Rheology of Dispersions of High-Aspect-Ratio Nanofibers Assembled from Elastin-Like Double-Hydrophobic Polypeptides”, *Int. J. Mol. Sci.*, **20**(24), 6262 (2019).

2. Ryohei Yamakado, Issei Kitamura, Mitsuo Hara, Shusaku Nagano, Takahiro Seki, Hiromitsu Maeda, “Photoisomerization-induced patterning of ion-based materials”, submitted.

Presentations at International Conferences

1. Issei Kitamura, Mitsuo Hara, Shusaku Nagano, Takahiro Seki, Photoinduced mass transfer driven by the surface hetero structure in photoresponsive liquid crystalline polymer films, The 11th SPSJ International Polymer Conference (IPC2016), Fukuoka, Japan (2016).

2. Issei Kitamura, Mitsuo Hara, Shusaku Nagano, Takahiro Seki, Photoinduced mass transfer driven by the surface tension difference on photoresponsive liquid crystalline polymer films, 9th International Conference on Molecular Electronics and Bioelectronics (M&BE9), Ishikawa, Japan (2017).

3. Issei Kitamura, Mitsuo Hara, Shusaku Nagano, Takahiro Seki, Photoinduced mass transfer triggered by the surface heterostructure in photoresponsive liquid crystalline polymer films, Nagoya Univ.-Tsinghua Univ.-Toyota Motor Corp.-Hokkaido Univ (NTTH) Joint Symposium, Gifu, Japan (2017).

4. Issei Kitamura, Mitsuo Hara, Shusaku Nagano, Takahiro Seki, Photoinduced mass transfer triggered by the surface tension difference on photoresponsive liquid crystalline polymer film, International Symposium on Advanced Display Materials and Devices (ADMD) 2017, Aichi, Japan (2017).

5. Issei Kitamura, Mitsuo Hara, Shusaku Nagano, Takahiro Seki, Photoinduced mass transfer by the surface tension difference fabricated by inkjet printing on photoresponsive polymer films, International union of materials research society-International conference of advanced materials (IUMRS-ICAM) 2017, Kyoto, Japan (2017).

6. Issei Kitamura, Mitsuo Hara, Shusaku Nagano, Takahiro Seki, Thermally and Photochemically Induced Mass Motion in Polymer Thin Films by Hetero-interface Strategy ESE symposium 2017-2, Rayong, Thailand (2017).

7. Issei Kitamura, Mitsuo Hara, Shusaku Nagano, Takahiro Seki, Thermally and Photochemically Induced Mass Transfer in Polymer Thin Films by Hetero-interface Strategy, 2017 VISTEC-NU Joint Seminar on New Optical Materials, Rayong, Thailand (2017).

8. Issei Kitamura, Mitsuo Hara, Shusaku Nagano, Takahiro Seki, Photoinduced Crater Pattern by the Surface Heterostructure Fabricated by Inkjet Printing on Photoresponsive Liquid Crystalline Polymer Films, 3rd International Conference on Photoalignment and Photopatterning in Soft Materials (PhoSM2018), Tampere, Finland (2018).

9. Issei Kitamura, Mitsuo Hara, Shusaku Nagano, Takahiro Seki, Photoinduced crater pattern by surface heterostructure fabricated by inkjet printing on liquid crystalline polymer films, International Liquid Crystal Conference (ILCC) 2018, Kyoto, Japan (2018).

10. Issei Kitamura, Mitsuo Hara, Shusaku Nagano, Takahiro Seki, Photoinduced Crater Pattern by the Surface Tension Difference Fabricated by Inkjet Printing on Photoresponsive Liquid Crystalline Polymer Films, KJF International Conference on Organic Materials for Electronics and Photonics (KJF-ICOMEP) 2018, Gifu, Japan (2018).

11. Issei Kitamura, Kazuaki Ooishi, Mitsuo Hara, Shusaku Nagano, Takahiro Seki, Photoinduced mass transfer driven by the surface hetero structure in photoresponsive liquid crystalline polymer films, The 12th SPSJ International Polymer Conference (IPC2018), Hiroshima, Japan (2018).

12. Issei Kitamura, Mitsuo Hara, Shusaku Nagano, Takahiro Seki, Photoinduced mass transfer directed by inkjet printing patterns on photoresponsive liquid crystalline polymer films, Photonics & Electromagnetics Research Symposium (PIERS) 2019, Roma, Italy (2019).

13. Issei Kitamura, Rafael B. Berk, Mitsuo Hara, Shusaku Nagano, Takahiro Seki, Photoinitiated mass transfer propagated from a topmost photoresponsive skin layer, 32nd International Microprocesses and Nanotechnology Conference (MNC2019), Hiroshima, Japan (2019).

Acknowledgements

This thesis is based on the studies under Prof. Takahiro Seki at the Department of Molecular and Macromolecular Chemistry, Graduate School of Engineering, Nagoya University.

First of all I would like to express my deepest appreciation to my supervisor Prof. Takahiro Seki for his helpful guidance and encouragement throughout my doctorates course, as well as for providing a lot of valuable opportunities to participate in conferences and to go abroad to study and research. I would like to show my gratitude to the laboratory staffs, Assoc. Prof. Yukikazu Takeoka, Prof. Shusaku Nagano (now; Department of Chemistry, Rikkyo University) and Assist. Prof. Mitsuo Hara for their sincere discussions, as well as detailed guidance and advice on experiments and measurements. I am particularly grateful to Prof. Nagano that he led my research in the right direction and brushed up it.

This thesis was also supported by researcher’s helps in other research institutions. Many thanks to Prof. Yuichi Masubuchi (Department of Materials Physics, Nagoya University), Assoc. Prof. Tetsuya Yamamoto (WPI-ICReDD, Hokkaido University) for all the valuable discussions and productive collaborations. I could not have performed my research works without their supports.

A part of this research was supported by the Japan Society for the Promotion of Science (JSPS) research fellow program for Young Scientist and Program for Leading Graduate Schools "Integrative Graduate Education and Research in Green Natural Sciences", MEXT, Japan.

I would like to thank Sakamoto donation foundation, Mr. Seishi Sakamoto, Ms. Haruyo Sakamoto and Mr. Seiichiro Sakamoto for Hoshizaki scholarship.

I wish to express my special thanks to all members of the Seki laboratory including alumni for their generous supports, encouragements and friendships. In

particular, I would like to thank Mr. Atsushi Hirakawa, Dr. Daisuke Tanaka, Dr. Ryota Imanishi, Dr. Koji Mukai, Mr. Keita Ohno, Mr. Tasuku Mizuno, Mr. Ryosuke Goto, Mr. Takashi Nakai, Mr. Reona Noda, Mr. Naoyuki Wakitani, Dr. Yui Naoi, Ms. Marina Ueda, Mr. Kazuaki Oishi, Mr. Kota Suetsugu, Mr. Keisuke Takishima, Mr. Ryota Higashi, Mr. Reona Kanazu, Mr. Ryohei Okayasu and Mr. Rafael Benjamin Berk as my collaborators. I received various cooperation and warm encouragement in my laboratory life from Ms. Yumi Otsuka, Ms. Yuumi Okaya, Mr. Taiki Orito, Mr. Keisuke Kato, Ms. Miho Nagai, Mr. Kenta Watanabe and Ms. Xiaoqian Zhang as my contemporary of the laboratory, and Mrs. Yuko Ohiwa as administrative assistant. I appreciate them sincerely.

Finally, I am grateful to my parents, my sister, my brother and my friends for their heartfelt encouragement, understanding, and helpful supports.

January, 2021

Issei Kitamura